2004

VALIDATION OF DETACHED EDDY SIMULATION USING LESTOOL FOR HOMOGENEOUS TURBULENCE

Sai Kumar Doddi
University of Kentucky, sai@engr.uky.edu

ABSTRACT OF THESIS

VALIDATION OF DETACHED EDDY SIMULATION USING LESTOOL FOR HOMOGENEOUS TURBULENCE

Detached Eddy Simulation (DES) is a hybrid turbulence model, a modification to the one-equation model proposed by Spalart and Allmaras (1997) [26]. It combines the advantages of both the RANS and LES models to predict any fluid flow. Presently, the focus is on using Homogeneous Turbulence to test the DES model. In an attempt to scrutinize this model, many cases are considered involving the variance of DES grid spacing parameter, C_{DES}, the grid density, Reynolds number and cases with different initial conditions. Choosing Homogeneous Turbulence for our study alienates complications related to the geometry, boundary conditions and other flow characteristics helping us in studying the behavior of the model thoroughly. Also, the interdependencies of the model grid spacing parameter, grid density and the numerical scheme used are also investigated. Many previous implementations of the DES model have taken the value of C_{DES}=0.65. Through this work, many issues including the sensitivity of C_{DES} will be made clear. The code used in running the test cases is called LESTool, developed at University of Kentucky, Lexington. The two main test cases considered are based on the benchmark experimental study by Comte Bellot and Corrsin (1971) [12] and the Direct Numerical Scheme (DNS) simulation by Blaisdell *et al*. (1991) [10].

KEYWORDS: Turbulence model, Detached Eddy Simulation, Homogeneous Turbulence, Grid Spacing Parameter, LESTool

Sai Kumar Doddi

01/14/2004

VALIDATION OF DETACHED EDDY SIMULATION USING LESTOOL FOR HOMOGENEOUS TURBULENCE

By

Sai Kumar Doddi

Dr. Thomas Hauser

Co-Director of Thesis

Dr. George Huang

Co-Director of Thesis

Dr. Raymond LeBeau

Director of Thesis

Dr. George Huang

Director of Graduate Studies

01/14/2004

(Date)

RULES FOR THE USE OF THESIS

Unpublished thesis submitted for the Master's degree and deposited in the University of Kentucky Library are as a rule open for inspection, but are to be used only with due regard to the rights of the authors. Bibliographical references may be noted, but quotations or summaries of parts may be published only with the permission of the author, and with the usual scholarly acknowledgements.

Extensive copying or publication of the thesis in whole or in part also requires the consent of the Dean of the Graduate School of the University of Kentucky.

THESIS

Sai Kumar Doddi

The Graduate School

University of Kentucky

2004

VALIDATION OF DETACHED EDDY SIMULATION USING LESTOOL FOR HOMOGENEOUS TURBULENCE

THESIS

A thesis submitted in partial fulfillment of the
requirements for the degree of Master of Science in Mechanical Engineering in the
College of Engineering at the University of Kentucky

By

Sai Kumar Doddi

Lexington, Kentucky

Co-Directors: Dr. Thomas Hauser, Assistant Professor of Mechanical Engineering,
Salt Lake City, Utah
and
Dr. George Huang, Professor of Mechanical Engineering,
Lexington, Kentucky
Director: Dr. Raymond LeBeau, Assistant Professor of Mechanical Engineering
Lexington, Kentucky

2004

Dedication

To my family, specially to my Dad
who inspired me to reach greater heights in life.

ACKNOWLEDGEMENTS

My special thanks go to my advisor Dr. Raymond LeBeau for giving me insight into the various aspects of my research and being very supportive at every stage. He was always ready to spare his valuable time liberally to patiently answer even trivial questions. I would also like to thank Dr. George Huang for guiding me throughout my research and sharing his pearls of wisdom aiding me to progress in my work. I would not have been successful at any stage without the assistance of Dr. Thomas Hauser. His useful comments and ideas have helped me a lot. I would like to thank Dr. Jacob for kindly agreeing to be in my committee.

I must thank my parents, brothers and sisters who saw in me a potential something more than I ever realized. They were so encouraging at all times and motivated me to tackle all barriers with determination and hard work. I cannot mention how many of them have been personally so helpful including my friends making my life so wonderful at UK. I enjoyed the company of my lab mates more like a family, at the same time gaining so much of knowledge from them.

I would like to thank KY NASA EPSCoR for supporting this research work. I would also like to thank NCSA for generously providing the computer resources to run my jobs on the IRIX cluster. I could have never completed my research work without availing the UKCFD Lab computers at University of Kentucky.

TABLE OF CONTENTS

LIST OF TABLES

LIST OF FIGURES

LIST OF FILES

Sai_Thesis.pdf…… 1.13 MB PDF File

CHAPTER 1

Introduction

1.1. Introduction to Turbulence

Turbulent flow is a highly complex phenomenon. Although researchers have studied the phenomenon for many years, it is not yet possible to characterize turbulence from a purely theoretical standpoint. Many important characteristics of turbulence are well-known, however, including the following:

- Turbulence is time-dependent, three-dimensional, and highly non-linear.
- Fully-developed turbulent motion is characterized by entangled eddies of various sizes. The largest eddies arise from hydrodynamic instabilities in the mean flow field, e.g., shearing between a flowing stream and a solid boundary or unstable stratification produced by heating the fluid from below.
- The largest eddies break down into smaller eddies which, in turn, break down into even smaller eddies. This process of eddy break-down transfers kinetic energy from the mean flow to progressively smaller scales of motion. At the smallest scales of turbulent motion, the kinetic energy is converted to heat by means of viscous dissipation.
- The dynamic and geometrical properties of the largest eddies are closely related to the corresponding properties of the mean flow field. For example, large, unstable vortices that form on the perimeter of a turbulent jet tend to possess well-defined toroidal structures.
- The time and length scales of the smallest turbulent eddies are many orders of magnitude greater than the time scales and free paths of molecular motion. As a result, the processes of viscous dissipation are statistically independent of molecular motion.
- Turbulent motion is not a random phenomenon. As a consequence, turbulent fields possess definite spatial and temporal structures.

1.1.1. Turbulence Modeling

To create a usable numerical model of a turbulent flow field, it is necessary to describe turbulent motion in terms of averaged quantities. Although it is theoretically

possible to directly apply the conservation equations to the entire flow field, it is unreasonably difficult to do so in practice. As noted above, turbulent flows involve entangled eddies the sizes of which encompass a wide range of length scales. To resolve an entire turbulent flow field by direct application of the conservation equations, it is necessary to employ a computational mesh with element sizes that are smaller than the smallest eddies. Such meshes are extremely dense and because computational cost increases dramatically with mesh density, this results in computations that are prohibitively expensive to resolve. By contrast, models that are based on averaged quantities characterize turbulent flows using meshes of reasonable density; therefore, they result in reasonable computational times and costs.

Turbulence modeling is one of the important features of computational fluid dynamics. It gives us a scope to estimate the flow properties of any fluid given the initial and boundary conditions. However, accurate prediction of the flow is not fully possible even now. The solution to complex physical phenomenon requires solving the complete Navier-Stokes equations with a proper numerical approach, not to mention the enormous usage of computer resources.

1.1.2. History of Turbulence Modeling

The primary emphasis is upon the time-averaged Navier-Stokes equations. The origin of this approach dates back to the end of 19th century when Reynolds (1895) published results of his research on turbulence. His pioneering work proved to have such profound importance for all future developments that we refer to the standard time-averaging process as one type of Reynolds averaging.

The earliest attempts at developing a mathematical description of turbulent stresses sought to mimic the molecular gradient-diffusion process. In this spirit, Boussinesq (1877) introduced the concept of a so-called eddy viscosity. The Boussinesq eddy-viscosity approximation is so widely known that few authors find a need to reference his original paper.

Much of the physics of viscous flows was a mystery in 19th century, and further progress awaited Prandtl's discovery of the boundary layer in 1904. Focusing upon turbulent flows, Prandtl (1925) introduced the mixing length (an analogy of the mean free

path of a gas) and a straightforward prescription for computing the eddy viscosity in terms of the mixing length. The mixing-length hypothesis, closely related to the eddy-viscosity concept, formed the basis of virtually all turbulence modeling research for the next twenty years. In modern terminology, we refer to a model based on the mixing-length hypothesis as an algebraic model or a zero-equation model of turbulence. By definition, an n-equation model signifies a model that requires solution of n additional differential transport equations in addition to those expressing conservation of mass, momentum and energy for the mean flow.

To improve the ability to predict properties of turbulent flows and to develop a more realistic mathematical description of the turbulent stresses, Prandtl (1945) postulated a model in which the eddy viscosity depends upon the kinetic energy of the turbulent fluctuations, k. He proposed a modeled partial-differential equation approximating the exact equation for k. Thus was born the concept of the so-called one-equation model of turbulence.

While having an eddy viscosity provides a more physically realistic model, the need to specify a turbulent length scale remains. Since the length scale can be thought of as a characteristic eddy size and since such scales are different for each flow, turbulence models that do not provide a length scale are incomplete.

A particularly desirable type of turbulence model would be one that can be applied to a given turbulent flow by prescribing at most the appropriate boundary and/or initial conditions. Ideally, no advance knowledge of any property of the turbulence should be required to obtain a solution. We define such a model as being complete. Note that our definition implies nothing regarding the accuracy or universality of the model, only that it can be used to determine a flow with no prior knowledge of any flow details.

Kolmogorov (1942) introduced the first complete model of turbulence. In addition to having a modeled equation for k, he introduced a second parameter ω that he referred to as `the rate of dissipation of energy in unit volume and time.' The reciprocal of ω serves as a turbulence time scale, while [$k^{1/2}/\omega$] serves as the analog of the mixing length and $k\omega$ is the analog of the dissipation rate, epsilon. In this model, known as k-ω model, ω satisfies a differential equation somewhat similar to the equation for k. The model is thus termed a two-equation model of turbulence.

Chou (1945) and Rotta (1951) laid the foundation for turbulence models that obviate use of the Bousssinesq approximation. Rotta devised a plausible model for the differential equation governing evolution of the tensor that represents the turbulent stresses, i.e., the Reynolds-stress tensor. Such models are most appropriately described as stress-transport models. Many authors refer to this approach as second-order closure or second-momentum closure. The primary conceptual advantage of a stress-transport model is the natural manner in which nonlocal and history effects are incorporated.

Thus, by the early 1950's, four main categories of turbulence models had evolved, viz.,

(1) Algebraic (Zero-Equation) Models

(2) One-Equation Models

(3) Two-Equation Models

(4) Stress-Transport Models

Finally, turbulence models have been created that fall beyond the bounds of the four categories cited above. This is because model developers have tried unconventional approaches in an attempt to remove deficiencies of existing models.

Among the numerical schemes available to the CFD community, DNS (Direct Numerical Simulation) is the most primitive one. In DNS, the flow is resolved temporally and spatially to the order of a length scale of the smallest eddy. Thus by such high resolution of the grid, the physics of the flow is being captured to the maximum extent by establishing continuity in the properties at the macro level. Though this is not attainable, the limit would be nearly reached. For simple flows with low Reynolds numbers, this is an excellent tool and the solution obtained using DNS is found to be very reliable. But some theories say that the grid size in DNS increases at the rate of $Re^{2.6}$. Thus, it is seen that this numerical scheme is possible only for simple geometries and low Reynolds number flows. For complicated geometries and high Reynolds number flows, i.e., to the applications of the present day even with the high-performance computational clusters much like the supercomputers, DNS is still not the primary choice mainly because of the computational time involved and economic consideration taken into account as well. Effective turbulence models are the need of the hour. LES (Large Eddy Simulation) is a very efficient turbulence model. Though the results of LES compared to DNS results are

not outstanding, they are still acceptable in the general sense and serve the requirement in most cases. More importantly, the simulation using LES is affordable compared to DNS cost or time in most cases. In LES, the large eddies of the flow are resolved and the smaller eddies are modeled using the SGS (sub grid scale) model. This has given the researchers good results for many cases. But for boundary layer flows, the grid has to be resolved to a high level and the total computations required to resolve around the boundary in most cases is not less even compared to DNS. So LES also turns out to be expensive in such cases. Hence the search for an optimum turbulence model is the present priority.

1.2. Homogeneous Turbulence

If a uniform stream of fluid passes through a regular array of holes in a rigid sheet, or a regular grid of bars, held at right angles to the stream, the motion downstream of the sheet consists of the same uniform velocity together with a superimposed random distribution of velocity. This random motion dies away with distance from the grid, and to that extent is not statistically homogeneous, but the rate of decay is found to be so small that the assumption of homogeneity of the turbulence is valid for most purposes. Thus there is available a convenient laboratory method of producing turbulence which is approximately homogeneous, the various stages of decay occurring at different distances from the grid.

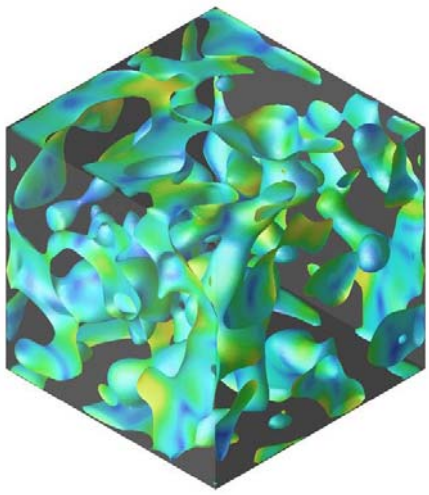

Figure 1.1: Homogeneous Turbulence simulation in a cube colored by Pressure fluctuations

"Homogeneous Turbulence is a random motion whose average properties are independent of position in the fluid"

- G. K. Batchelor

1.2.1. Mathematical Description of Homogeneous Turbulence

We shall confine our attention to the case of a fluid which is effectively incompressible (indeed, it would be difficult to proceed on any other basis on account of the complexity of the problem). The equation of continuity is then

$$\nabla \cdot u = 0 \tag{1.2.1}$$

where u is the velocity vector of the turbulent motion at a position in the field specified by the vector coordinate x, where both u and x are referred to axes such that the fluid has no average motion.

The density, ρ and viscosity, υ are assumed to be constant. Also, the Navier Stokes equation is assumed to be valid. The variation of u with x and time t then satisfies

$$\frac{\partial u}{\partial t} + u \cdot \nabla u = -\frac{1}{\rho}\nabla p + \upsilon \nabla^2 u \tag{1.2.2}$$

where ∇ represents the gradient operator with respect to the coordinate system x, and p represents pressure. The validity of this equation is taken as the fundamental premise.

Hence, as suggested by Batchelor [13], the mathematical formulation of the problem of homogeneous turbulence is this: *Given an infinite body of uniform fluid in which motions conform to the equations* (1.2.1) *and* (1.2.2), *and that at some initial instant the velocity of the fluid is a random function of position described by certain probability laws which are independent of position, to determine the probability laws that describe the motion of the fluid at subsequent times.*

1.2.2. Brief History of Homogeneous Turbulence

The origin of the subject lies in G. I. Taylor's pioneering work in 1935. Prior to this time there had been no clear recognition and acceptance of the fact that the velocity of the fluid in turbulent motion is a random continuous function of position and discontinuous collisions between discrete entities that have been studied in the kinetic theory of gases. When these ideas became popular, Taylor introduced the correlation

between the velocities at two points as one of the quantities needed to describe turbulence. As soon as the statistics of continuous random statistical homogeneity simplified the analysis, Taylor went further still and considered isotropic turbulence. In this same paper Taylor described measurements which showed that the turbulence generated downstream from a regular array of rods in a wind tunnel was approximately homogeneous and isotropic. Thus a clear guide to further theoretical and experimental work was established.

Other important contributions to the subject were made by Taylor in 1938. The first was a consideration of the mechanical processes represented by the non-linear term in the equation for the decay of mean-square vorticity. This work demonstrated clearly two important consequences of the non-linearity of the dynamical equation. The second contribution was the introduction into turbulence theory of a result obtained in pure mathematics, viz. that the Fourier transform of the correlation between two velocities is an energy spectrum function in the sense that it describes the distinction of kinetic energy over the various Fourier wave-number components of the turbulence.

Soon after Taylor's work, T. Von Karman perceived that mean values of the products of the velocities at two (or more points) were tensors, which immediately enabled the analysis to be expressed more concisely and greatly facilitated the deductions from the assumption of isotropy.

The required physical basis for one kind of similarity of the turbulence was suggested some years later by A. N. Kolmogoroff. Kolmogoroff's hypothesis was that the small-scale components of the turbulence are approximately in statistical equilibrium. These small-scale components owe their existence to the non-linear interchange of energy between different wave-number components, and Kolmogoroff postulated that the equilibrium would be universal, apart from the effect of variation of two parameters, one the viscosity of the fluid and the other determined by the large-scale components of the turbulence. Thus, when these two parameters are given, the complete statistical specification of the small-scale components of the turbulence is determined, and many definite predictions may be made from dimensional analysis.

On the experimental side, a large number of measurements of mean values of different velocity products has been made since 1935, principally with the hot-wire

anemometer. This instrument is capable of giving an electrical signal which is proportional to the instantaneous velocity of the fluid at the point where the wire is placed. Examples of the kinds of measurements of which the hot-wire anemometer is capable are to be found in the papers by A. A. Townsend who has supplied many of the measurements on which our present ideas about homogeneous turbulence are based, and S. Corrsin.

One of the recent benchmark experiments performed on Homogeneous Turbulence is the study by Comte Bellot and Corrsin[12]. His results on isotropic turbulence have given way to many recent developments by lending a standard basis of comparison and the calibration of the developing hybrid turbulence models, for e.g., the grid sensitivity parameter, C_{DES} which is one of the critical parameters in a recent turbulence model developed called Detached Eddy Simulation (DES)[26] is obtained from the Homogeneous Turbulence simulation.

1.3. Description of Present Work

1.3.1. Motivation

"Current CFD (turbulence modeling) capabilities do not permit the reliable prediction of separation onset/progression characteristics. Efforts currently underway to address this deficiency…need to be accelerated. Major advancements are needed"

- Letter to NASA ASTAC Chair from Airframes Systems Subcommittee, 21 March 2000

As stated in the above quotation and also widely known, the turbulence models available cannot predict the separation in flows satisfactorily and hence progress has to be made to develop models which can handle many practical problems and complicated flows.

Direct Numerical Simulation (DNS) is the earliest tool used to solve flow problems by solving for the Navier Stokes Equations computationally. But the grid size increases dramatically as the Reynolds number is increased. This rules out DNS for complicated cases. If we talk about Large Eddy Simulation (LES), it is not much different from DNS at the boundary. Away from the boundary it may be affordable, but the grid becomes very dense as it approaches the boundary. Hence we cannot use LES as our

primary model for a wide variety of cases. Also, it is well known that Reynolds Averaged Navier Stokes (RANS) does not predict separated flows well though it is good at dealing with cases without separation. From the above mentioned reasons, we definitely need to develop a model which suits our requirements and yet is affordable which gives us worthy results.

"The conversion of a typical RANS code to DES is rapid as far as the modification of this model goes, but achieving the required spatial and temporal accuracy for LES can demand deep improvements…Thus, DES can address some very challenging flow physics but the burden on the user is, not surprisingly, even higher than for a RANS study.

- from the concluding remarks, "Detached Eddy Simulation of Massively Separated Flows", M. Strelets, AIAA 2001-0879

As stated by Dr. Strelets, Detached Eddy Simulation (DES) can handle challenging problems and give us good results. But understanding the model and investigating it thoroughly is necessary before it can be used as a perfect model. Every model has its own pros and cons, but we believe that DES could work out to be a very cheap and realistic model and its advantages could be utilized to the fullest. With this hope we begin to explore the model within our limits. Our goals are stated in the next section.

As will be seen in the future chapters, we have chosen two different cases, one is the Blaisdell's case with a Reynolds number, Re=3640 and other is a CBC case with a mesh Re=34000. Since *Detached Eddy Simulation* is an important tool to study specially cases where there is separation, it would also be interesting to study homogeneous turbulence at low *Re*. In this case, we would understand the basic *DES* model and investigate the subtle intricacies in the model. The numerical scheme and the amount of artificial added to the model could drastically affect the fashion in which the model behaves. Understanding such model behavior would help us a long way in studying even complicated cases.

1.3.2. Objectives and Summary

In this present research work, we will discuss the simulation of Homogeneous Turbulence in detail using Detached Eddy Simulation (DES). We will scrutinize the underlying parameters of DES using our test cases. Our main objectives are

1. To understand the sensitivity of the DES grid spacing parameter, C_{DES} by applying this turbulence model to Homogeneous Turbulence.
2. To see the effect of grid density when using DES and judging the interdependency of C_{DES} and grid density.
3. Understanding the effect of initial conditions on homogeneous turbulence simulation using two different test cases.
4. Test and observe the sensitivity of the model to Reynolds number
5. Analyze the behavior of the model with respect to the numerical schemes applied, 5^{th} order upwind scheme or 6^{th} order central scheme.
6. Understanding the effect on dissipation rate of the model (from the slope of the energy spectrum and temporal energy decay) by varying the numerical scheme and C_{DES} and evaluating the interdependencies.

CHAPTER 2

Survey of Previous Work

2.1. Introduction

Direct numerical simulation (DNS) is potentially the most accurate way to numerically study a turbulent flow. In this approach, the flow field in solved directly from the Navier-Stokes equations and no averaging or turbulence modeling is applied. Thus only the numerical methods affect the accuracy of the solution. From some point of view DNS is the most straightforward approach to CFD. As a drawback DNS requires a huge amount of computer capacity and high order numerical methods for good results.

When direct numerical simulation is applied, the computational domain must be large enough and the computational grid dense enough. Otherwise all features of turbulence will not be described correctly. The proper length of the domain is set by the so called integral length scale. It is the distance after which the self correlation of the velocity components vanishes. The number of grid points is set by the Reynolds number. As Reynolds number grows the ratio of the integral length scale to the smallest length scale in the flow grows and thus smaller eddies will be present in the flow field. The grid must be able to capture these smallest scales of motion. For the two above mentioned reasons, direct numerical simulation requires so much computer capacity that it is not adaptable for engineering type flows. The value of DNS lies in the huge amount of information it provides from the flow field. It is a valuable tool for the study of physics of turbulence.

In large eddy simulation (LES) the small scale motion is extracted from the main flow field by filtering. While the main flow field is solved from the Navier-Stokes equations, the smallest eddies are modeled. LES is conceptually close to RANS, but as a method it is more closely related to DNS. In RANS the turbulence model damps out the smallest scales of motion no matter how dense a grid is used, while in LES the grid density (or filter width) defines the amount of damping. This means that as we use a denser grid in LES the turbulence model includes less damping and we approach direct numerical simulation. One essential consequence is that with LES we obtain a three dimensional flow field for two dimensional geometries, which never happens with RANS.

Also large eddy simulation requires a huge amount of computer capacity and is not yet applicable to most engineering problems. However, RANS is not able to describe properly flows over non-streamlined bodies, where the flow is massively separated and there exists also other time dependency than turbulence. Still RANS behaves very well in boundary layers and requires considerably fewer grid points than LES. This has led to the development of so called hybrid methods which combine RANS and LES. They apply RANS in the boundary layers and LES in the other parts of the flow field. The open problem in the hybrid methods is numerics. While RANS-calculations require damping the same feature may spoil the LES result.

As seen in the Figure 2.1 below as we move from RANS to LES, there is this so called 'grey area' where it behaves as a combination of LES and RANS models and to what degree is of each is unclear. In this region we do not know how the turbulence model behaves. We need to find a unified approach to understand the grey area. There have been several suggested approaches to address this problem.

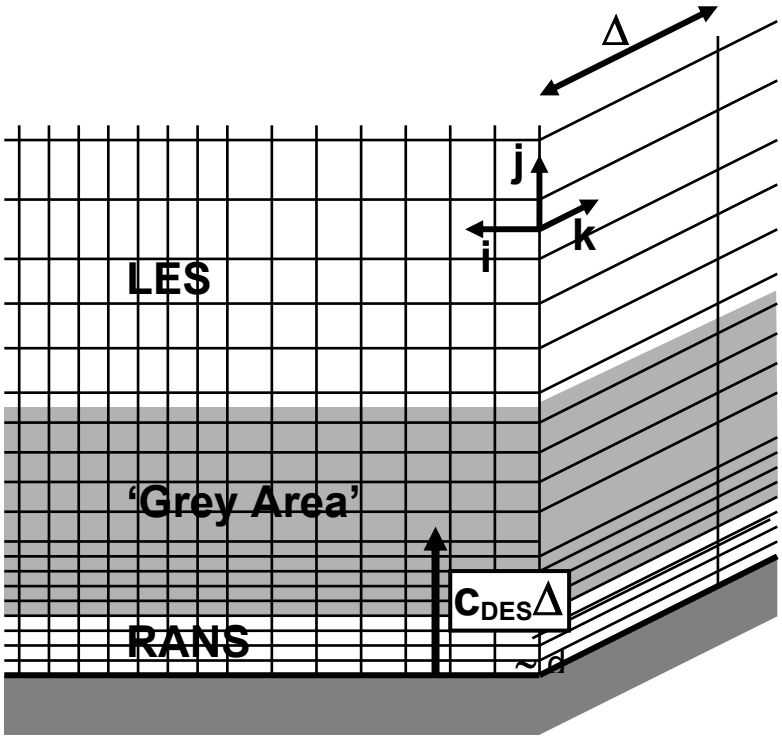

Figure 2.1: Transition from RANS model to the LES model introducing the concept of 'grey area'.

Some of the unified approaches which address the 'grey area' issue and provide a smooth transition between the RANS and LES are:

1. Speziale's Reynolds Stress Model (Speziale, 1998)

$$\tau_{ij}^{SGS} = [1 - \exp(-\beta\Delta / L_k)]^n \tau_{ij}^{RANS}$$

This is the explicit algebraic Reynolds Stress model proposed by Speziale. Here τ_{ij}^{SGS} is the sub grid scale Reynolds shear stress and τ_{ij}^{RANS} is the Reynolds averaged Navier - Stokes shear stress.

2. DES Model or S-A Model (Spalart, 1997)

$$\widetilde{d} = \min(d, C_{DES}\Delta)$$

This is the Detached Eddy Simulation obtained by modifying *d* in the one-equation model proposed by Spalart and Allmaras, combining the advantages of Reynolds Averaged Navier Stokes (RANS) model and the Large Eddy Simulation (LES) model. $C_{DES}\Delta$ is the product of grid sensitivity parameter C_{DES} and the maximum of the grid spacing in any of the directions.

3. DES SST Model (Travin, 2000)

$$D_{DES}^{k} = \rho k^{3/2} / \widetilde{l}\,,\ \widetilde{l} = \min(l_{k-\omega}, C_{DES}\Delta),$$
$$l_{k-\omega} = k^{1/2} / (\beta^* \omega)$$

This model is the Shear Stress Transport based model of DES proposed by Travin. The dissipation term of DES is given by D_{DES}^{k} and the length scale $\widetilde{l}$ and $k-\omega$ length scale $l_{k-\omega}$ are defined as seen above.

4. KE1E-SAS Model (Menter, 2003)

$$\widetilde{L}_{vK-SAS} = \max(L_{vK-SAS}, C_{SAS}\widetilde{\Delta}),\ with$$
$$\widetilde{\Delta} = \min(\Delta x, \Delta y, \Delta z), C_{SAS} = 0.6$$

This model is based on a one-equation model using the v. Karman length-scale L_{vK-SAS} to adapt to the underlying turbulent structures. The model can be operated in RANS and in LES mode and is termed Scale-Adaptive Simulation (SAS) model.

In our present research, we shall apply the Spalart-Allmaras' Detached Eddy Simulation (DES) Model to study the Homogeneous Turbulence case. More about this model will be explained in section 3.1. The benchmark homogeneous turbulence experiment was performed by Comte Bellot and Corrsin [12] using their wind tunnel which was about 10 m long. Turbulence was generated using a bi-plane square rod grid with mesh sizes of 1 inch and 2 inches. The Reynolds number corresponding to the 2 inch mesh is 34000. The results obtained were recorded at three locations downstream of the wind tunnel.

2.2. DES studies in the Research World

Detached Eddy Simulation is not a very old concept. The one-equation model was proposed by Spalart *et al.* [27] in 1997. Since then, other researchers have implemented this model, which has added weight to this model in the world of computational modeling of flows. It would be helpful to study the kind of work others have done in order to show how our work is relevant in the present scenario and how it would help the current research industry.

2.2.1. Analysis of DES Model

In the work on 'Detached-eddy simulation of an airfoil at high angle of attack', Shur *et al.* (1999) in their research on turbulence modeling and experiments related to DES of an airfoil at high angle of attack made some studies on Homogeneous turbulence. They have taken two grids 32^3 and 64^3 to perform their studies. They seem to get strong ripple effects in the case of 32^3 grids. However, they get good results using the 64^3 grid when they simulate the CBC case. They obtain a –5/3 slope for the energy decay. They give little information about this case in their paper but do conclude that they finally fix the value of C_{DES} as 0.65 based on their simulations. Finally they stress that the cut-off slope in the CBC energy spectra is very sensitive even to a very slight change in C_{DES} (~ +0.05 or –0.05). Also, as we have noticed, they state that this sensitivity is seen not only in the value chosen for C_{DES} but also on the grid resolution.

In their conclusions, they want to make more studies in the direction of checking how sensitive the *DES* parameters and grid resolution are in terms of getting good results

including studies how the Reynolds number and numerical differencing scheme would affect the model. DES mainly being a 3D model, they have not got good results when they have used the model for 2D simulations.

In the work on 'An Approach to Wall Modeling in Large-Eddy Simulations', Nikitin *et al.* (July 2000) applied the DES model without adjustment as an SGS model in the LES of channel flow. The range of Reynolds number Re_τ is from 180(a QDNS) to 80,000(a full LES). This allows us to see how the transition occurs and how it is affected.

The value of C_{DES} is set from the isotropic homogeneous turbulence experiment as 0.65. Three different codes were used to test the case. The discretization effects as opposed to the modeling effects are what could be mainly scrutinized though their effort. The results obtained were stable and fairly accurate though there was some acceptable disagreement due to the resolution of the grid. Finally they conclude saying that these results raise hope for gradual improvements that could lead to a simple, stable and accurate approach to wall modeling.

In the work on 'Detached Eddy Simulation of a Supersonic Axisymmetric Base Flow with an Unstructured Solver', Forsythe *et al.* [15] studied the base flow (normally seen behind a missile, rocket or a projectile) using DES and (Monotone Integrated LES) MILES schemes. While dealing with the S-A DES scheme, they have used varying values of C_{DES} as they were unsure about which was the best value that had to be used in their modeling. The C_{DES} values used were 0.25, 0.5 and 0.65. Though 0.5 is listed here, very little studies and discussion is provided in this paper (a reference quoted by Forsythe *et al.* has more information related to C_{DES}=0.50). From the explanation given in the paper it can be concluded that the C_{DES}=0.65 performed very poorly. However, when C_{DES}=0.25 was used, the results were encouraging. When comparing results for the reattachment location and downstream velocity profile, MILES results matched well. And the DES results got better and approached close to MILES results as the C_{DES} was reduced from 0.65 until it reached 0.25. Forsythe *et al.* use two unstructured grids in their simulations (Short Grid-1.7 Million cells and Long Grid-2.8 million grids.)

In conclusion, Forsythe *et al.* state that the lower value of C_{DES}, i.e., C_{DES}=0.25 is a better value and hence the C_{DES} value should be reduced when an unstructured grid consisting of tetrahedrons is used. Also, they state that when capturing the boundary

layer, DES did a better job than MILES in general when the LONG (fine) grid was used as the RANS mode of DES modeled the boundary layer better than what MILES did. They also conclude that since using the right value for C_{DES} is important, computations of isotropic turbulence should be performed using the grids that they have used to explore the right value of C_{DES}.

2.2.2. Application of DES Model

In the paper published in the Journal of Fluids Engineering on "Detached-eddy simulation with compressibility corrections applied to a supersonic axisymmetric base flow", Forsythe *et al.* [14] used two models to perform studies on base flows. The objective of this paper was to predict the base pressure correctly which is used to calculate the base drag. The two models used were: a) Spalart-Allmaras' DES Model and b) Mentor's Shear Stress Transport model of DES. In the case of S-A DES Model, the C_{DES} is taken as 0.65 based on the paper by Shur *et al.* [21] (discussed previously). In the Menter's SST model of DES [9], the k-ε and k-ω DES have their respective C_{DES} calibrated by Strelets isotropic turbulence experiment as $C^{k-\varepsilon}_{DES}$=0.61 and $C^{k-\omega}_{DES}$=0.78. Menter's SST model is based on the blending of and k-ε and k-ω models. For the testing of cases in this paper, four grids are used (both structured and unstructured). Finally, unstructured grids gave far better results as against structured grids when compared to the experiment and fine grids have predicted the flow better than coarse grids. Also, in general S-A DES results were better than the SST DES results.

In the concluding remarks, Forsythe *et al.* state that though base flows can be predicted well using hybrid models like DES than using pure LES or pure RANS, careful consideration must be made while choosing the grid size and density.

Also in the work on 'Detached Eddy Simulations of Supersonic Flow Over Cavity', Hamed *et al.* [1] assess the capability of DES in predicting cavity flow fields involving interactions between acoustics, turbulence and shock waves. They used Menter's SST model of DES [9] in their study to predict the flow over cavity. Their motivation to use a hybrid model comes from the fact that URANS simulations have failed in general to capture the flow unsteadiness. They do not mention the C_{DES} values that they have used in their paper; the best assumption is that they have used the values

suggested by Strelets for the Menter's SST DES model in his isotropic turbulence experiment. The grid that they have used has 0.8×10^6 grid points as against 21×10^6 (205x94x40) grid points used by Rizzetta *et al.* (comparative results). Their results are quite comparable with what Rizzetta *et al.* obtained.

Hamed *et al.* conclude that the SST model of DES has worked in predicting the supersonic cavity flow.

Related to some of the details revealed at the Aerospace Sciences Meeting 2003, Reno, Nevada, on "Detached Eddy Simulation around a Forebody at High Angle of Attack", Viswanathan *et al.* [4] performed studies around a rectangular ogive forebody based on the body width/diameter D, the forebody length is 2D while the length of the aft section is 4D. The cross-section is a rounded-corner square with corner radius D/4. Simulations are performed using the S-A DES model. The C_{DES} value is chosen as 0.65 as suggested by Shur *et al.* [21]. No further investigations are made on determining the value of right C_{DES}. The grid is of three resolutions a) base line grid (6.5×10^6 cells) b) fine grid (8.75×10^6 cells) and c) coarse grids (2.1×10^6 and 3.5×10^6 cells). The grid is an unstructured grid consisting of tetrahedra and prisms. The Reynolds number variation was from 8×10^4 to 2.25×10^6 (based on the freestream speed and diameter D). The grid was clustered near the ogive surface and geometrically stretched at a rate of 1.2 away from the wall. The distance from the wall to the first cell center was less than 2×10^{-6}D, within one viscous unit on average. The results obtained are compared with URANS results and experimental results by Pauley *et al.*

Excellent results have been obtained by the S-A DES simulations which compare pretty well with the experimental results and are far better than the URANS results. In the concluding remarks, Viswanathan *et al.* point out that when they run the static geometry with varying grid resolutions, as the grid density increased, the turbulence model effect reduces and the technique (DES) ultimately would approach Direct Numerical Simulation.

Also, in the work on "Film Cooling Analysis Using DES Turbulence Model", Roy *et al.* [31] use Spalart-Allmaras based Detached Eddy Simulation (DES) model that is applied to a film cooled flat plate.

The code used is a finite volume based parallel, implicit, unstructured Euler/Navier-Stokes flow solver called 'Cobalt'. GridPro multiples grid generator was used to develop a multi-block (15) grid with approximately 1,300,000 cells. Gridgn14.03 is used to convert this grid into Cobalt compatible unstructured grid containing a single block and 899584 cells. The value of C_{DES} taken is 0.65. Comparisons are made with the RANS model which shows that the DES simulation greatly enhances the realistic description of the dynamic mixing processes.

2.3. Present Research Overview

In the Figure 2.2, we see a summary of the research done which has been documented in this thesis. As explained in section 3.2, there are two test cases. The CBC case simulated using LESTool is compared to the standard experimental results by Comte Bellot and Corrsin [12] and some other results obtained from the studies by Knight *et al.* [6] and Shur *et al.* [21]. The Blaisdell's case that is simulated is compared to the DNS studies performed by Blaisdell *et al.* [10].

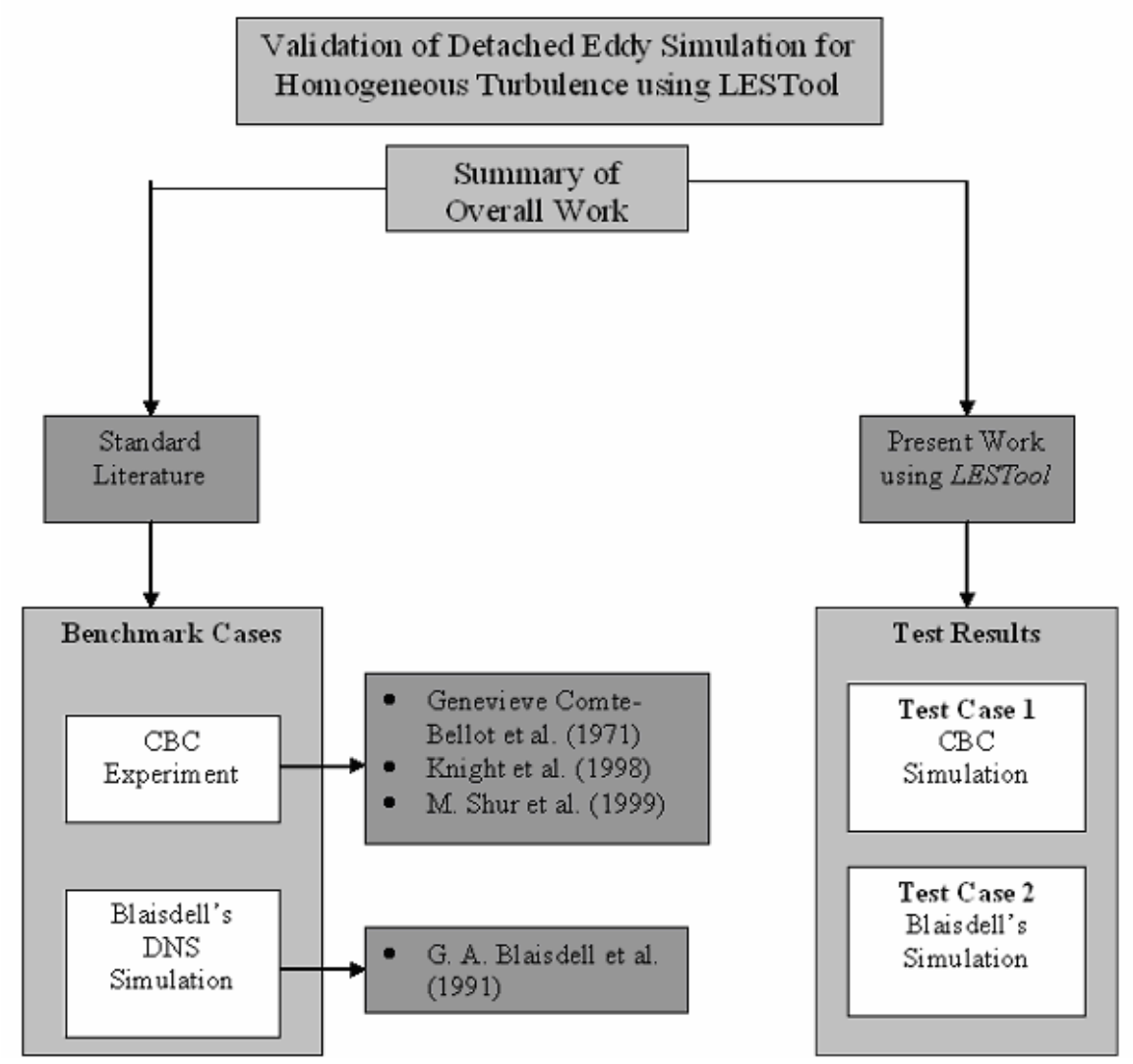

Figure 2.2: Overview of the present research work

CHAPTER 3

Theory and Test Cases

The focus of this chapter will be on giving an outline of the DES model and also introducing to the research work that has been done on Homogeneous Turbulence earlier.

3.1. Detached Eddy Simulation

The present DES model is a simple variation of the S-A one-equation eddy-viscosity RANS model. The DES modification concerns the destruction term, and hinges on the length scales d and $\tilde{d}$. In the S-A model, d is the distance to the nearest wall and expresses the (inviscid) confinement of eddies by the wall. In the DES model, we replace d with $\tilde{d}$, which is defined as

$$\tilde{d} \equiv \min(d, C_{DES}\Delta) \text{ with } \Delta = \max(\Delta x, \Delta y, \Delta z)$$

The role of Δ is to allow the energy cascade down to the grid size; roughly, it makes the pseudo-Kolmogorov length scale, based on the eddy viscosity, proportional to the grid spacing. We use the largest dimension of the grid cell as defined by the DES model, in contrast with the often-used cube-root definition of Δ.

The model is as follows. The transition terms were removed from the S-A model [26] and would have no impact except maybe near the buffer layer. The eddy viscosity is given by

$$\nu_t = \tilde{\nu} f_{v1},\ f_{v1} = \frac{\chi^3}{\chi^3 + c_{v1}^3},\ \chi \equiv \frac{\tilde{\nu}}{\nu}$$

where ν is the molecular viscosity, $\tilde{\nu}$ is the working variable and obeys the transport equation

$$\frac{D\tilde{\nu}}{Dt} = c_{b1}\tilde{S}\tilde{\nu} + \frac{1}{\sigma}\left[\nabla.((\nu + \tilde{\nu})\nabla\tilde{\nu}) + c_{b2}(\nabla\tilde{\nu})^2\right] - c_{w1}f_w\left[\frac{\tilde{\nu}}{\tilde{d}}\right]^2$$

Here S is the magnitude of the vorticity,

$$\tilde{S} = S + \frac{\tilde{\nu}}{\kappa^2\tilde{d}^2}f_{v2},\ f_{v2} = 1 - \frac{\chi}{1 + \chi f_{v1}},$$

The function f_w is

$$f_w = g\left[\frac{1+c_{w3}^6}{g^6+c_{w3}^6}\right]^{1/6},\ g = r + c_{w2}(r^6 - r),\ r \equiv \frac{\tilde{\nu}}{\tilde{S}\kappa^2\tilde{d}^2}$$

The wall boundary condition is $\tilde{\nu} = 0$. The constants are $c_{b1} = 0.1355$, $\sigma = 2/3$, $c_{b2} = 0.622$, κ=0.41, $c_{w1} = c_{b1}/\kappa^2 + (1+c_{b2})/\sigma$, $c_{w2} = 0.3$, $c_{w3} = 2$, $c_{v1} = 7.1$.

In a structured grid, Δx and Δz are independent of y while Δy is refined near the wall, so that there is a layer near the wall in which $\tilde{d} \equiv d$, loosely called the "RANS region", and a region away from the wall in which $\tilde{d} \equiv C_{DES}\Delta$, called the "LES region".

3.2. Background of Homogeneous Turbulence

Homogeneous Turbulence is the simplest of all cases in turbulence with less complexity involved compared to any other turbulence case as the boundary conditions are periodic and the properties change only with time. This gives us scope to study the DES model in a well-defined way without having to worry about intrusion of other complexities that would affect our study. In effect, we can have an isolated study of the model. As we shall see, there are two well-known studies that have been done on Homogeneous Turbulence. One of them is experimental and the other is numerical. Both of them have different initial conditions (energy spectra), Reynolds numbers and initialization parameters. In the present study, two test cases have been considered corresponding to each of these research studies. The setup, working and comparison of the results of the test cases will be discussed in the future chapters. In this chapter, we shall look at the underlying cases that have led to the present research work and also look at the results they have obtained.

The two cases which form the basis for comparing our simulations are:

1. The Experimental study performed by Comte Bellot and Corrsin [12] and
2. The Direct Numerical Simulation studies made by Blaisdell *et al.* [10]

3.2.1. Comte Bellot and Corrsin Experiment

Isotropic turbulence is turbulence whose statistical properties are invariant under all axis rotations and reflections. Since physically interesting properties include joint

probabilities of field variables at two or more space points, isotropy requires homogeneity as well. For simplicity the motion is restricted to be that of a constant density, Newtonian fluid with zero mean velocity everywhere, in an inertial frame.

The benchmark isotropic turbulence experiment performed by Comte Bellot and Corrsin [12] will be described here. The closed wind tunnel, **Figure 2.1** is about 10m long. All turbulence data is generated by a biplane, square-rod, polished dural grid with mesh size of 5.08 cm and solidity of 0.34. A few correlation values were measured far behind a similar grid of mesh size 2.54 cm, to permit reaching larger dimensionless distances and times in the decaying turbulence. The slight (1.27:1) contraction was located 18 mesh lengths downstream of the grid. The streamwise ($\overline{u_1^2}$) and transverse ($\overline{u_2^2}$, $\overline{u_3^2}$) components' turbulent energies remained nearly equal to each other as they decayed along the length of the test section:

$$\frac{U_0^2}{\overline{u_1^2}} = 21\left(\frac{U_0 t}{M} - 3.5\right)^{1.25},$$

$$\frac{U_0^2}{\overline{u_2^2}} = \frac{U_0^2}{\overline{u_3^2}} = 20\left(\frac{U_0 t}{M} - 3.5\right)^{1.25}$$

Here, t is elapsed time in traveling at the mean flow velocity from the grid,

$$t = \int_0^{x_1} \frac{dx_1}{\overline{U}(x_1)}$$

The velocity approaching the grid is U_o = 10 m/sec, and hence a grid mesh Reynolds number, Re= U_0M/ν = 34000 for Mesh size, M = 5.08 cm. Hence the viscosity can be calculated as v=1.494117E-5 m^2/sec.

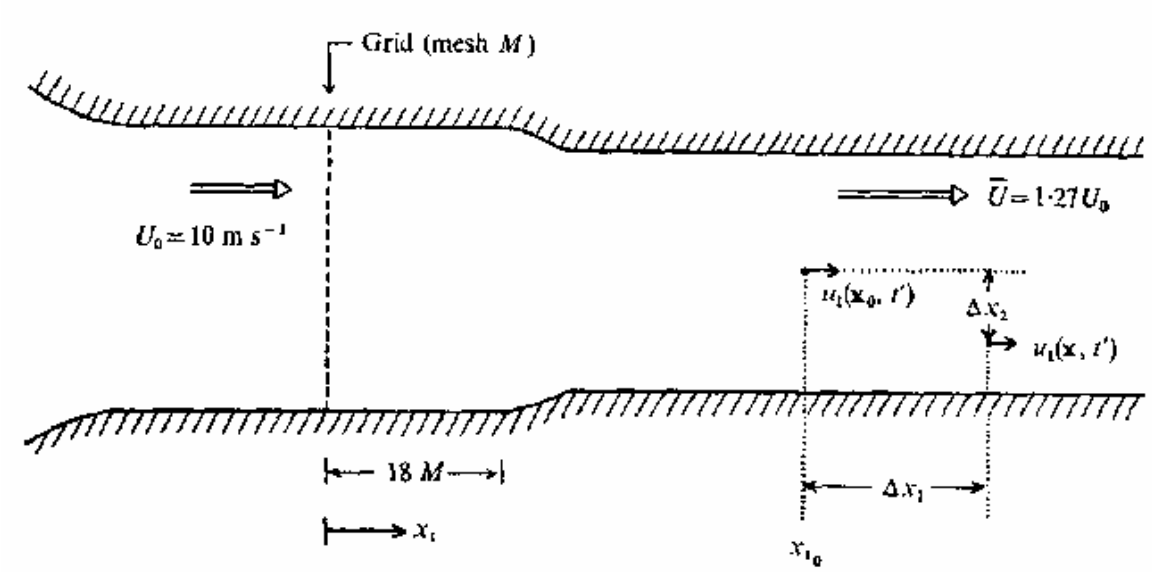

Figure 3.1: Qualitative sketch of upstream end of wind-tunnel test section. [12]

If $\bar{U}$ were exactly constant, t would be just proportional to downstream distance. The schematic sketch of the wind tunnel used in the CBC experiment is shown here. The u_1 energy spectra measured from single probe at U_0t/M=42, 98 and 171 are tabulated in the CBC paper [12]. They are measured as frequency spectra, but, since the relevant Taylor approximation is well satisfied, they are interpreted as 'one-dimensional' wave-number spectra, $E_{11}^{(1)}(k_1, t)$.

Under the assumption of isotropy, the 'three-dimensional' turbulent energy spectra $E(k\ , t)$ can be computed from the one-dimensional data as

$$E(k\ , t) = \frac{1}{2} k^3 \frac{\partial}{\partial k} \left\{ \frac{1}{k} \frac{\partial}{\partial k} E_{11}^{(1)} k_1, t) \right\}.$$

This expression is carried out by the graphical differentiation of faired curves.

The numerical data for three-dimensional spectra for 3-d grid is given in **Table 3.1.**

In **Table 3.1**, E(*k,t*) (defined as U_0t/M) cm^{2}sec^{-2} is the energy spectrum and *k* is the wave number.

The Kolmogorov wave-numbers, $k_K = \eta^{-1} = \left(\frac{\varepsilon}{\nu^3} \right)^{1/4}$ associated with the dissipative eddies, are 34, 21 and 15 cm^{-1} for stations $U_0t/M=42$, *98* and *171*, respectively. We observe that most of the dissipation occurs in scales a bit large than η.

The dissipation rate is obtained most accurately from the actual energy decay rate, as is the Taylor microscale:

$$\varepsilon = -\frac{3}{2}\overline{U}\,\frac{d\overline{u_1^2}}{dx_1}\,,$$

$$\lambda = \left\{\frac{10\nu\overline{u_1^2}}{\overline{U}\,\dfrac{d\overline{u_1^2}}{dx_1}}\right\} = \left(\frac{15\nu\overline{u_1^2}}{\varepsilon}\right)^{\frac{1}{2}},$$

$$R_\lambda = \sqrt{u_1^2}\,\lambda/\nu\ .$$

Table 3.1: Numerical data for three-dimensional spectra behind 2 in grid computed from 1-d spectra. [12]

***k* cm^{-1}**	***tU$_0$/M=42***	***tU$_0$/M=98***	***tU$_0$/M=171***
0.15	--	--	4.97×10^{1}
0.20	1.29×10^{2}	1.06×10^{2}	9.20×10^{1}
0.25	2.30×10^{2}	1.96×10^{2}	1.20×10^{2}
0.30	3.22×10^{2}	1.95×10^{2}	1.25×10^{2}
0.40	4.35×10^{2}	2.02×10^{2}	9.80×10^{1}
0.50	4.57×10^{2}	1.68×10^{2}	8.15×10^{1}
0.70	3.80×10^{2}	1.27×10^{2}	6.02×10^{1}
1.00	2.70×10^{2}	7.92×10^{1}	3.94×10^{1}
1.50	1.68×10^{2}	4.78×10^{1}	2.41×10^{1}
2.00	1.20×10^{2}	3.46×10^{1}	1.65×10^{1}
2.50	8.90×10^{1}	2.86×10^{1}	1.25×10^{1}
3.00	7.03×10^{1}	2.31×10^{1}	9.12×10^{0}
4.00	4.70×10^{1}	1.43×10^{1}	5.62×10^{0}
6.00	2.47×10^{1}	5.95×10^{0}	1.69×10^{0}
8.00	1.26×10^{1}	2.23×10^{0}	5.20×10^{-1}
10.00	7.42×10^{0}	9.00×10^{-1}	1.61×10^{-1}
12.50	3.96×10^{0}	3.63×10^{-1}	5.20×10^{-2}

15.00	2.33×10^{0}	1.62×10^{-1}	1.41×10^{-2}
17.50	1.34×10^{0}	6.60×10^{-2}	--
20.00	8.00×10^{-1}	3.30×10^{-2}	--

3.2.1.1. Results of CBC Experiment

The results were noted at three locations, $U_0t/M = 42$, *98* and *171*. These results are shown below. We shall perform our simulations using the initial conditions of the 2 inch mesh (or 5.08 cm) grid used by CBC in their experiment.

In the Figure 3.2, there are three different curves representing the energy spectrum at each of these time stages. $U_0t/M=42$ is the initial time or at physical time equal to zero at which we construct the initial conditions. This is shown as the *circular* symbols. Then we see the *triangular* symbols representing the energy spectrum at $U_0t/M=98$ and then we also look at the *square* symbols which represent the energy spectrum at the last recorded time stage or at $U_0t/M=171$.

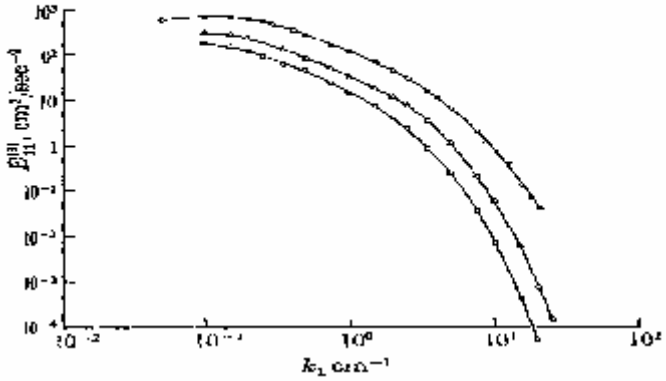

Figure 3.2: Downstream evolution of one-dimensional energy spectrum. $U_0=10ms^{-1}$, 5.08 cm grid, U_0t/M: circle-42 (topmost), triangle-98 (curve in between), square-171 (lowermost). [12]

Also, as seen from the above figure, the energy decays and hence as the time increases, the peak of the curve decreases evident from Figure 3.2. This trend is rather obvious but the exact shape of the curve and the recorded experimental results play an important role.

We shall use these standard experimental results obtained by Comte Bellot and Corrsin to compare our simulated results using LESTool.

The Figure 3.3 shown below is a representation of the energy spectra at the three different time stages as explained above, i.e., at $U_0t/M=42$, $U_0t/M=98$ and $U_0t/M=171$.

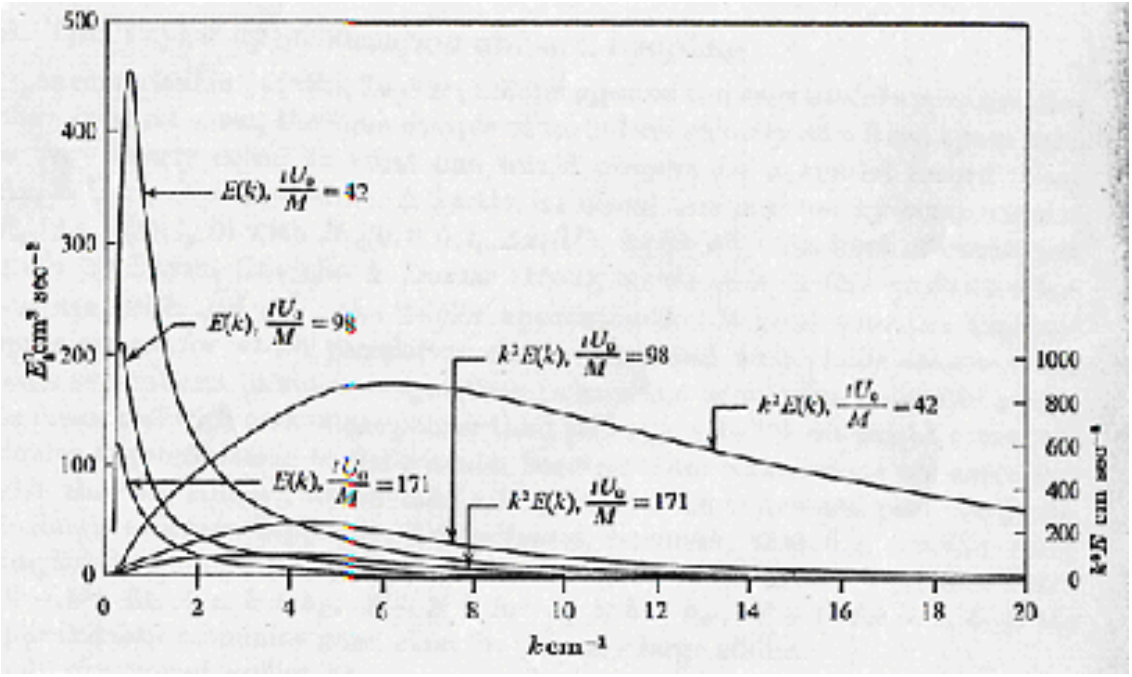

Figure 3.3: Downstream evolution of three-dimensional energy and dissipation spectra 5.08 cm grid. [12]

In fact, the figure above is a culmination of representations of energy spectra in two different scales, one is in the *linear scale* and the other is in the *log scale*. Also, it is a clear representation of understanding how the energy spectrum evolves in time. As seen in the Figure 3.3, the peaks of E(k) for tU_0/M=42, 98 and 171 have reducing heights in that order representing the dissipation of turbulent kinetic energy with time.

CBC Experiment Decay Curve

Another important investigation in the CBC case is analyzing the decay rate. The energy decay seen in Figure 3.4 is obtained by Comte Bellot and Corrsin in their experiment. This decay rate and the slope of the curve depend on various factors which we shall analyze and present in the results section in Chapter 5. We shall see how the

decay results will be affected by the initial conditions, more specifically the shape of the initial energy spectrum. Also the numerical dissipation and the grid sensitivity parameter C_{DES} which defines the artificial dissipation added to the DES model affect the shape of the decay curve. Only the standard experimental results are presented in this chapter. The experimental decay curve produced by Comte Bellot and Corrsin is shown in Figure 3.4.

The corresponding results obtained by computer simulation using LESTool will be shown in the following chapter and comparisons will be made with the experimental results.

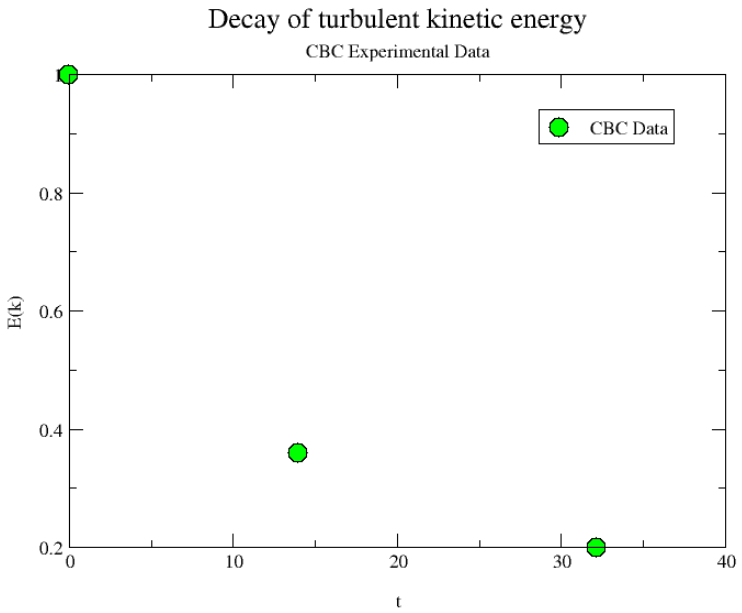

Figure 3.4: Decay curve points for the CBC Experiment. [12]

3.2.2. Blaisdell's Direct Numerical Simulation (DNS)

The Direct Numerical Simulations (DNS) of decaying isotropic turbulence are presented by Blaisdell *et al.* Simulations were performed at low initial rms Mach numbers (roughly M_0=0.05), moderate initial rms Mach numbers (M_0=0.3), and higher initial rms Mach numbers (M_0=0.7).

The first simulation run in their study was a repetition of the nearly incompressible decaying isotropic test case of Feiereisen *et al.* For this test, an initial program was written to produce initial turbulent fields in the same manner as Feierensen. Feireisen's initial conditions consist of a uniform density field, a random solenoidal velocity field

with a specified velocity spectrum, and a pressure field obtained by solving a Poisson equation. The initial turbulent Mach number used by Blaisdell *et al.* was M_0 ~0.06. The initial spectrum is a tophat energy spectrum with energy between wavenumbers k_0=8 and k_0=16. (The low value of the spectrum at the right end occurs because the energy containing range is $8 \le k \le 16$.) The computational Reynolds number was Re = 3640, which gave a turbulent Reynolds number $\mathrm{Re}_T = \overline{\left(\rho u_i'' u_i''\right)}^2 / \varepsilon\tilde{\mu} = 319$ and a Taylor microscale Reynolds number $\mathrm{Re}_{\lambda_{11}} = \bar{\rho} q \lambda_{11} / \tilde{\mu} = 40$.

The first test case run was using a 64^3 grid. Blaisdell *et al.* designated this test a label ia64f. The calculations were carried out to t=7.0 and the initial eddy turn-over time defined by $\tau = \bar{\rho}\bar{k} / \varepsilon$ was 12.3. Figure 3.6 shows the three-dimensional velocity spectra at t=7.0. This spectra is defined as

$$E(k) = \iint \hat{u}_i'' u_i''^{\otimes} dA(k)$$

Here $\otimes$ denotes a complex conjugate and the integrals are taken over spherical shells of radius k.

The test case was rerun using a 96^3 grid. Blaisdell *et al.* called this new simulation ia96f. This velocity spectrum at t=7.0 can be seen in Figure 3.7. With the finer mesh the enstrophy spectrum is adequately resolved. The calculations are continued to t=12.0 which is approximately one initial eddy turn-over time. The velocity spectrum at t=12.0 develops from the tophat spectrum of Figure 3.5 into a spectrum of low Reynolds number turbulence. Note that there is on inertial subrange, which would be indicated by an extended region with $E(k) \sim k^{-5/3}$. The presence of an inertial subrange requires a separation between the length scales of the energy containing eddies and the dissipative eddies. Since the range of the length scales increases with Reynolds number, the number of grid points needed to resolve the range of length scales for such a simulation is prohibitive, and hence Blaisdell *et al.* limit their simulations to low Reynolds numbers.

The Blaisdell's DNS initial spectrum shown in Figure 3.5 is

1. A top hat spectrum with energy in the wave number band $8 \le k \le 16$
2. $E(k) \sim k^4 e^{-2(k/k_0)^2}$ with k_0=6

The initial temperature and pressure fluctuations obtained by solving a Poisson equation for the pressure following Feireisen (1981).

The results corresponding to cases ia64f and ia96f in Blaisdell *et al.*'s study will be used for judging our results.

The initial 3-d energy spectrum, E(k) used in Blaisdell's DNS Simulation [10], for simulation for the 64^3 grid is shown in Figure 3.5. The initial parameters for the isotropic simulations are given in Table 3.2.

Table 3.2: The initial parameters for the isotropic simulations [12]

Case	**Ia96f**
Grid	96^3
$E_0(k)$	1
$\left(\overline{\rho'\rho'}\right)_0^{1/2}$	0.0
χ_0	0.0
M_0	0.06
Re	3640
M_{rms_0}	0.0598
Re_{T_0}	318.7
t_f / τ_0	1.0

3.2.2.1. Blaisdell's DNS Simulation Curves

Shown below are the simulations of Blaisdell *et al.* First the initial top hat energy spectrum is shown in Figure 3.5. Later the figures corresponding to 64^3 and 96^3 grid are shown at time, t=7 seconds.

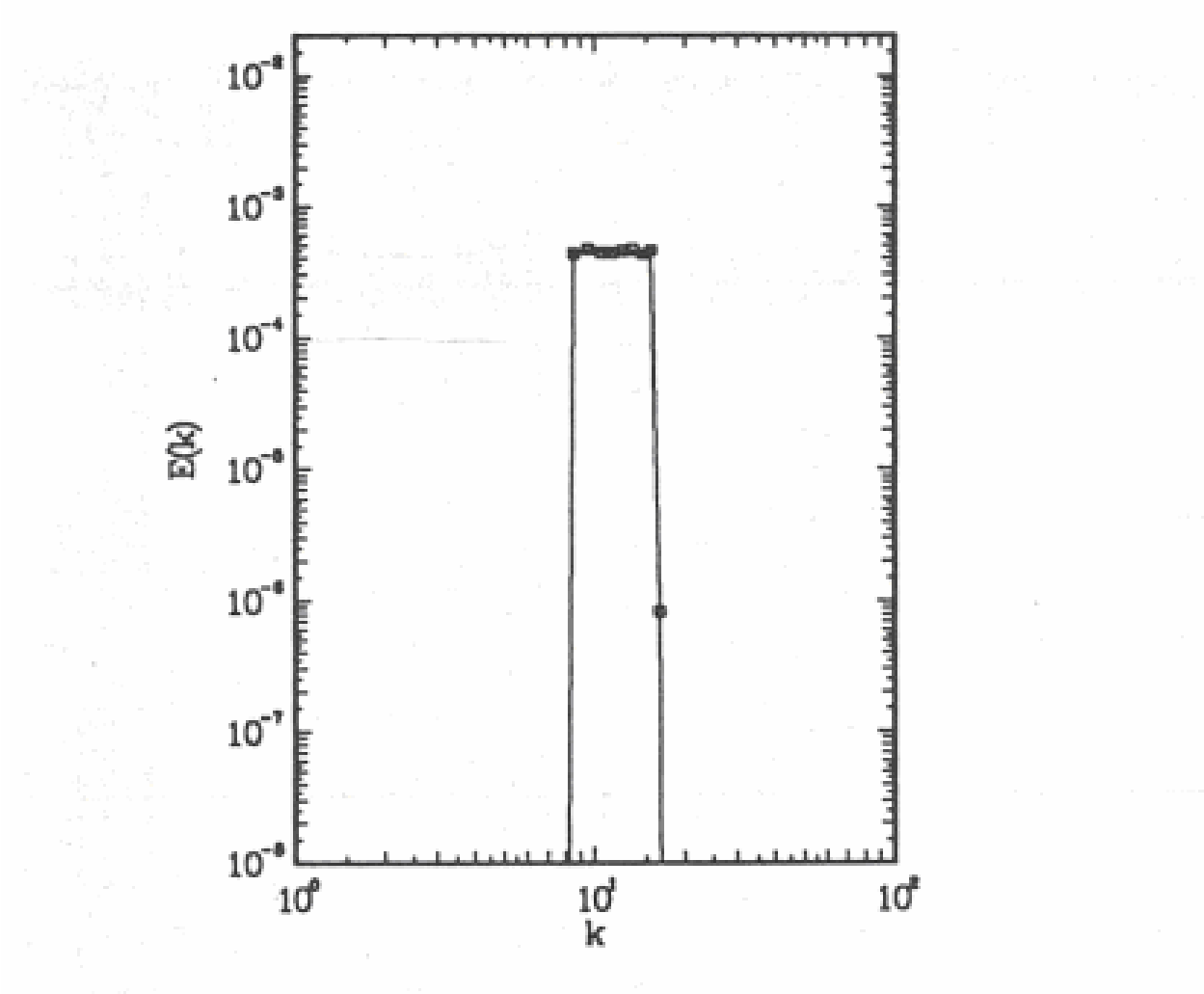

Figure 3.5: Blaisdell et al.'s (1991) Initial 3-d Energy Spectrum, E(k) used in their DNS simulation for ia64f. A similar tophat spectrum shape is used for most of the simulations.

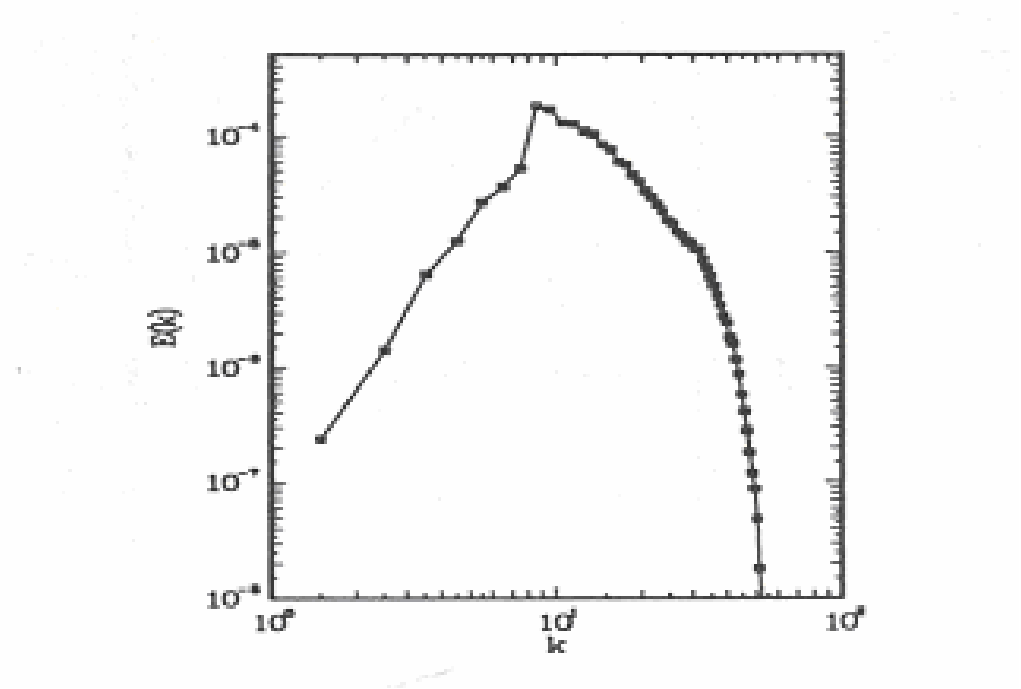

Figure 3.6: 3-d velocity spectrum, E(k) for ia64f at t=7, 64^3 grid. [10]

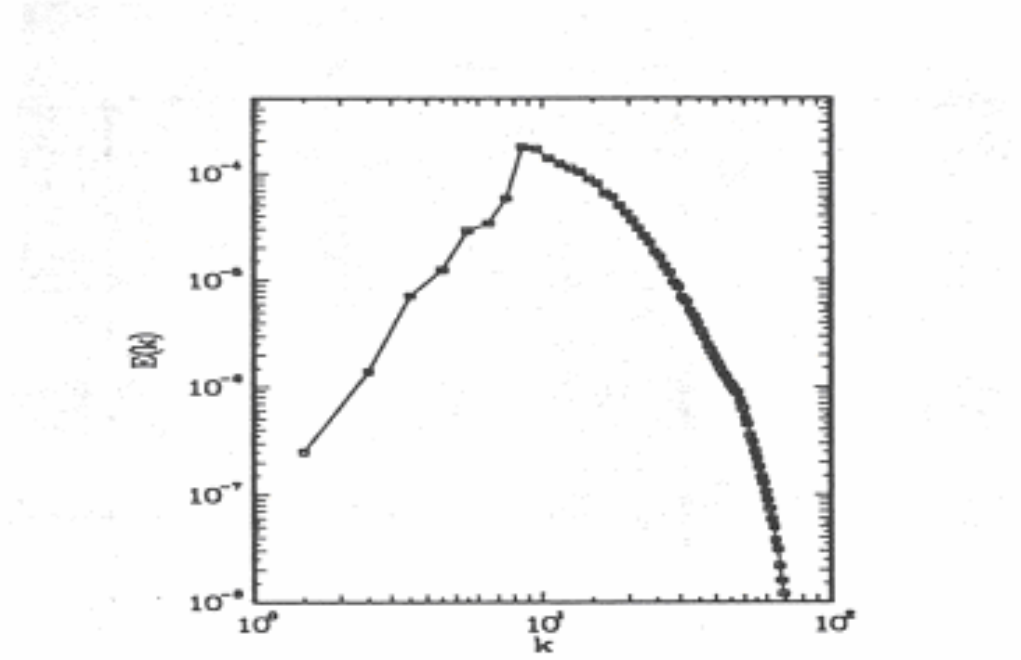

Figure 3.7: 3-d velocity spectrum, E(k), for ia96f at t=7, 96^3 grid. [10]

These results shown in the previous sections obtained from CBC experiment [12] and Blaisdell's DNS simulation [10] will become the basis of comparison for all our numerical simulations and results that follow.

With reference to the CBC case, there have been some simulations performed by other researchers available in the literature. These results are seen in the sections below.

3.3.1. Knight et al.'s Results

The decaying turbulence was simulated by Knight *et al.* considering the fluid to be inside the cube of length L_c with periodic boundary conditions on all surfaces, provided that the length L_c is large compared to the turbulence length scales. The cube dimension was taken to be L_c=43.787 cm which represents the zero-intercept of the polynomial fit (Figure 5.11) of the energy spectrum E(k).

For $42 \leq U_o t_{cbc}/\mathrm{M} \leq 171$, the cube length L_c is significantly larger than both the experimental velocity integral length scale L_v given by

$$L_v = 0.048M\left(\frac{U_0 t_{cbc}}{M} - 3.5\right)^{0.4}$$

and wavelength L_m corresponding to the peak in the energy spectrum E(k) as indicated in table below.

Table 3.33: Ratio of Length Scales [6]

$U_o t_{CBC}/M$	T	L_c/L_v	L_c/L_m
42	0	41.7	3.48
98	139.6	29.2	2.79
171	321.6	23.2	2.09

where

L_c = Length of cube

L_m = Experimental wavelength for peak in E(k)

L_v = Experimental velocity integral length scale

M = grid mesh spacing in experiment (5.08 cm)

t_{CBC} = Dimensional time in experiment

t = Dimensional time in computation
(non-dimensionalized by L/U_∞)

Some of Knight *et al.*'s results which will be useful in comparing to our simulations are listed below:

1) Decay of filtered turbulent K.E for Grid 1 (32^3)

2) Decay of filtered turbulent K.E for Grid 2 (64^3)

3) Turbulence energy spectrum at $U_o t/M = 98$ for Grid 1(32^3)

4) Turbulence energy spectrum at $U_o t/M = 171$ for Grid 1(32^3)

5) Turbulence energy spectrum at $U_o t/M = 98$ for Grid 1 (32^3) and Grid 2 (64^3)

6) Turbulence energy spectrum at $U_o t/M = 171$ for Grids 1 and 2.

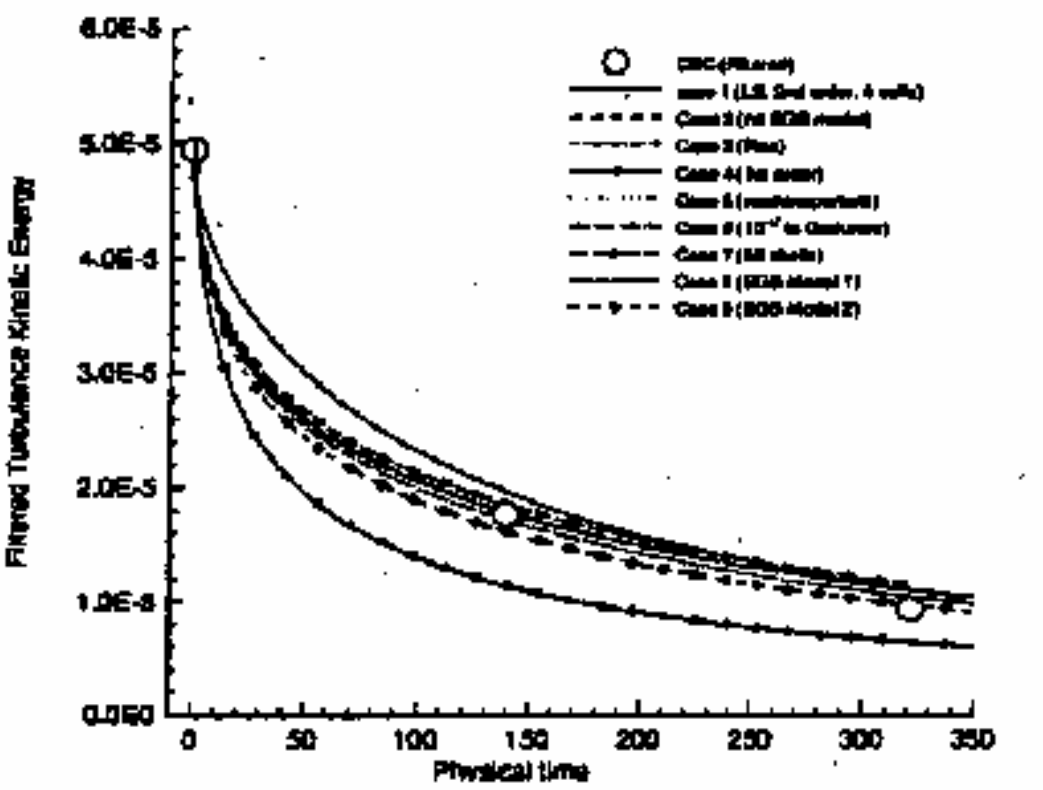

Figure 3.8 a: Decay of filtered turbulent kinetic energy for Grid 1 (32^3 grid). CBC experimental data is shown in circular symbols. [6]

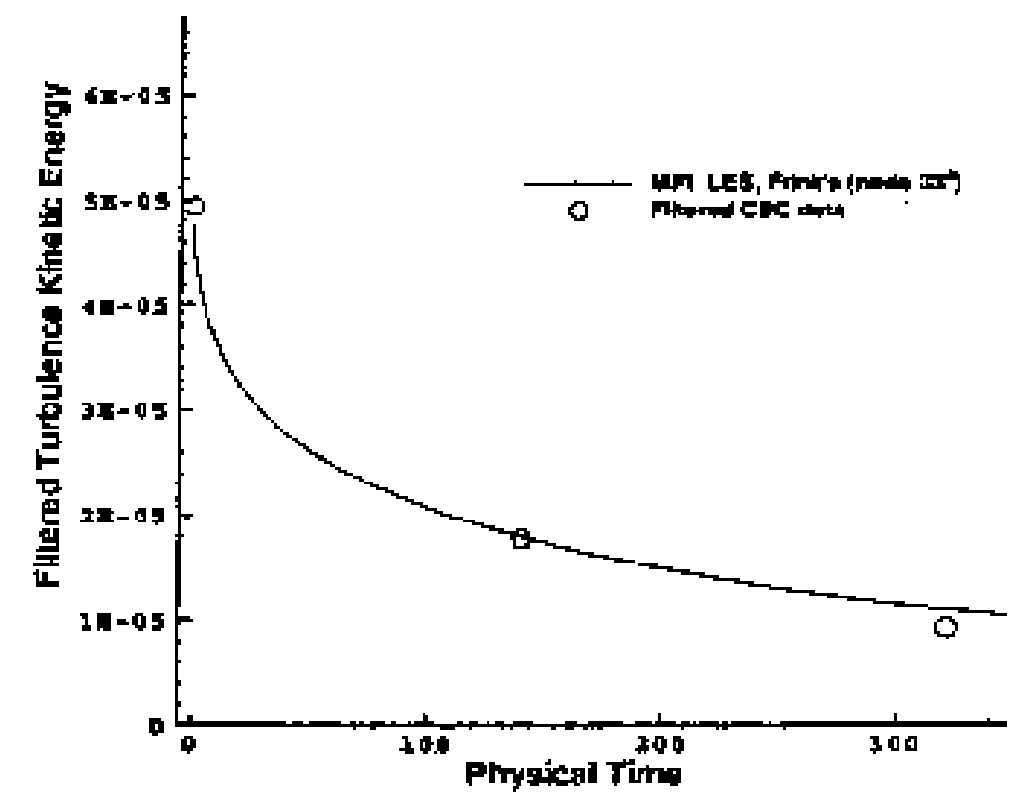

Figure 3.8 b: Decay of filtered turbulent kinetic energy for Grid 1 (33^3 grid). [6]

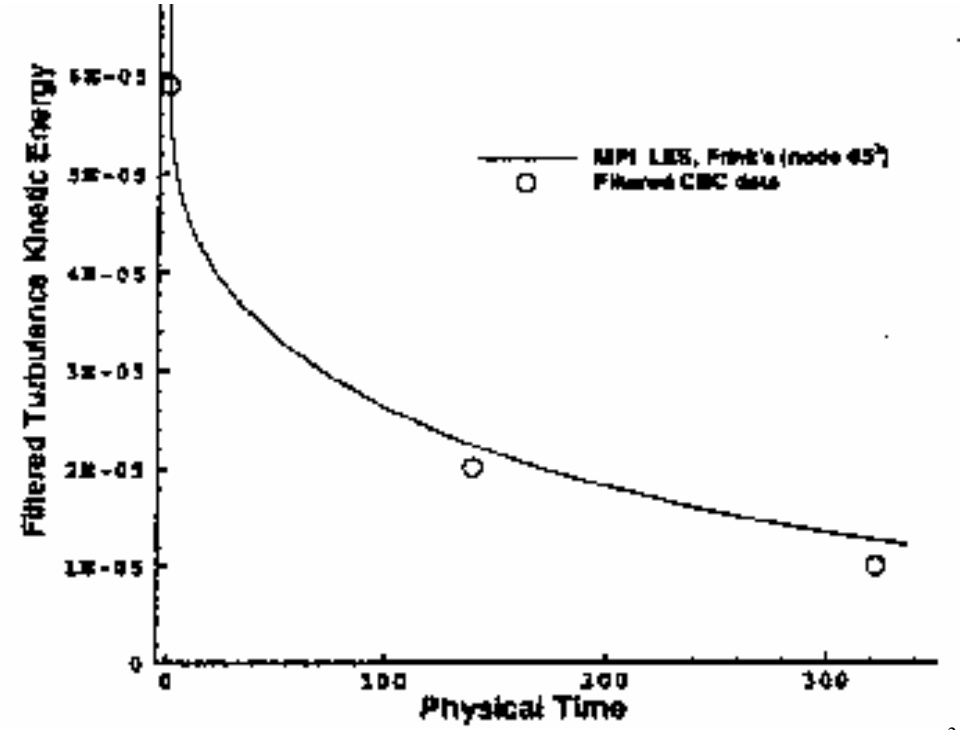

Figure 3.9: Decay of filtered turbulent kinetic energy for Grid 2 (65^3 grid). [6]

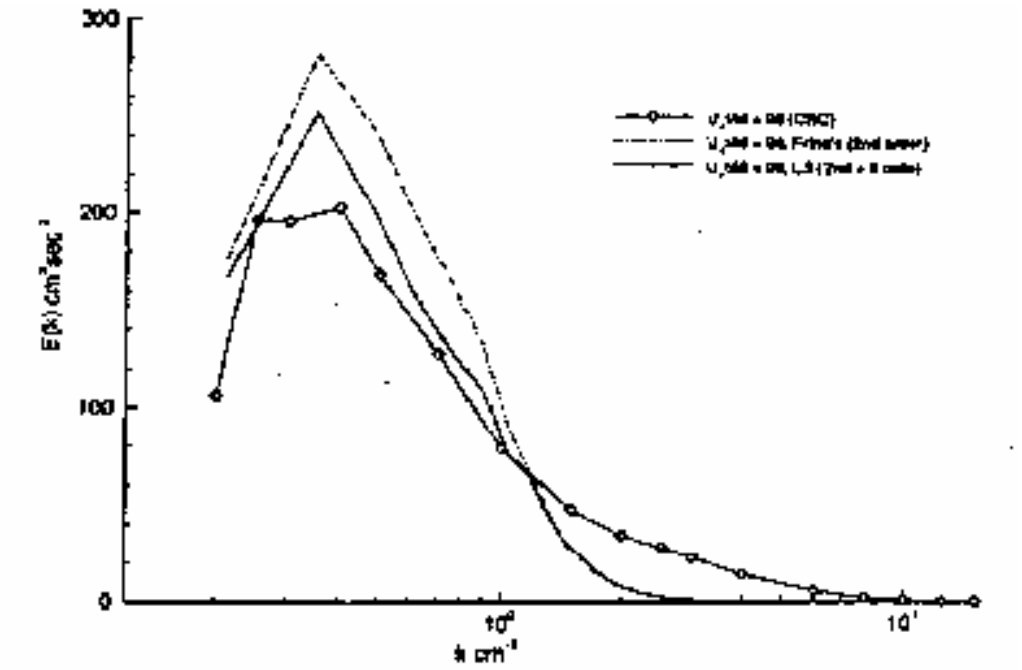

Figure 3.10 a: Turbulent energy spectrum, E(k) at *Ut/M*=98 for Grid 1 (33^3 grid). [6]

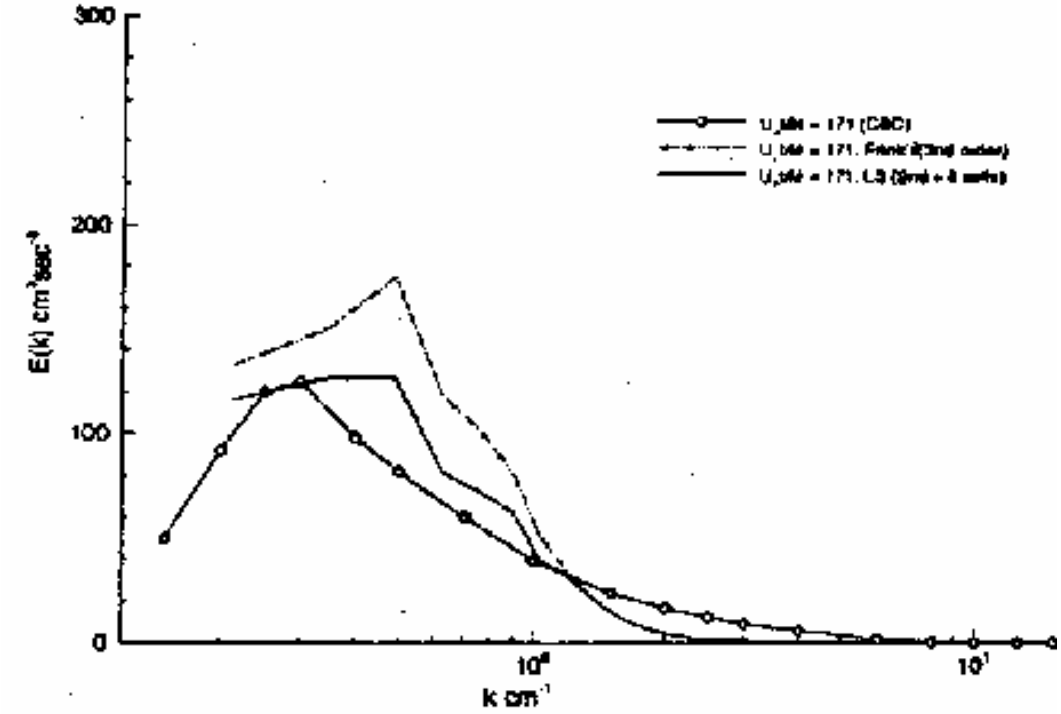

Figure 3.10 b: Turbulent energy spectrum, E(k) at *Ut/M*=171 for Grid 1 (33^3 grid). [6]

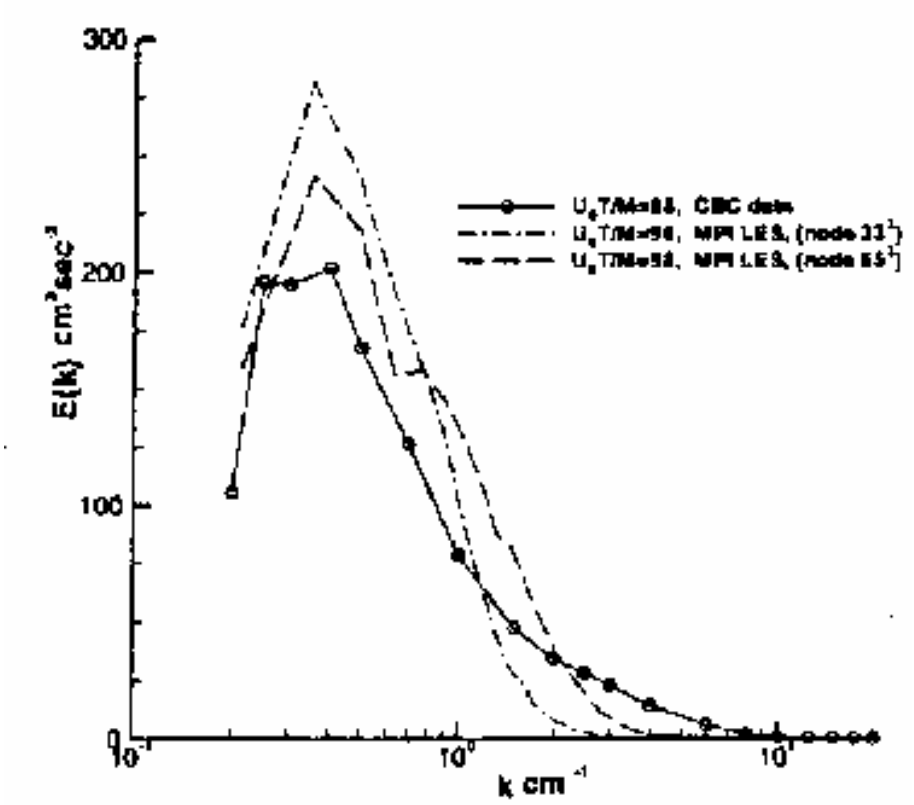

Figure 3.11 a: Turbulent energy spectrum, E(k) at *Ut/M*=98 for Grid 1 and 2. [6]

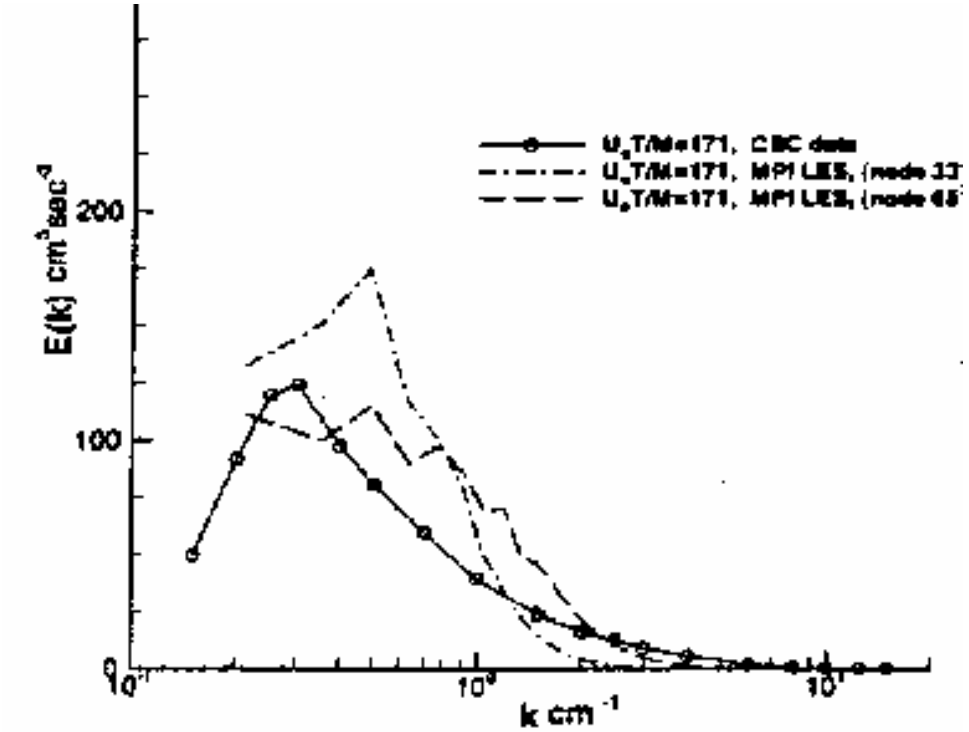

Figure 3.11 b: Turbulent energy spectrum, E(k) at *Ut/M=171* for Grid 1 and 2. [6]

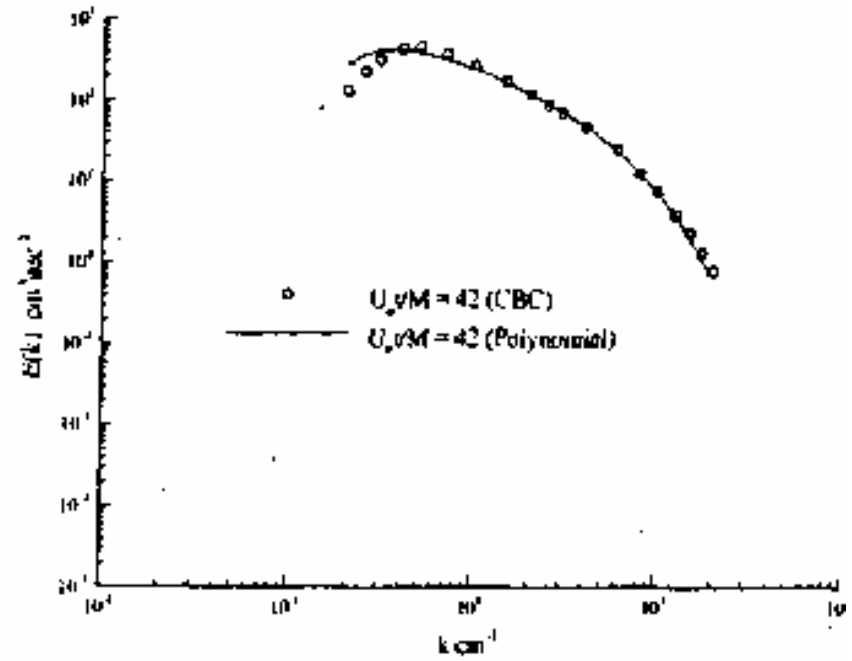

Figure 3.12: Experimental data (circular symbols) of Comte-Bellot and Corrsin for E(k) *Ut/M*=42 and polynomial interpolation (solid curve) at initial non-dimensional time. [6]

3.3.2. Strelets et al.'s Results

Figures 3.13 and 3.14 show the results of Strelets *et al.* [22] at non-dimensional times *Ut/M*=98 and *Ut/M*=171.

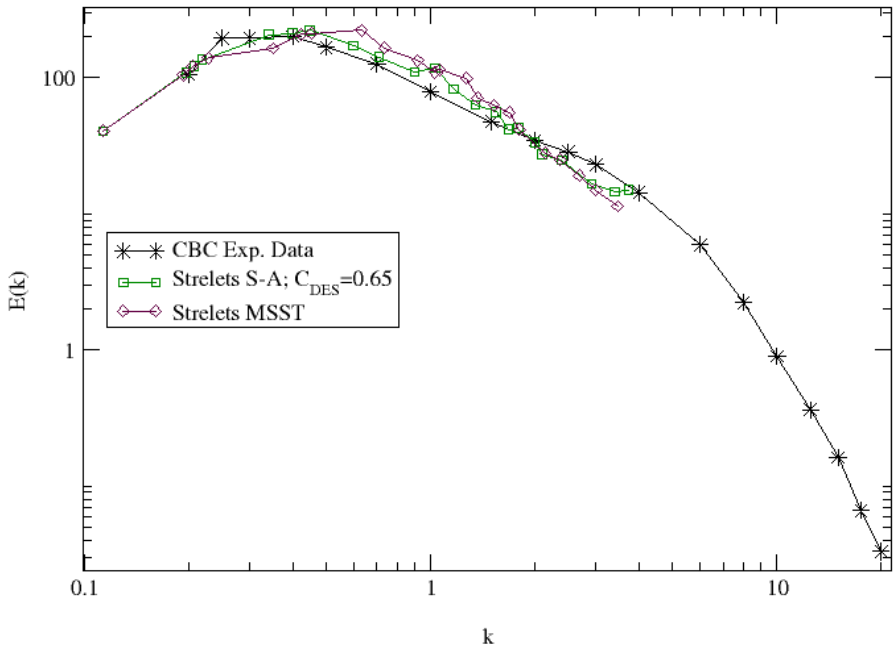

Figure 3.13: Energy Spectrum produced by Strelets *et al.* [22] at non-dimensional time *Ut/M*=98 for 64^3 grid.

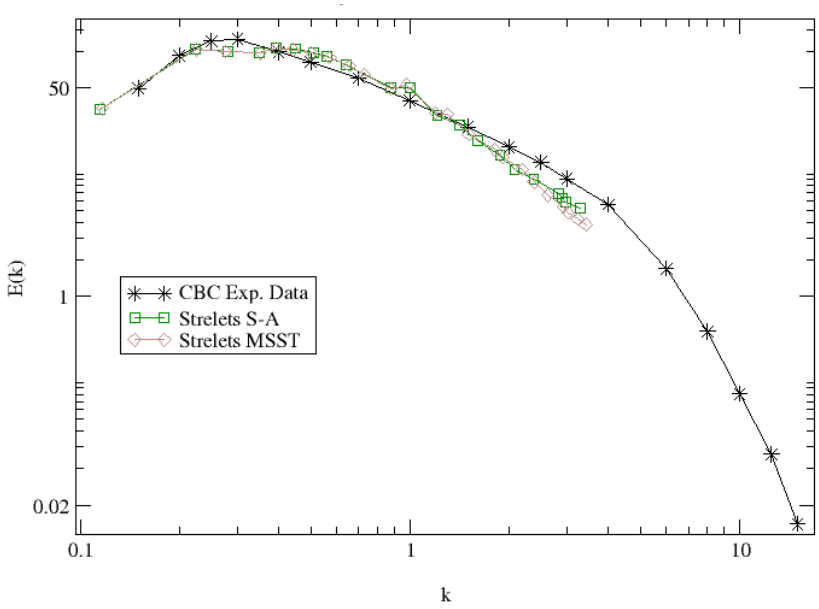

Figure 3.14: Energy Spectrum produced by Strelets *et al.* [22] at non-dimensional time Ut/M=171 for 64^3 grid.

Apart from the standard results shown in section 3.2, we shall also compare our results shown in section 3.3.1 and 3.3.2.

Chapter Four

Computer Simulation Setup and Background

4.1. Initial Conditions

In the previous chapter, we have examined the initial conditions of the Comte Bellot and Corrsin's case and the Blaisdell's case. The discussion of the creation of initial conditions is explained in the code 'Crecomp'. Appendix A provides details about the processes involved in generating initial conditions using Crecomp, but this chapter will discuss some aspects of the process.

Initial conditions form the starting point for any simulation. For unsteady problems, initial conditions dictate how the flow behaves eventually. So the solution obtained at any point of time is a function of initial conditions unlike steady state problems. Erratic initial conditions will reflect their discrepancy in the due course. Hence it is necessary and important that the initial conditions are setup with proper care.

Based on the specifications of test case, the data is fed to LESTool using the input file called 'homo.inp'. The required parameters for this input file can be seen in section 4.3.3.1. The initial energy spectrum and the grid for the simulation of homogeneous turbulence experiment is created using Crecomp. These input files are then given as input to LESTool along with homo.inp. While setting up the simulation run, we can prescribe for how long we would like to run the simulation. Also we can prescribe on how many processors we would like the code to be run. The scheme to be used and the numerical dissipation to be allowed are prescribed in LESTool code. After setting up the initial conditions right and starting the simulation, we collect the obtained output data files and then perform post-processing to study the details. Obviously, the run time would be proportional to the size of the grid and the amount of physical time we would want the initial conditions to be developed. Before setting up the run, we would also decide whether we would want to use the No Model or DES model. If we use the DES model, we would prescribe the required C_{DES} value in the input file.

4.1.1. Blaisdell's Initial Conditions

The initial conditions generated using Crecomp are used as the input for LESTool, the code which solves the turbulence equations. The velocity fields needed for LESTool are given by Crecomp in such a way that irrespective of the grid density, the energy spectrum produced has the same energy for all the initial spectra. The rms velocities are taken as the input decides the total energy under the curve. This energy is divided across the range of wavelengths available. Since the maximum wave number (k_{max}) in the case of 32^3 is 17 and is much smaller than in the case of a 96^3 grid where the k_{max}=49. But since the total energy has to be conserved, the peak of the lower density grid is seen to be located higher than the denser grid to accommodate for the excess energy which would be distributed across high wave numbers for the denser grids. The shape of the initial spectrum curve is a top-hat energy spectrum in the case of the Blaisdell's case and the shape in the case of CBC's initial spectrum is given by the experimental data provided by Comte Bellot and Corrsin. The initial condition in the Blaisdell's case has the following characteristics. It has a zero-mean with periodic random velocity field. The divergence of velocity is zero. It has the shape of a Top-hat energy spectrum for the velocity field. The temperature and density are constant throughout the simulation. The RMS values are prescribed to the energy spectrum initially. The compressibility is zero. The shape of the energy spectrum is seen in Section 3.2.2.1.

4.1.2. Comte Bellot and Corrsin's (CBC) Initial Conditions:

For creating the initial conditions for the CBC case, the scheme explained by Knight *et al*. [6] is followed.

The experimental data of Comte-Bellot and Corrsin for the one-dimensional energy spectrum, E_{11} at U_0t/M=42 can be approximated by the logarithmic polynomial

$$\log_{10} E_{11} = a_0 + a_1 \log_{10} k + a_2 (\log_{10} k)^2 + a_3 (\log_{10} k)^3 + a_4 (\log_{10} k)^4$$

where E_{11} is in cm^3/sec^2 and k is in cm^{-1}. In isotropic turbulence, the energy spectrum E(k) can be obtained from E_{11} by

$$E(k) = \frac{1}{2} k^3 \frac{\partial}{\partial t}\left(\frac{1}{k}\frac{\partial E_{11}}{\partial k}\right)$$

This yields,

$$E(k) = E_{11}\left\{\begin{aligned}&\frac{1}{2}\left[\alpha_1 + 2\alpha_2 \log_e k + 3\alpha_3 (\log_e k)^2 + 4\alpha_4 (\log_e k)^3\right]^2 + \alpha_2 - \alpha_1 + (3\alpha_3 - 2\alpha_2)\log_e k \\ &+ (6\alpha_4 - 3\alpha_3)(\log_e k)^2 - 4\alpha_4 (\log_3 k)^3\end{aligned}\right\}$$

In the Figure 4.1 we see the polynomial fit for the 1-d energy spectra, E_{11}. The polynomial fit is done using simple mathematical curve fitting using the fourth order polynomial curve fitting. The experimental CBC data are taken as the points between which and beyond which interpolation and extrapolation is done to obtain the curve fit. The polynomial by obtained by Knight *et al*. [6] has the coefficients as indicated in Table 4.1.

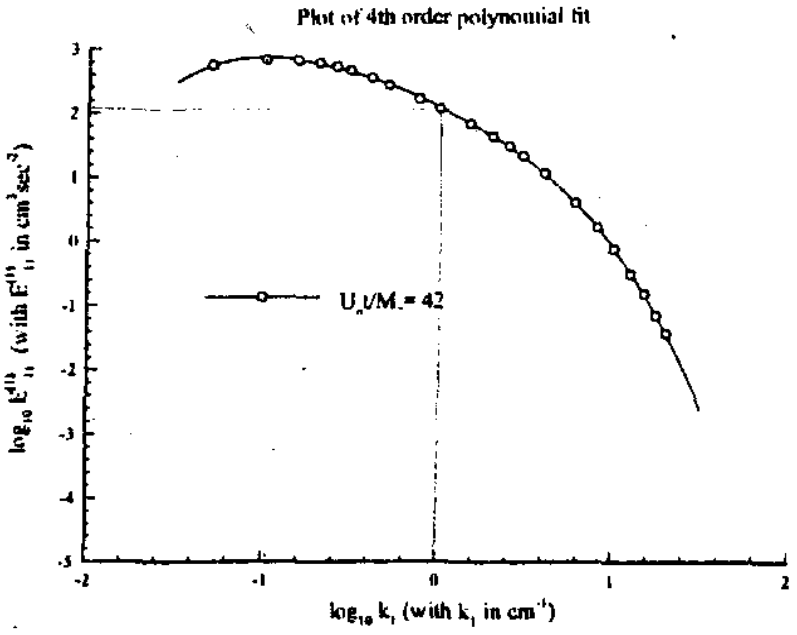

Figure 4.1: Experimental data of Comte-Bellot and Corrsin for $E_{11}(k)$ at $U_o t/M=42$ (circular symbols) and the polynomial fit produced by Knight. [6]

Table 4.1: Knight's coefficients for his logarithmic polynomial fit. [6]

Term	*Value*
α_0	4.7935398
α_1	-1.3284141
α_2	-0.2146974
α_3	-0.0314604
α_4	-0.0169870

4.1.3 More about initial conditions

Several attempts have been made to improve the initial conditions. Improving the initial conditions means generating initial profiles that are closer to the experimental initial conditions. Since the initial conditions could have an effect on the temporal evolution of the energy spectrum during the simulation, the closer the initial condition produced by LESTool is to the experimental initial condition [12] the better. The initial conditions are produced using Crecomp (Appendix A1). The initial spectrum, at t=0, is denoted as q.homo in this simulation of homogenous turbulence evolution.
Some of these cases are described below which aid in understanding the initial conditions obtained.

Figure 4.2 is a plot of all the attempts made to bring the obtained original initial condition curve (q.homo) closer to the CBC initial spectrum (with asterisk symbols). We shall make the idea conveyed in this graph clear by splitting up the idea in the plots that follow. The colors and symbols used will help identify the curves picked from this plot while discussing them separately.

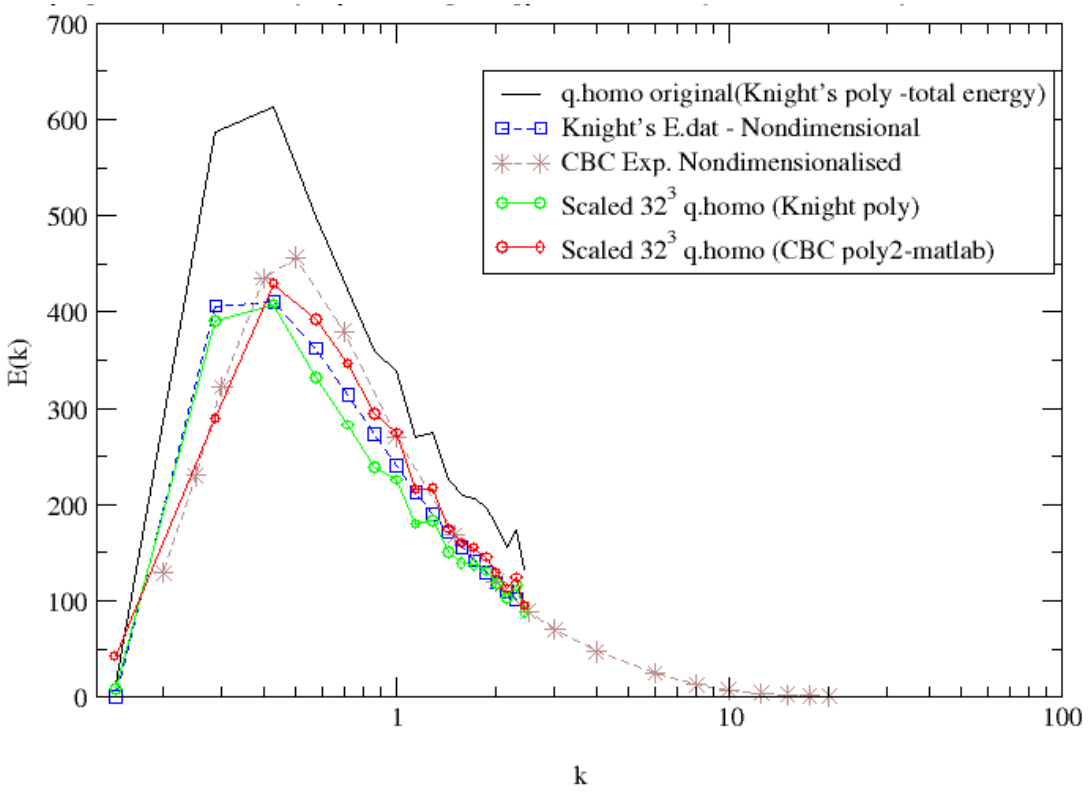

Figure 4.2: Initial curve produced by 'Crecomp' for 32^3 grid and the polynomial fit produced using matlab compared with Knight's Initial Energy Spectrum and CBC Data along with some scaled versions.

In the Figure 4.3 we see how Knight's non-dimensional energy spectrum compares to the CBC initial spectrum. As explained before the idea proposed by Knight will be implemented in our simulations but the idea has been modified to produce slightly better initial conditions as will be seen in the next plot. However both the energy spectra shown below in Figure 4.3 will be used for the purpose of comparison of our simulations for the CBC case.

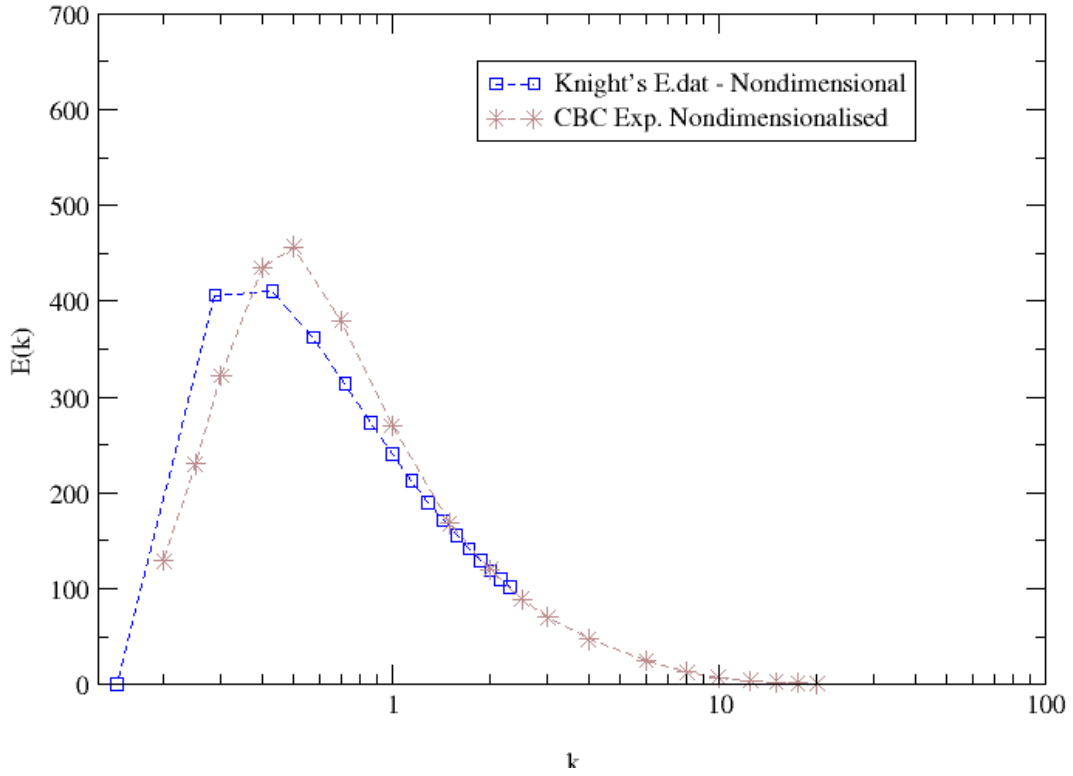

Figure 4.3: Knight's Initial Energy Spectrum compared with CBC Data at initial time, Ut/M=42.

In order to get better than what Knight has produced, we have used a linear curve fitting (will be seen in Figure 4.4) instead of a logarithmic curve fitting (Knight's idea). This gives us a better initial spectrum as shown below in Figure 4.4 (compared to Knight's energy spectra compared to CBC experimental data shown in Figure 4.3). This curve fitting is performed in matlab using a 4^{th} degree polynomial. The comparison of the linear curve fit (diamond shaped symbols) made with the standard CBC initial spectrum (asterisk symbols) is seen in Figure 4.4.

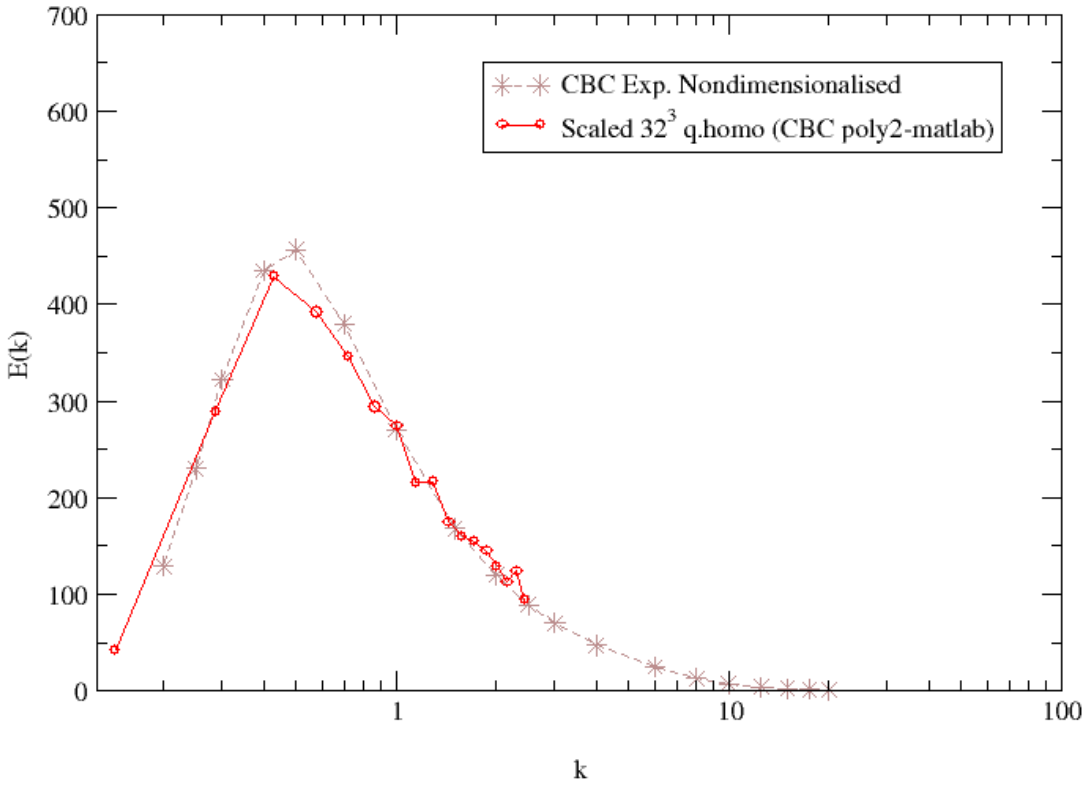

Figure 4.4: Initial Energy Spectrum produced using matlab compared with CBC Data at initial time *Ut/M*=42. This curve is also termed as 'polyfit', short for polynomial curve fit.

In the Figure 4.5 below, the same plot seen in Figure 4.4 is shown but now it is a log plot. We see that the comparison is very good matching the CBC data well indicating that the linear fit is a better match than the logarithmic fit approach of Knight. Later we shall see how this initial spectra will compare to the standard comparison cases after performing simulation using LESTool.

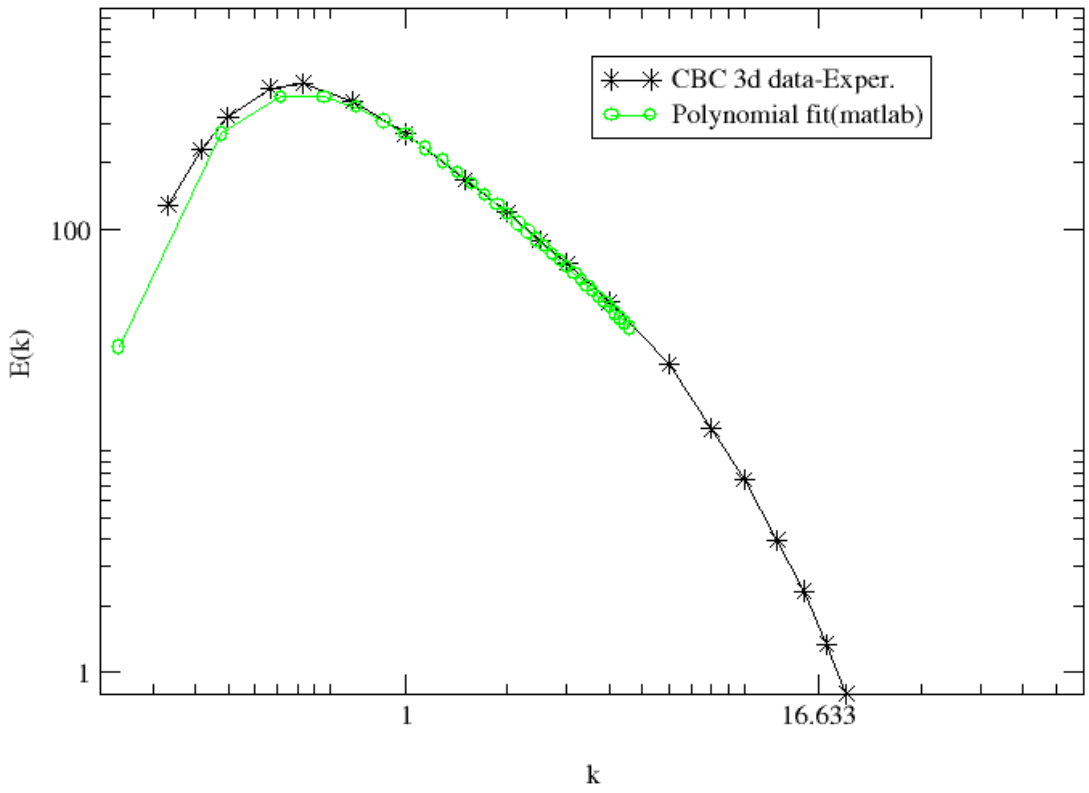

Figure 4.5: The logarithmic plot of the same polyfit, polynomial curve fit shown in Figure 4.4

At this point it becomes important to explain the concept of scaling. Whenever the initial conditions (q.homo) are produced using Crecomp, it is made sure that the energy spectrum contains the same amount of energy as the original energy spectrum or the experimental energy spectrum. But we know that the k_{max} or the maximum wave number used to plot the energy spectra decreases as the grid density decreases. The total number of values of k representing the energy spectrum in the case of 128^3 grid is 65, 49 in the case of 96^3 grid, 33 in the case of 64^3 grid and 17 values of k in the case of 32^3 grid. So, it is natural that if the k_{max} decreases as the grid density decreases, to accommodate for the decrease in the area under the curve of higher k value range in higher density grids, the lower density grid energy spectra has to be shifted up. This implies that the peak of the lower density grid will the highest of all among the initial spectra produced using Crecomp. The initial spectra shown below as the black curve is for the 32^3 grid shown without symbols produced using Crecomp. In order to match this curve with the experimental initial spectrum, we could scale the energy of this 32^3 spectra. The scaling factor would be nothing but the excess area under the experimental energy spectra (CBC curve) beyond k=17(in the linear scale) to the right of the curve in the case of 32^3 grid. In the Figure 4.6, we see how our initial curve (in black) looks after it is scaled (in green diamonds). It compares well with the Knight's initial spectrum (blue squares). Hence by scaling the curve, we can make the initial curve look much better in comparison. But would this affect the simulation is the question. As seen at the end in the latter part of the thesis, it does not affect much.

Thus after scaling we see that the produced scaled energy spectra (diamond symbols) is much closer to Knight's energy spectra (square symbols).

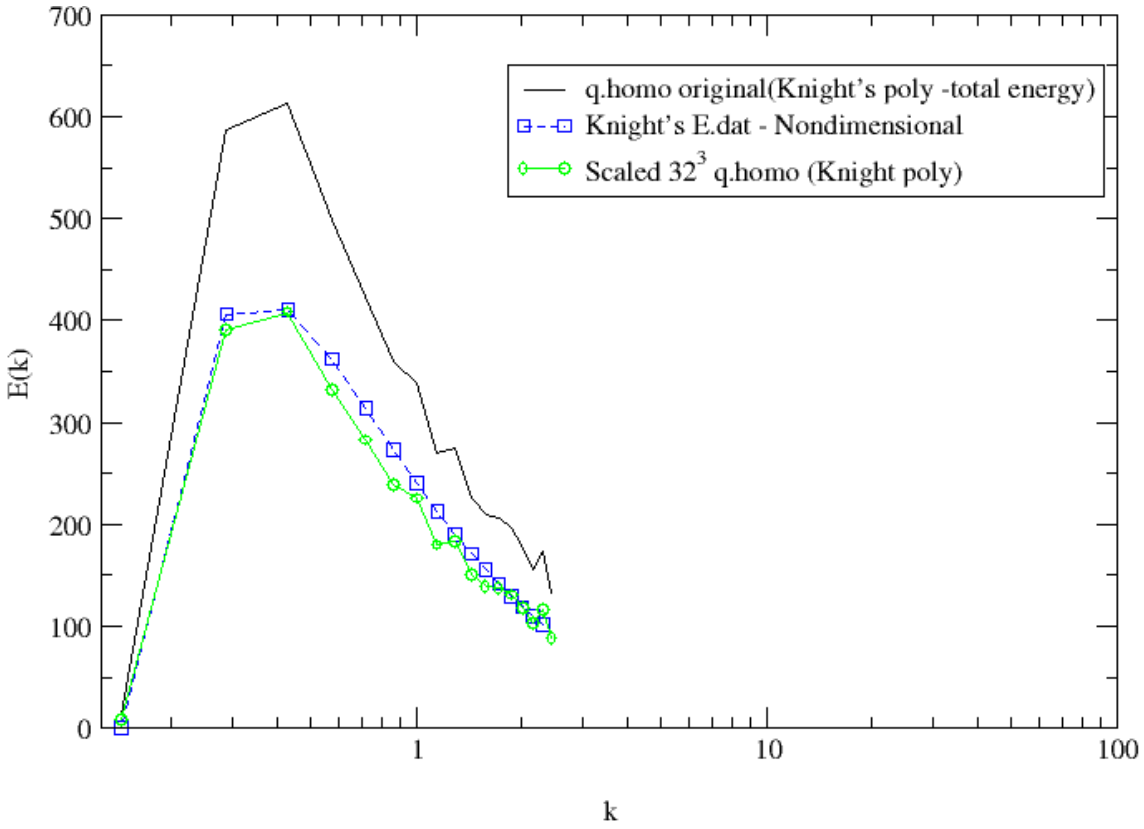

Figure 4.6: Our initial energy spectrum, 'q.homo' produced using 'Crecomp' is scaled and compared with Knight's Initial Energy Spectrum at initial time, *Ut/M*=42

In the Figure 4.7, we can see the initial condition produced using the idea suggested by Knight (same as seen in Figure 4.3) but produced by Crecomp. Here there is no scaling used. Hence our curve is much higher than the CBC curve. We perform most of our 32^3 grid simulations using the q.homo curve shown. The quality (slope of the curve) of the results after performing the simulations is not affected whether we scale the initial energy spectrum curve of not. There would only be a magnitude difference in the results produced which can be nullified by scaling the resultant curves appropriately using the scaling factor explained before without any loss of generality. The scaled version of the initial condition curve (q.homo) matches pretty well with Knight's spectrum (seen in Figure 4.6), especially when we take the higher density initial spectrum (say 96^3 grid-will be seen later). What is shown below is for the 32^3 grid. We shall see that as long as the energy spectrum slope matches the actual slope (CBC spectrum slope), the simulation should run fine. This means that both the scaled version and the non-scaled version of the initial energy spectrum will not have any difference in the energy

spectrum slope at t=7 after performing the simulation. We are mainly interested in comparing the slope of the energy spectrum after we evolve in time. Thus by scaling, we will be comparing the slopes of the curves without any interference of initial magnitudes under the energy spectrum. It is important to compare the shape of the energy spectrum rather than the overall magnitude of energy under the curve. Specially, the shape of the curve after the peak of the energy spectrum is what we would be comparing. So by scaling the curve, we can appropriately compare the slopes of the simulations with other simulations as well as the experiment.

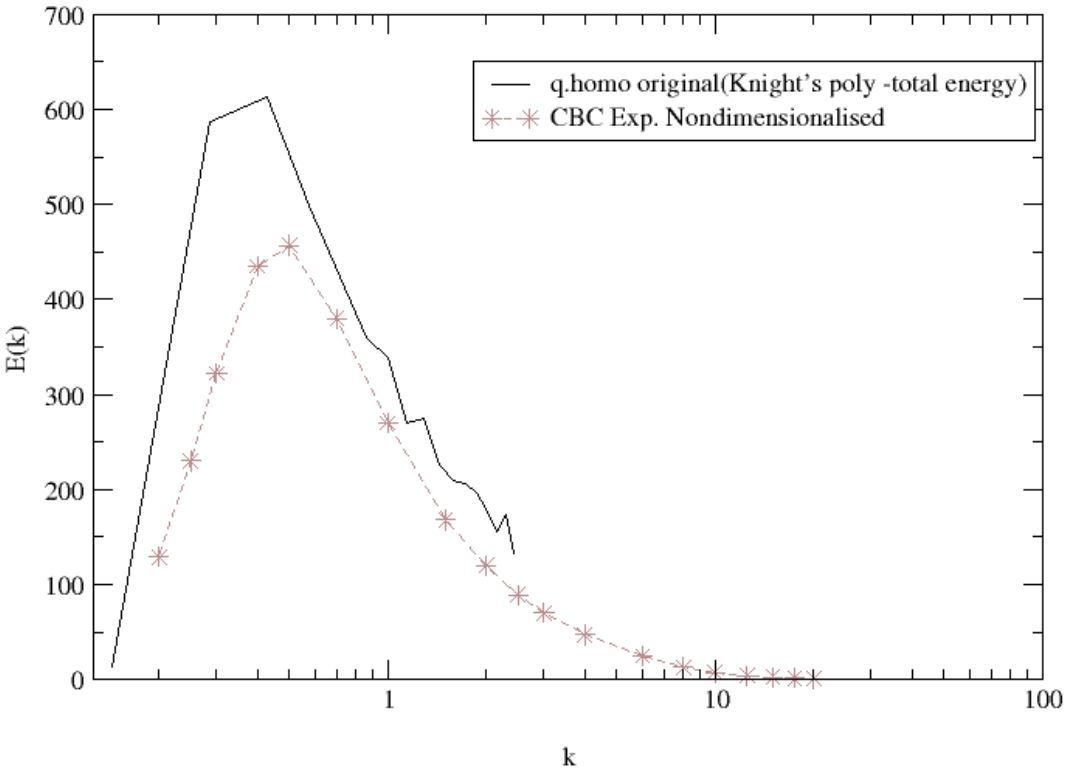

Figure 4.7: Our initial energy spectrum, 'q.homo' produced using 'Crecomp' is compared with Experimental CBC Initial Spectrum at initial time, *Ut/M*=42

Once we produce our initial energy spectra, we go ahead and run all our simulations. Apart from mainly using the above initial condition (q.homo) for simulations, we have also tested with a variation in initial conditions using the polynomial fit to see how our results vary. These simulation case can be seen later in the results section.

4.2. Parameters Setup

The input file detailed below is used to generate the initial conditions using Crecomp.

```
&statistic_nml iseed=12345678 /
&domain_nml ni=64, xbegin=0.0, xend=6.283185 /
&initial_nml
 r_mean=1.0, t_mean=1.0, u_mean=0.0, v_mean=0.0, w_mean=0.0,
 r_rms2=0.0, t_rms2=0.0, u_rms2=0.000040333, v_rms2=0.000040333, w_rms2=0.000040333,
 chi=0.0, spectrum_type=2/
&fluid_nml gamma=1.4, rgas=0.714285614286 /
!&exponent_spec al0=6.00 /
&topHat_spec  kstart=8, kend=16 /
```

4.2.1. Blaisdell's Case

Most of the parameters in the input file seen in section 4.2 are self explanatory though some more explanation will be given below. In the above input file, the spectrum_type=1 corresponds to the Blaisdell's case and spectrum_type=2 corresponds to the CBC case. Hence we would run the Crecomp.exe available from Crecomp with the corresponding parameter to obtain the desired initial spectrum.

4.2.2. CBC Case

Our cube length in LESTool is 2π hence our non-dimensional length scale is given by L= 2π . The two quantities which we would focus on non-dimensionalising in the input file 'homo.inp' are velocity, U and viscosity, mu_ini. From the CBC experiment, the viscosity, $\nu = 1.494117647 \times 10^{-5}\ m^2 sec^{-1}$. Also, the velocity is known to be $U = 10 msec^{-1}$.

4.2.2.1Explanation of the velocity parameters

$$M_t = 0.011 = \frac{\sqrt{u_{rms}^2 + v_{rms}^2 + w_{rms}^2}}{\hat{a}_\infty} = \frac{u_{rms}\sqrt{3}}{1.0}$$

Thus we have, $u_{rms}^2 = 4.0333 \times 10^{-5}$ $cm^2 sec^{-2}$. The turbulent mach number in this case is given by $M_t = 0.011$. The definition of Mach number gives us the root mean square velocity which can be used to define the energy spectrum in the input file for Crecomp. Since we deal with homogeneous turbulence, $u_{rms}^2 = v_{rms}^2 = w_{rms}^2$ as seen in the *cbc.inp* file [4.2].

4.2.3. LESTool Parameter study

This section focuses on two aspects:

1. Obtaining all the initial condition parameters to complete the input file, homo.inp.
2. Obtaining the initial condition file, q.homo using Knight's polynomial with details of non-dimensionalization.

A typical input file for LESTool is shown in Figure 4.8. Before we run our simulations, we have to input the data in the below input file correctly based on the case and criterion we choose. The critical parameters below are given an explanation.

4.2.3.1. The input file, homo.inp

```
&global_nml  rgas=0.714285714286, rho_ini=1.0, u_ini = 0.06, T_ini=1.0,
        mu_ini=0.000006268953951, dtime = 1.0e-3, rhs_method=1,
        restart=true restart_name='q.homo'/
&FlowEquationSet_nml SourceTerm=0, turbulenceModel=0/
&LES_model_nml tk_model=true, heat_flux_model=true /
&Smagorinsky_model_nml cr=0.012, ci=0.0066, SGS_Prandtl=0.4/
&DES_model_nml c_des=0.65/
&kepsilon_model_nml /
&grid_nml grid_name='Homo' /
&bc_input_nml bc_type=10, bc_dir=-1, start=-1, 1, 1, end=-1,-1,-1 /
&bc_input_nml bc_type=10, bc_dir= 1, start= 1, 1, 1, end= 1,-1,-1 /
&bc_input_nml bc_type=10,  bc_dir=-2, start= 1,-1, 1, end=-1,-1,-1 /
&bc_input_nml bc_type=10,  bc_dir= 2, start= 1, 1, 1, end=-1, 1,-1 /
&bc_input_nml bc_type=10, bc_dir=-3, start= 1, 1,-1, end=-1,-1,-1 /
&bc_input_nml bc_type=10, bc_dir= 3, start= 1, 1, 1, end=-1,-1, 1 /
&time_nml itime_max=12000, itime_out=50, method = 20 /
&modified_adi_nml inner_max=3, i_diagonal=false, j_diagonal=false,
                  k_diagonal=false /
&post_pro_nml nplot=250, output_format=1//
```

Figure 4.8: A typical example of input file, 'homo.inp' used in LESTool simulations

So the parameters that we would need to run any given case in the in the initial file homo.inp are rgas, rho_ini, u_ini, T_ini and mu_ini.

4.2.3.1. Parameter determination

- The parameter, 'rho_ini' is defined as 1.0.
- Also, T_ini is defined as 1.0.
- The parameter, 'rgas' is given by rgas = 1/γ as the sound speed is defined as 1.0 and T_ini is defined as 1.0 and the ratio of specific heats for air is γ = 1.4. Thus, rgas = 1/1.4 = 0.714285714286.
- The parameter, 'u_ini' is taken the way Knight *et al.* define it. Knight *et al.* define the speed of sound as 1/10 the regular speed of sound. So the turbulent Mach number,

  $$M_t = 10 * M_{CBC} = 0.011.$$

  Since, the speed of sound is defined as 1.0,

  $$u\_ini = 0.011$$

- The parameter, mu_ini is obtained as follows:

$$\mathrm{Re} = \frac{a_K(k_s^{-1})}{\nu_{CBC}} = \frac{a_{us}(L_{us})}{\nu_{us}}$$

$$\Rightarrow \frac{a_K(k_s^{-1})}{\nu_{CBC}} = \frac{(1)(1)}{\nu_{us}}$$

Thus we get the viscosity in the LESTool simulation as shown below.

$$\nu_{us} = \frac{\nu_{CBC}}{a_K(k_s^{-1})_K} = \frac{U_{CBC} M_{CBC}}{\mathrm{Re}_{CBC}\, a_K(k_s^{-1})_K}$$

$$= \frac{(10 ms^{-1})(5.08 \times 10^{-2} m)}{(34000)(34.2 ms^{-1})(6.96889 \times 10^{-2} m)}$$

$$= 6.268953951 \times 10^{-6} kgm^{-1}s^{-1}$$

where subscript 'us' refers to the simulation performed using LESTool, subscript 'CBC' refers to CBC experiment and subscript 'K' refers to Knight *et al.*'s simulation.

Thus the parameter for viscosity in the LESTool input file, mu_ini=0.000006268953951 is obtained.

4.3. Machine Configuration

To do a detailed analysis of homogeneous turbulence modeling using DES, efficient coding with a probable extension to MPI platform to enable multiprocessing for optimization of time, proper generation of initial conditions, and use of different grid densities and appropriate manipulation of DES parameters is necessary. Keeping this in mind the grid densities that are considered are 32^3, 64^3, 96^3 in the CBC case and 32^3, 64^3, 96^3 and 128^3 grid in the Blaisdell's case. The motive behind selecting these grid densities for each of the cases will be explained later. The numerical schemes that have been adopted are 5^{th} order upwind scheme and 6^{th} order central scheme. The code has been mainly run on UTA, 8 250 MHZ IP27 processors, MIPS R10000 Processor Chip, an IRIX based SGI machine. The 96^3 and higher grid cases have been run on the resources supplied by NCSA. Some computations have also been done on the LINUX Platform Clusters.

Typically, it takes about 60-65 hours to run the 64^3 No Model (MILES) case until time, t=12 on UTA, whereas the DES cases take about 35-40 hours more time. The 96^3 take a very large amount of time when run of UTA and hence the option of running those cases on UTA is ruled out. These cases have been run using the NCSA computing resources on the IRIX platform. Typically each case takes about week to finish. The 128^3 cases take very long time. These too have been run on the NCSA machines and took about a month to finish. Because of the amount of time that it takes, the 128^3 case has been restricted only to the No Model case. Also, the 96^3 case also has been restricted to the important cases, whereas the 64^3 cases have been run liberally.

4.4. LESTool

LESTool has been developed at University of Kentucky, Lexington. Originally built specifically for turbomachinery applications, LESTool has now been modified to apply to many different CFD simulations, including fields beyond aerospace and mechanical engineering. LESTool is designed to be a comprehensive platform, and is continuously adapted for new developments in turbulence-transition modeling, computational numerics, and computer science. The code is portable to most parallel

systems, based on standard FORTRAN90, OpenMP, and MPI. Complex engineering flows are simulated using high-order numerical schemes and Chimera overset grids to solve the time-depended, three-dimensional Navier-Stokes equations. LESTool has been optimized for SGI multi-platforms, leading to high floating-point performance and good scaling characteristics.

4.5. Post Processing

The post processing is done using ‘grace’. Grace is a WYSIWYG 2D plotting tool for the X Window System and Motif. Grace runs on practically any version of Unix-like OS. As well, it has been successfully ported to VMS, OS/2, and Win9*/NT/2000/XP (some minor functionality may be missing, though).

The application is mainly used to plot the energy spectrum curves and energy decay curves. It has many features including curve fitting, transformations, integration etc.

Chapter 5

Results

5.1. Introduction

In this section, we shall include all primary results that meet our objectives. As indicated earlier, the two test cases are the CBC case and Blaisdell's case. Hence this chapter is divided into two sections dealing with each of the test cases.

In exploring the behavior of Detached Eddy Simulation (DES) model, we shall specifically target the effects of

a. Reynolds number
b. Grid Density
c. Grid sensitivity parameter, C_{DES}

We shall also see the effect of numerical dissipation and the variation of the numerical scheme used. As listed, results of each of the two cases will follow.

5.2. CBC Case

5.2.1. Generation of Initial Conditions

Once the *cbc.inp* (section 4.2) input file for Crecomp (Appendix A) is given, the initial conditions at non-dimensional time Ut/M=42 can be generated. The initial conditions generated using Crecomp for the CBC case are shown in Figures 5.1, 5.2 and 5.3. These figures correspond to three cases with grid densities of 32^3, 64^3 and 96^3. These initial condition (also referred to as q.homo) curves are compared to Knight *et al.*'s initial condition (E.dat) in each of the plots. In addition, the areas under each of the curves, representing the total energy in each case, is presented. Knight *et al.*'s initial condition curve is produced by the logarithmic polynomial fit explained in Chapter 3. These Knight *et al.*'s polynomial fits curves are produced for each of the grid densities of 32^3, 64^3 and 96^3 with the largest wave number (k_{max}) equal to 17, 33 and 49 respectively. As explained previously, the initial condition q.homo produced by Crecomp tries to keep a constant amount of theoretical energy under the curve irrespective of k_{max}. This is because the rate of energy decay is a function of total energy and not the energy vs. *k* spectrum. So irrespective of the grid density, Crecomp make sure that the total energy under the energy spectrum is maintained. In this attempt, the greater the value of k_{max}, the more complete

is the representation of the energy and therefore the initial curve is closer is the curve to the experimental curve. Hence we see that as the grid density increases, q.homo matches more closely with Knight *et al.*'s curve (E.dat). Hence the difference between the quantitative areas under the curve in Figure5.3 is the least among the three figures considered.

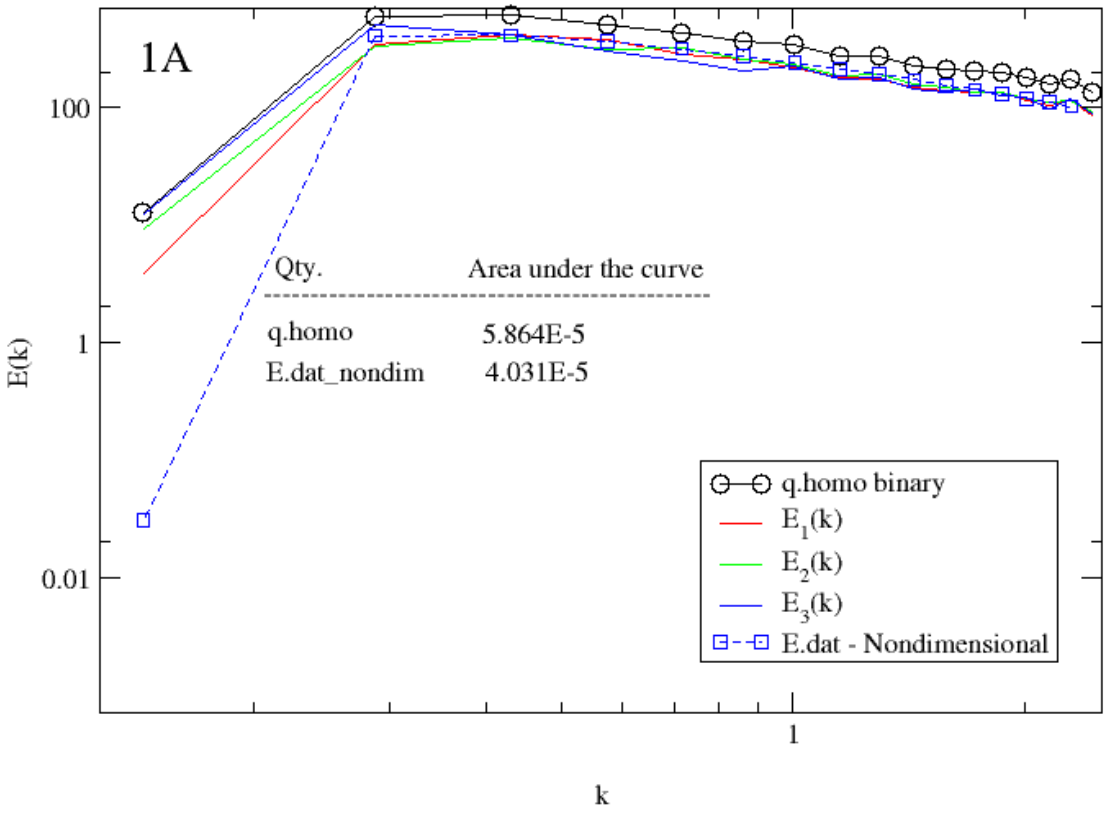

Figure 5.1: Energy Spectrum produced by 'Crecomp' for 32^3 grid at non-dimensional time *Ut/M*=42. Comparison shown with Knight *et al.*'s Initial Energy Spectrum

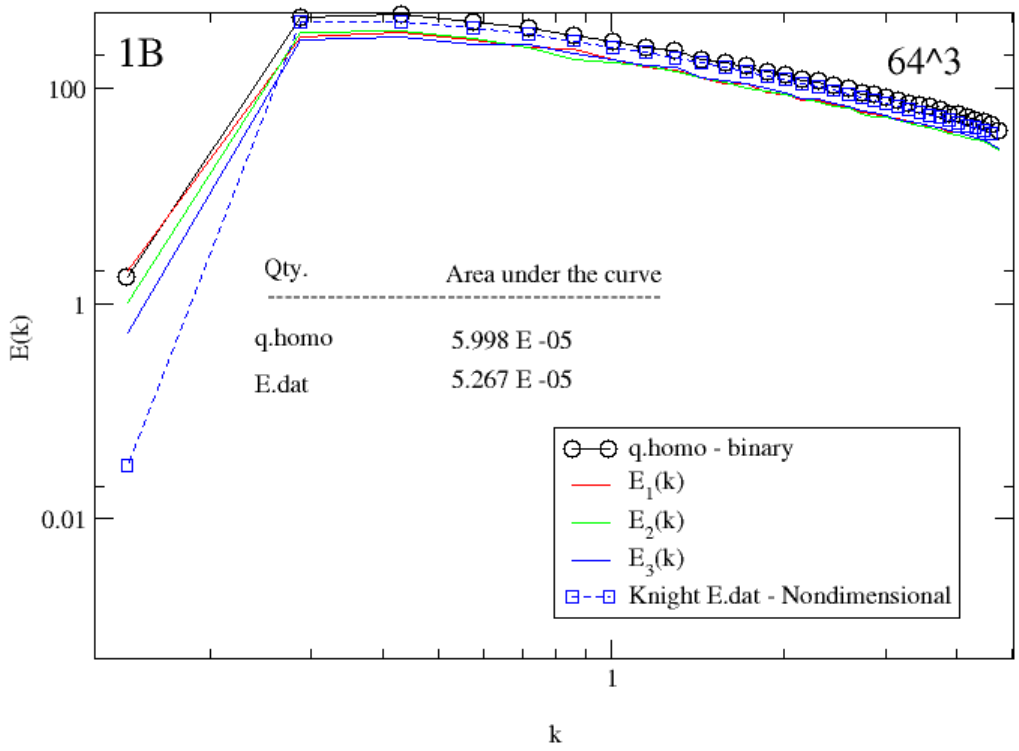

Figure 5.2: Energy Spectrum produced by Crecomp for 64^3 grid at non-dimensional time *Ut/M*=42. Comparison shown with Knight *et al.*'s Initial Energy Spectrum.

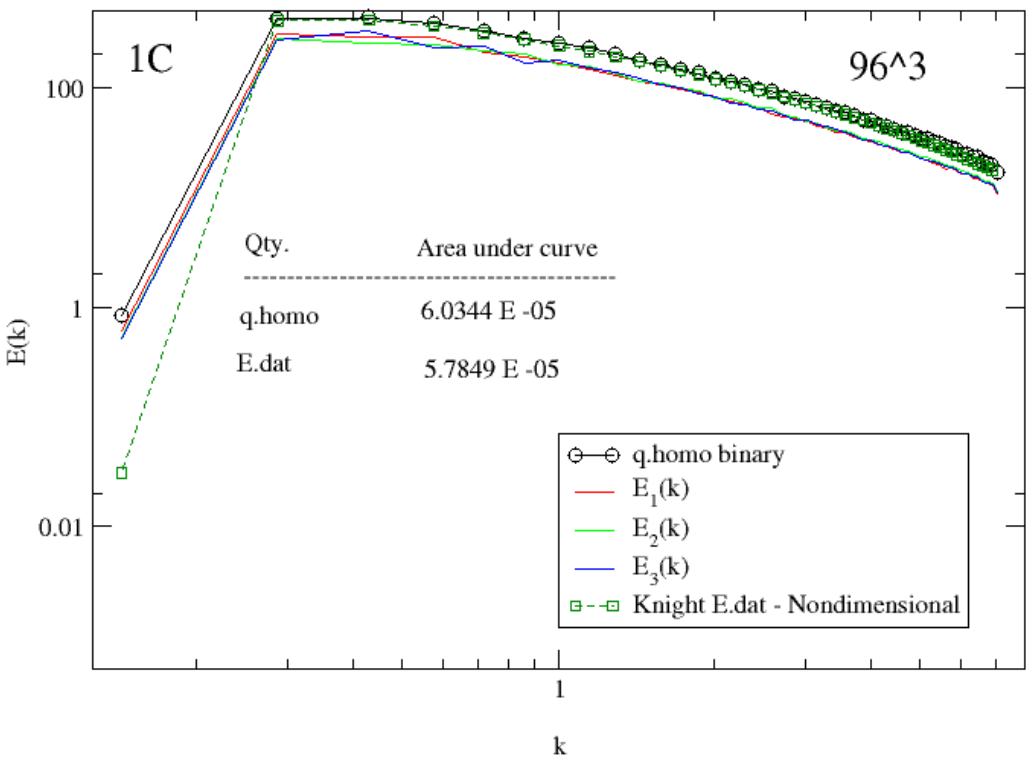

Figure 5.3: Energy Spectrum produced by Crecomp for 96^3 grid at non-dimensional time *Ut/M*=42. Comparison shown with Knight *et al.*'s Initial Energy Spectrum.

Figures 5.1, 5.2 and 5.3 each have four curves:

a. The initial condition curve (q.homo) using Crecomp
b. Components of q.homo – $E_1(k)$, $E_2(k)$ and $E_3(k)$
c. Knight *et al.*'s initial curve (E.dat) whose method we have incorporated in generating the initial conditions.

We can see that as the grid density increases from the 32^3 curve to the 96^3 curve (q.homo), the curve approaches Knight *et al.*'s initial condition and matches better. To produce the initial conditions curve (q.homo), the method proposed by Knight *et al.* (1998) has been used. A logarithmic polynomial fit through the experimental points of 3-d energy spectrum taken from CBC paper [12] has been used, and hence it makes sense that as the grid density is increased, the curve matches the Knight *et al.*'s initial spectrum better because we essentially follow the same approach suggested by Knight *et al.* while producing these initial conditions using Crecomp.

The energy under 'q.homo'(LESTool initial condition) produced by Crecomp is

5.864 x 10^{-5} m^2sec^{-2} for the 32^3 grid case from Figure 5.4 and the energy under Knight *et al.*'s polynomial curve (E.dat) is 4.031 x 10^{-5} m^2sec^{-2}. Similarly, these values of energies for the 64^3 and 96^3 grids can be seen from Figures 5.5 and 5.6. The energy difference between the two curves (q.homo and Knight *et al.*'s curve, E.dat) gets smaller as the grid density increases. In fact, it actually approaches the energy under Knight *et al.*'s curve (E.dat) as we move from Figure 5.4 to 5.6. And it can also be seen that the energy under E.dat also approaches some value which is the exact theoretical value that is supposed to be under the curve. This can be calculated mathematically as seen in the next section.

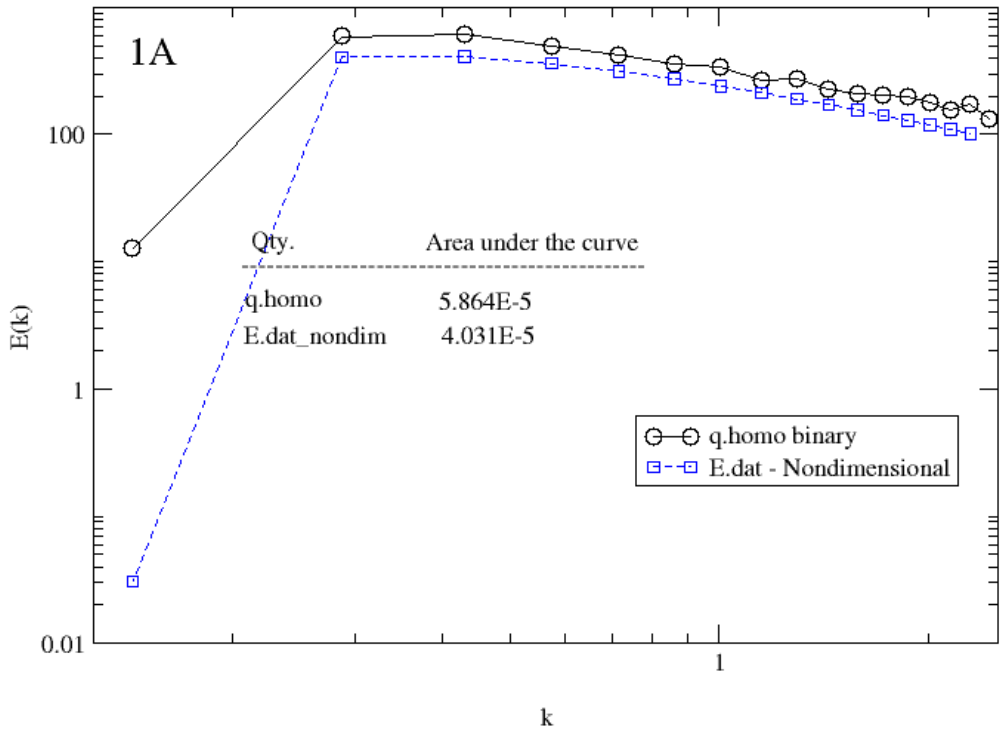

Figure 5.4: Comparison of Energy under the initial curve produced by 'Crecomp' for 32^3 grid and Knight *et al.*'s Initial Energy Spectrum

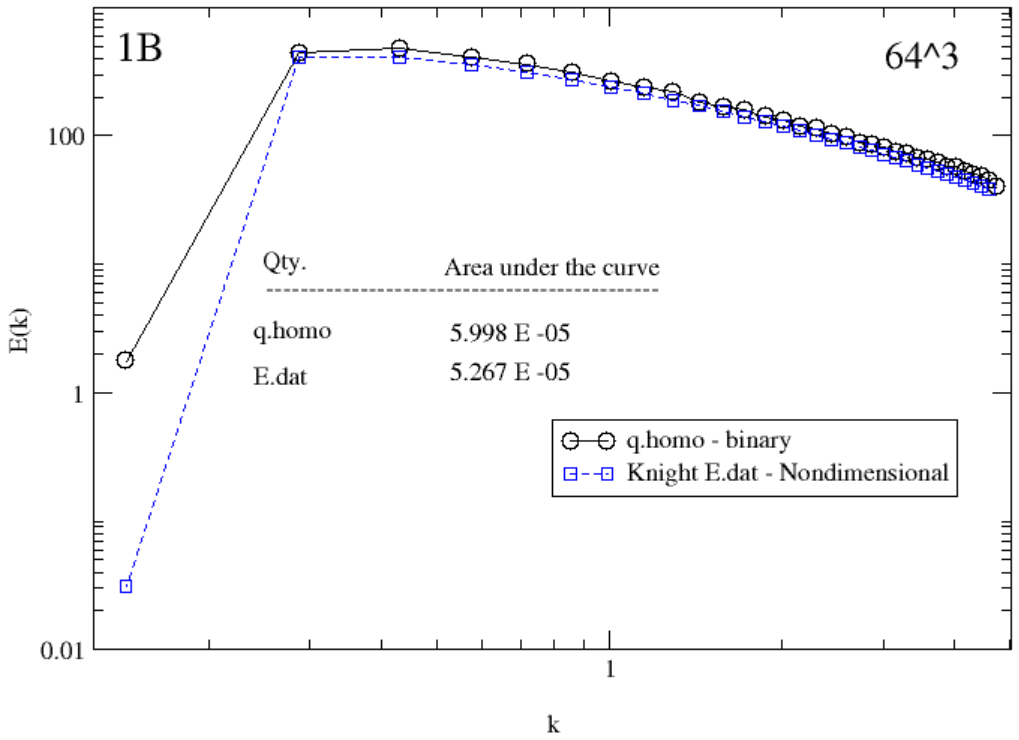

Figure 5.5: Comparison of Energy under the initial curve produced by 'Crecomp' for 64^3 grid and Knight *et al.*'s Initial Energy Spectrum

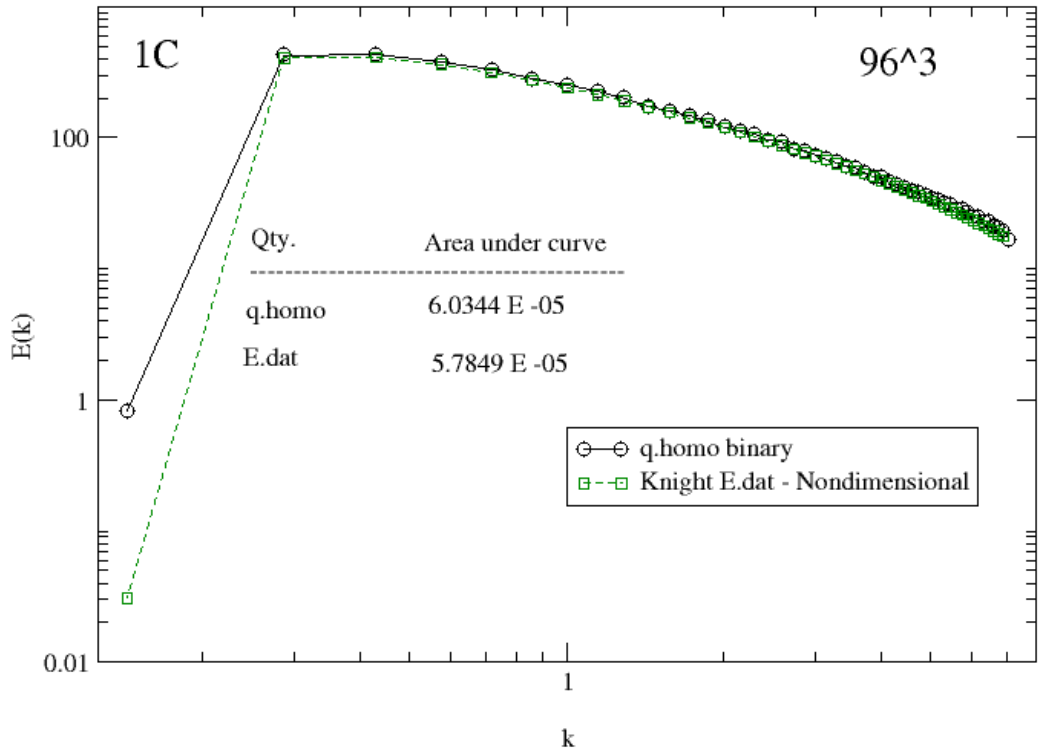

Figure 5.6: Comparison of Energy under the initial curve produced by 'Crecomp' for 96^3 grid and Knight *et al.*'s Initial Energy Spectrum

5.2.2. Mathematical interpretation of energy under the curve

The total energy under the energy spectrum is defined by

$$k' = \frac{u_{rms}^2 + v_{rms}^2 + w_{rms}^2}{2} = \frac{3}{2} u_{rms}^2 = 6.04995 \times 10^{-5} m^2 \sec^{-2}$$

In the 32^3 grid, there are only 17 grid points to define the energy spectrum and hence k_{max}=17. In the case of 64^3 initial energy spectrum k_{max}=33 and in the case of 96^3 grid, k_{max}=49. If k_{max} is high the span of the curve along the k axis (horizontal axis) will increase. Theoretically, as k_{max} tends to infinity, the energy under the curve will converge to 6.04995×10^{-5} $m^2 sec^{-2}$ as calculated above.

The initial energy spectra, be it 32^3, 64^3 or 96^3 always tries to hold the specified amount of theoretical energy (6.04995×10^{-5} $m^2 sec^{-2}$) under the curve. But k_{max} for 32^3, 64^3 or 96^3 is different (17, 33 and 49 respectively). So to maintain the same energy under the curve, the curve in the case of 32^3 rises up to accommodate for the lower k_{max}. Hence as seen in Figure 5.4, q.homo in the case of 32^3 is situated much above the Knight *et al.*'s initial condition. However, as seen the total amount of energy is actually held up well in the case of higher density grids as the discreteness decreases. Thus, eventually as the grid density increases to a high value, q.homo converges with Knight *et al.*'s initial curve (E.dat) which in turn attains the theoretical amount of energy under it. But for the purpose of simulation, the way the 32^3 is constructed and the amount of energy it holds is very reasonable to obtain good results. Also, it will be seen in this chapter in the section 5.2.10 (Effect of Scaling) that the initial shape of the curve is more important in deciding how good our results will be rather than the amount of energy it holds. Hence as seen in Chapter 4 in section 4.1.3, there have been various attempts to improve the shape of the initial condition spectrum and match it in the best possible way with the experimental CBC initial spectrum.

5.2.3. Simulations Tree

All our simulations are performed using LESTool. To observe the behavior of the DES model and the trend that each of the cases follows many simulations were performed. The simulations run with respect to the CBC case are shown in Figure 5.7.

These included cases with three kinds of grid densities 32^3, 64^3 and 96^3. Each of these cases has been tested with multiple dissipation rates. Also whenever the DES model is incorporated, the C_{DES} has been varied over a wide range wherever possible up to C_{DES}=0.10 to 2.00.

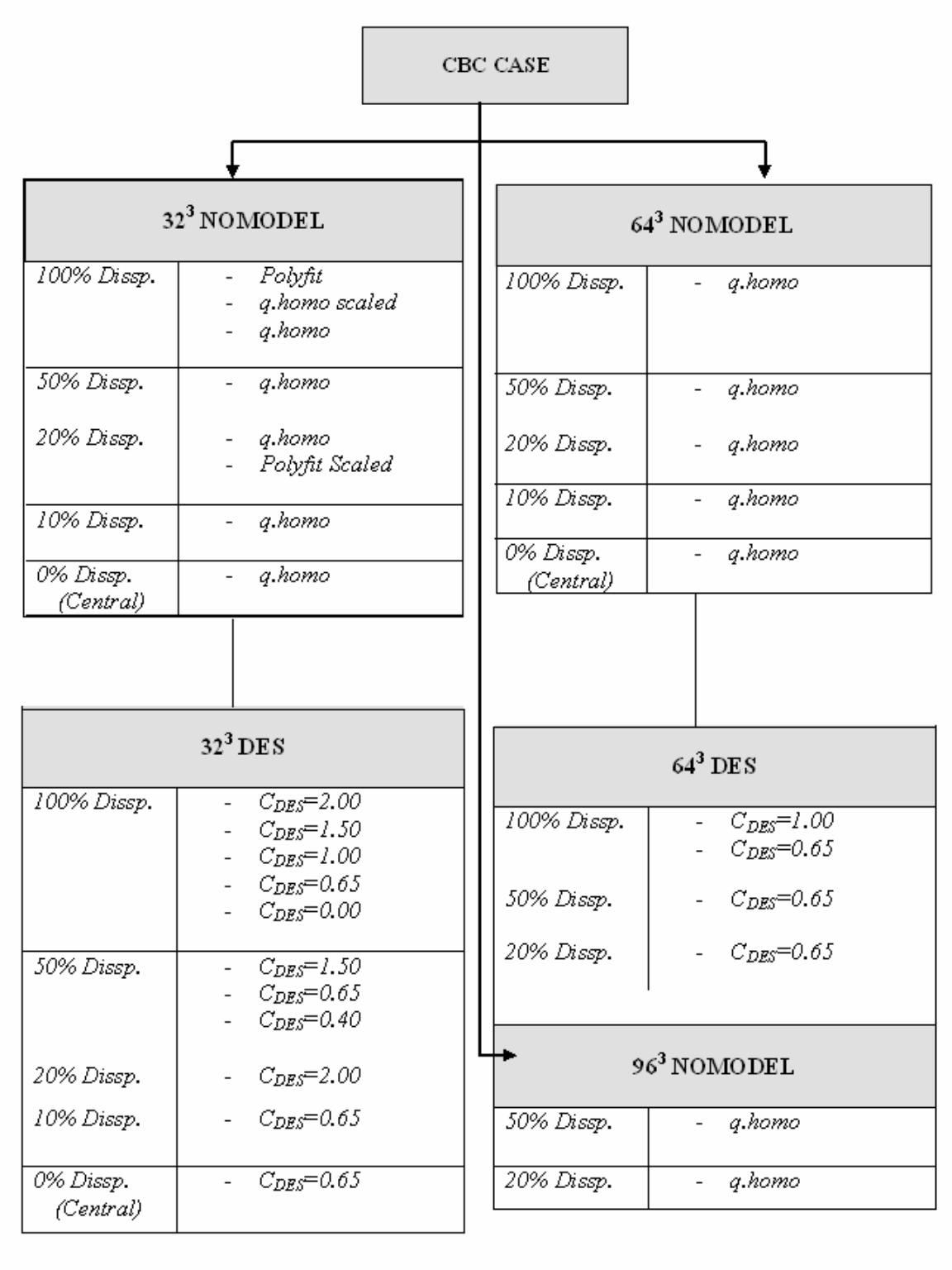

Figure 5.7: Simulations run with respect to the CBC case.

5.2.4. Decay Results

The decay of turbulent kinetic energy with time is very useful to us in interpreting the rate of change of dissipation with time. This would help us know how the model is behaving. If the dissipation rate is very low then in most cases it turns out that the model becomes unstable. So a minimum amount of dissipation is added to make the model stable. But adding too much of dissipation would make the model deviate from reality. Various energy decay plots resulting from different simulation cases are presented in Figure 5.8. The variables considered while running these cases are the grid density, the numerical dissipation of the model and the grid sensitivity parameter of DES, C_{DES}. Simulations performed using LESTool are compared with experimental CBC and Knight *et al.*'s results. The experimental CBC result only provides us with three points (shown in solid green circles) to compare our dissipation rate. These three points represent the results at non-dimensional times Ut/M=42, 98 and 171. Among Knight *et al.'s* results, only his best fit decay curve along with his most deviating curves have been shown to compare the results produced by LESTool with results obtained from CBC experiment and from the literature. Since this plot is cluttered with many curves, useful content shall be extracted out and discussed separately.

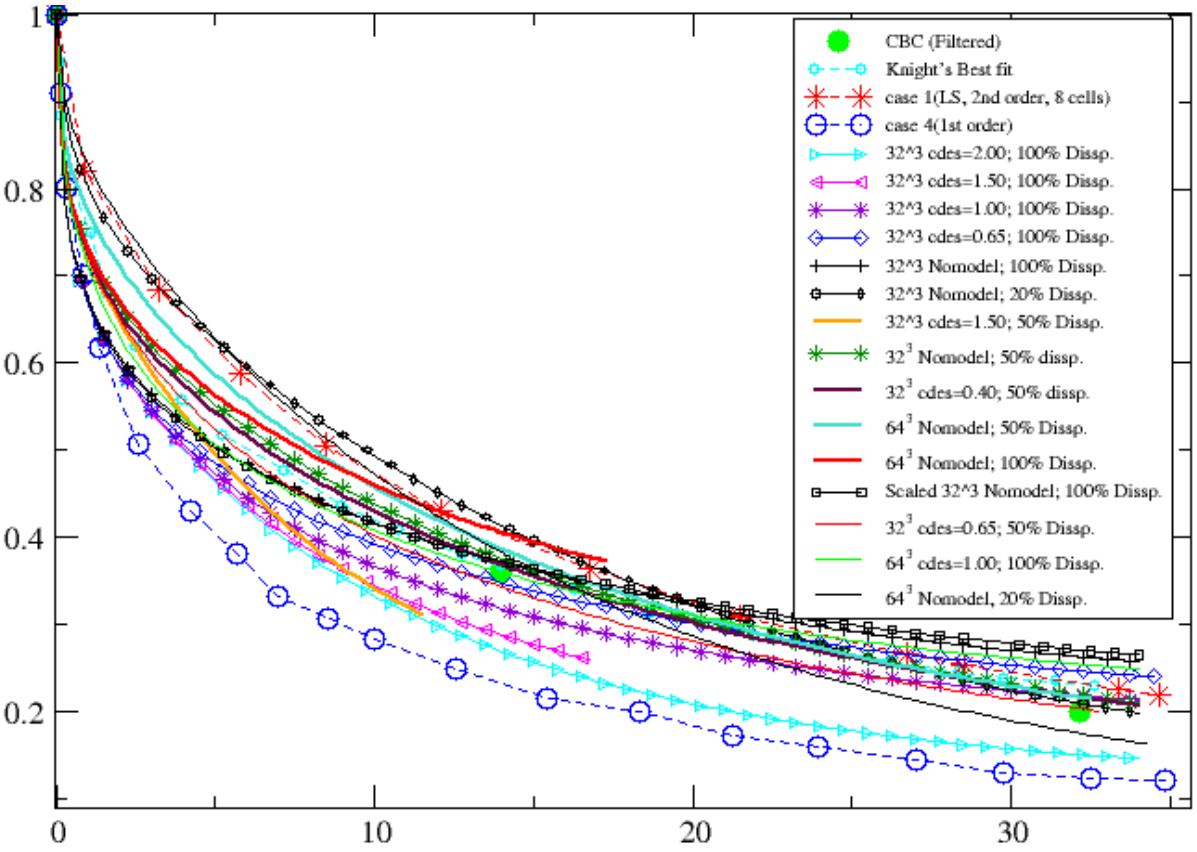

Figure 5.8: Decay curves showing the decay of turbulent kinetic energy, *E(k)* with respect to time *t* for various values of C_{DES},, dissipation rates and grid with the experimental CBC result.

In the Figure 5.9 below, the change in the turbulent kinetic energy with time or the dissipation rate for different cases of dissipation can be seen. The higher the dissipation rate (square symbols), the steeper is the initial slope (starting from t=0 at the origin) and when the dissipation is small, the dissipation rate is also small. Hence the dissipation rate seems to be proportional to the numerical dissipation at initial time non-dimensional time Ut/M=42 or physical time t=0. In addition, higher the dissipation rate, the faster is the flattening of the curve at longer times (around Ut/M=171). The 100% dissipation curve flattens faster than 20% dissipation curve. Here the dissipation rate seems to become inversely proportional to the numerical dissipation of the curve after some dissipation of energy initially.

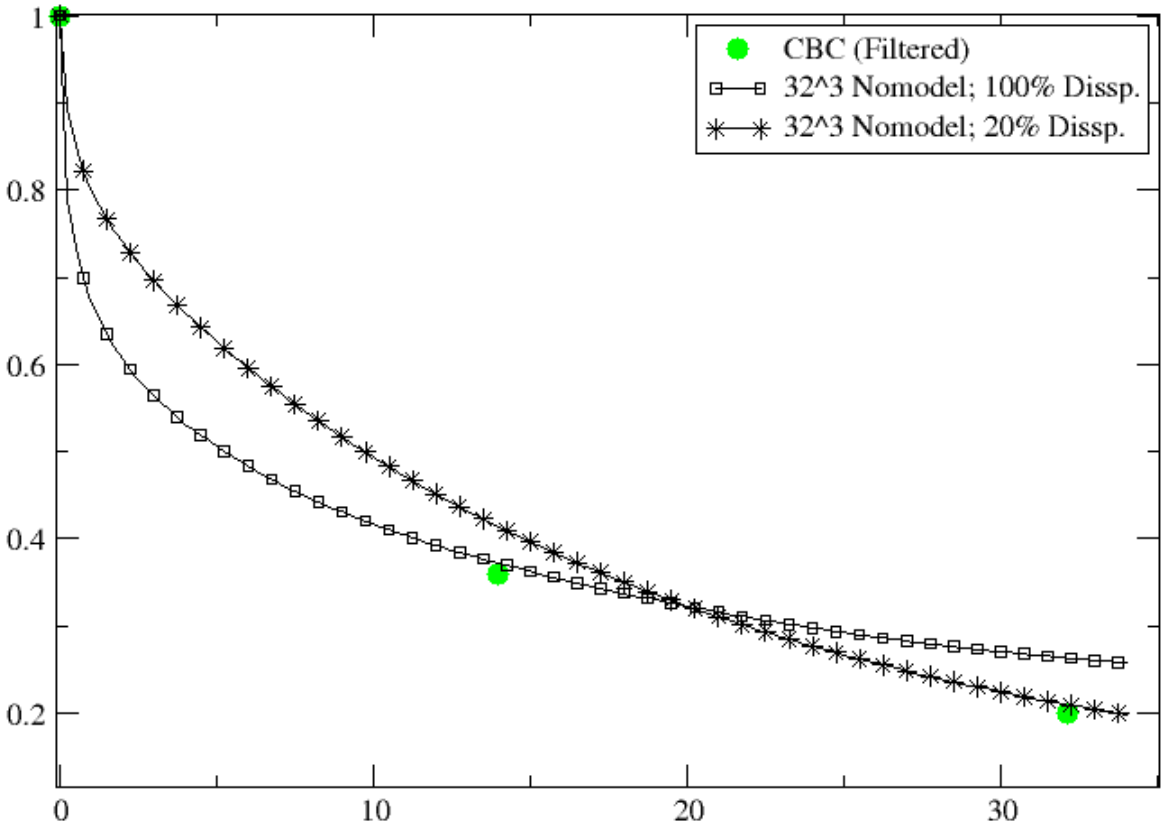

Figure 5.9: Comparison of decay curves with different dissipation rates with the experimental CBC Decay points.

Intermediate dissipation simulations (dissipation between 20% and 100%) may follow intermediate patterns and the trend that is expected (lying between the two curves in Figure 5.9). This motivates us to try the 50% dissipation to match the experimental CBC points (green circles above) better. As seen in Figure 5.10, the 50% dissipation case actually behaves as expected. But this would still be the No Model case with 50% dissipation. As seen in Figure 5.8 above, for the DES case when the C_{DES} is increased, the initial dissipation rate increases and later the dissipation rate remains almost the same as other cases with different values of C_{DES}. This places the curve with a higher C_{DES} below the curve with a lower C_{DES} and running parallel to it along the curve. Thus when a C_{DES} of 0.65 is incorporated in the DES model of the corresponding No Model case, it matches the experimental CBC points (solid green circles) very well as seen in section 5.2.6.

5.2.5. Best Fit Decay

As seen below in Figure 5.10, the decay curves match the CBC experimental decay points very well. We see four different curves of which one of them corresponds to Knight *et al.*'s result (red open circle symbols) and the other three are plots with grid densities of 32^3 and 64^3. Among the cluster of curves in Figure 5.8, these curves are the closest match to CBC curve as evident from Figure 5.10. It can be seen the plots with a numerical dissipation closer to 50% produce the best fit curves. Also notice that these are also the DES model plots with a grid sensitivity parameter, C_{DES}=0.65. As explained in the previous section, it is really the combination of the right amount of numerical dissipation and C_{DES} which gives us the best results and in our case it is evident that the best fit decay curves are produced with a DES case of C_{DES}=0.65 and 50% numerical dissipation.

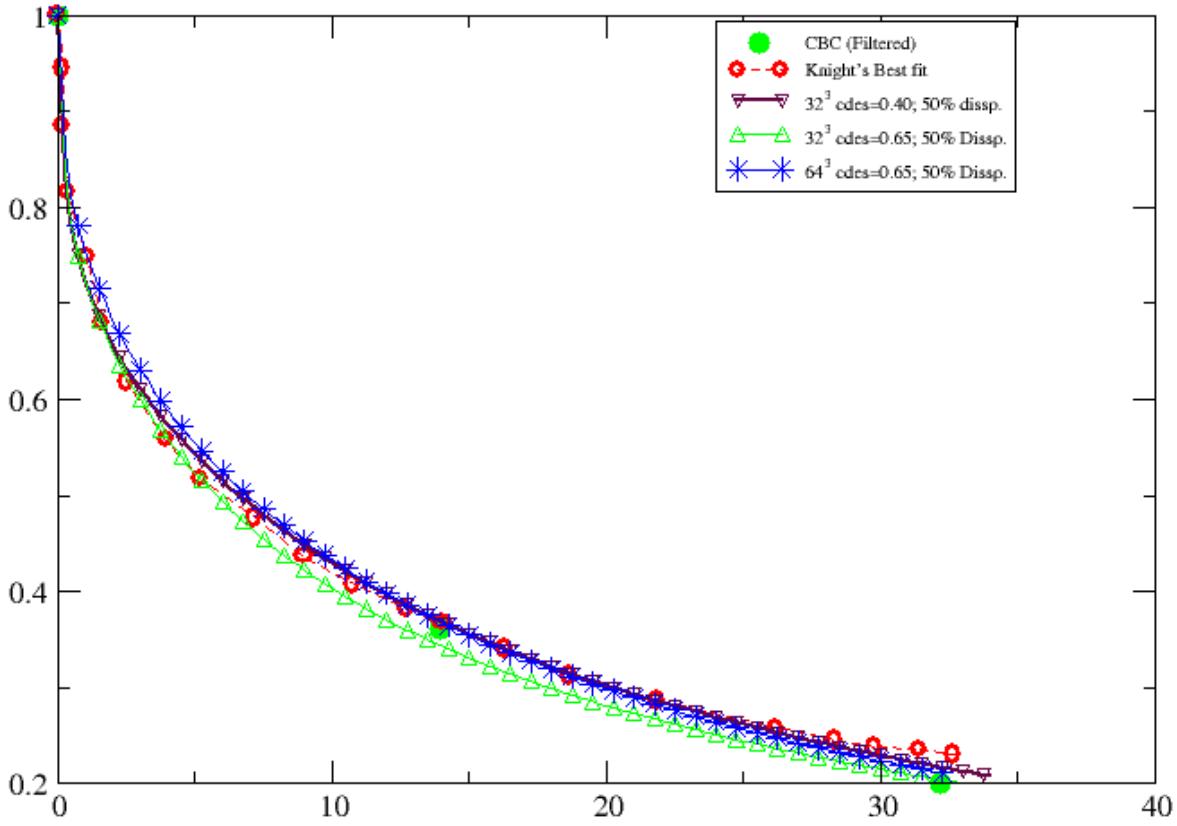

Figure 5.10: Best decay curve fits shown in comparison to experimental CBC decay points for different grid densities and C_{DES} values.

5.2.6. Energy Spectra Results

In the Figure 5.11, the results of the evolution of energy spectra obtained using LESTool are seen at non-dimensional time *Ut/M*=98. Results obtained using LESTool are compared with the CBC curve (bold stars) and with Knight *et al.*'s results (black and red diamond symbols). It is seen that 20% dissipation produces good results. Even Strelets [22] points out that central differencing scheme produces good results compared to the 5th order upwind scheme as the 5th order upwind produces too much dissipation. So better results are obtained as we keep decreasing the numerical dissipation. When 0% dissipation is reached, effectively the 5th order upwind scheme merges with the 6th order central difference scheme. But, in this case, LESTool goes unstable for numerical dissipation less than 10%. So the central scheme is run in a stable manner for this case by adding at least 10% numerical diffusion. The cases with 100% dissipation are the No

Model cases which like the MILES (Monotone Integrated Large Eddy Simulation) cases of Knight *el al.* unless they are run by the DES model. Really, all cases with No Model are like MILES or ILES, but the higher numerical dissipation cases should be more comparable to this method. The C_{DES} corresponding to the DES case can be seen in the legend. Figure 5.11 gives an idea of the range of results and some of the trends followed by varying various parameters. However, these trends and comparisons will be discussed more clearly in subsequent sections and in the next chapter.

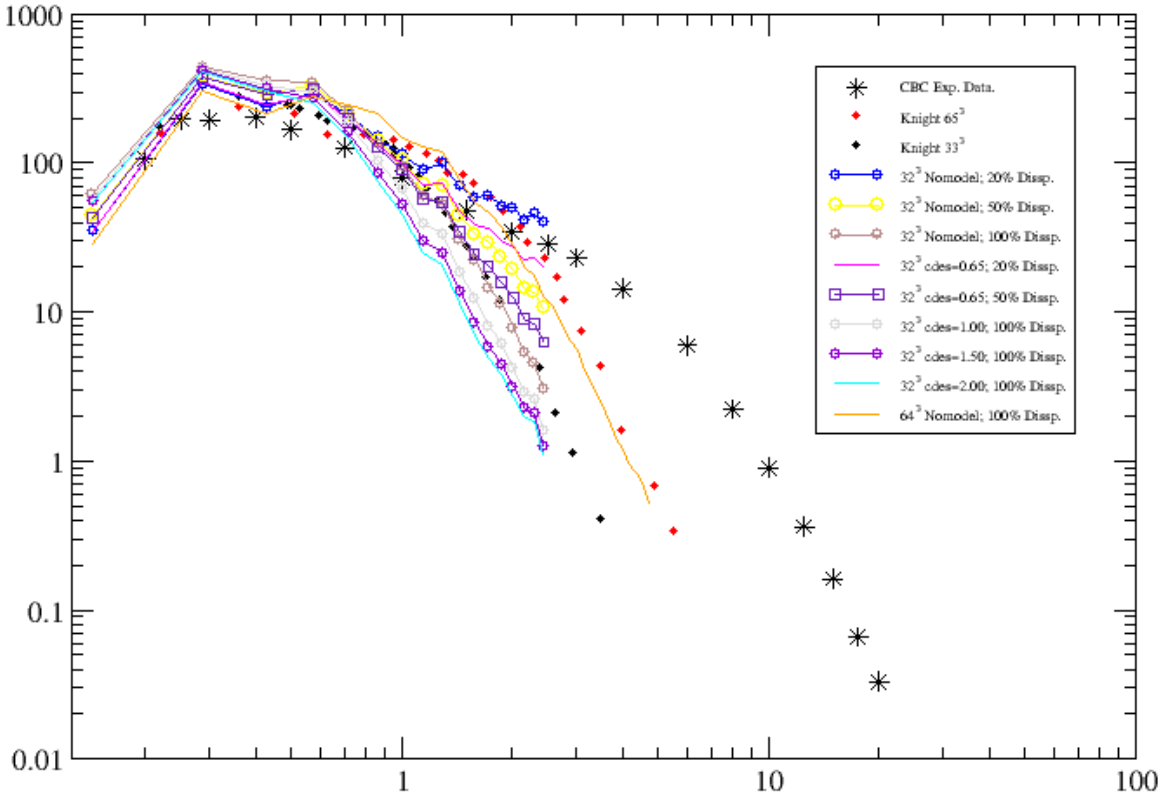

Figure 5.11: Comparison of turbulent kinetic energy spectra results obtained using LESTool for various simulations at non-dimensional time *Ut/M*=98 with Knight *et al.*'s and CBC results.

In the Figure 5.12, we see the plot of the energy spectra results obtained using LESTool after a time evolution of non-dimensional time *Ut/M*=171. As seen in the figure, the blue circular symbols correspond to the unscaled initial spectrum which is scaled after evolution through time at *Ut/M*=171 whereas the brown diamond symbols represents the

curve which has been scaled at *Ut/M*=42 and then evolved in time until *Ut/M*=171. Also this curve (brown diamond syymbols) has been obtained from the linear polynomial fit (explained in section 4.1.3) as against the logarithmic polynomial fit method of Knight *et al*. It is also seen that since both the curves in discussion merge pretty well as seen in the figure, it shows that comparing the curves after a simulation time of *Ut/M*=171, the scaling performed at initial time does not differ much from the curve where scaling has been performed at a later time. The results look much like what they look at *Ut/M*=98. Also they consistently match with the CBC experimental results in a similar way.

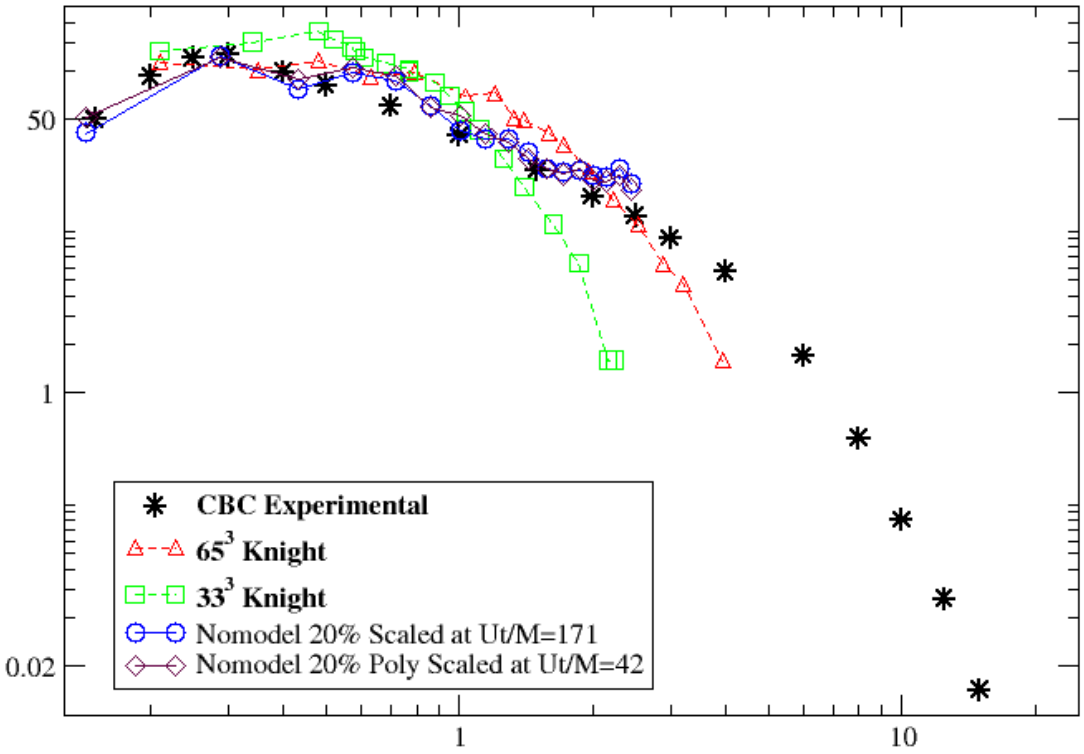

Figure 5.12: Energy spectra results obtained using LESTool compared with Knight *et al.*'s results and CBC results at non-dimensional time *Ut/M*=171

5.2.7. Best Fit Energy Spectra Results

In Figure 5.31, we shall compare our results obtained using LESTool with

1. CBC experimental data
2. Strelets' simulations
3. Knight *et al.*'s simulations

As seen in Figure 5.13, the results match the CBC experimental data very well at time *Ut/M*=98. Results are shown for both 32^3 and 64^3grids. The 64^3 results (small purple circles) are slightly better than the 32^3 grid results (inverted red triangles). Also, we have seen that the initial condition of 64^3 matches better than the 32^3 initial spectrum with the experimental CBC initial spectrum. Hence, it is plausible that as the spectrum evolves 64^3 is a better match to the CBC spectrum than the 32^3 grid at both *Ut/M*=98 and *Ut/M*=171 (Figure 5.14).

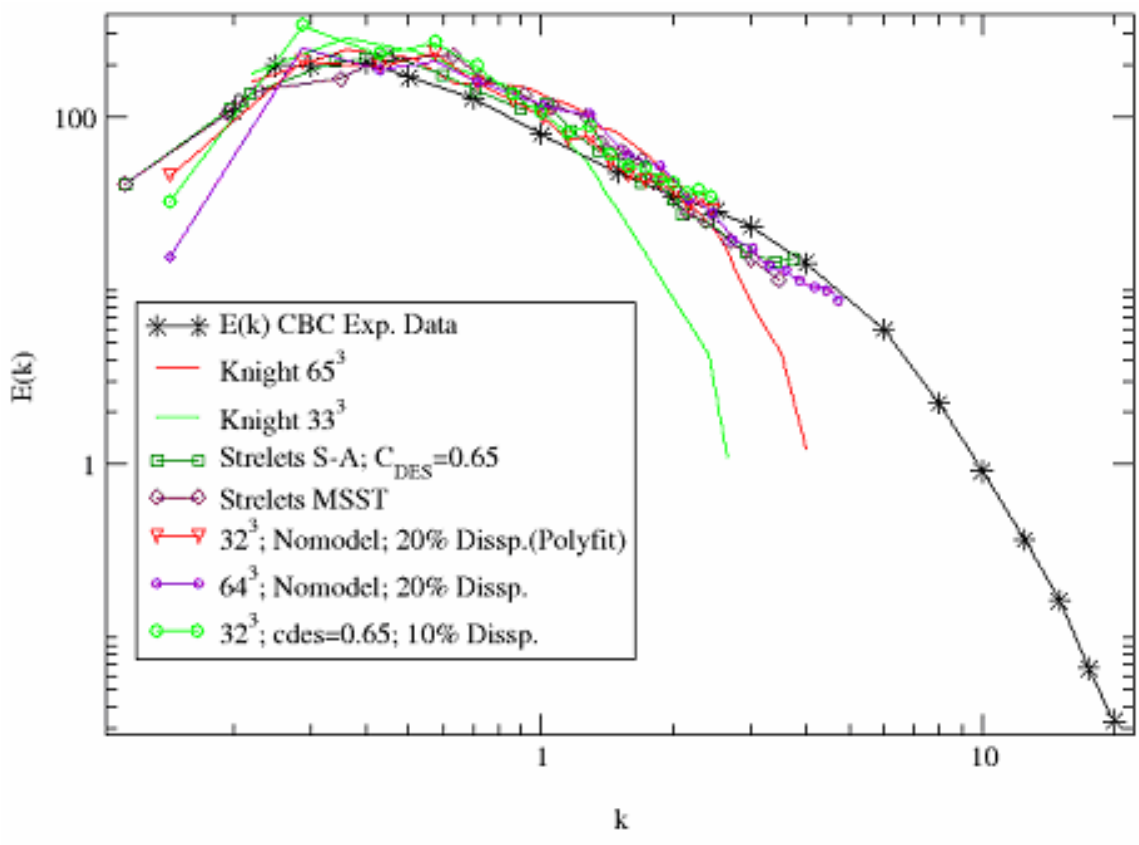

Figure 5.13: Best fit energy spectrum results compared with Knight *et al.*'s results, Spalart's results and Experimental CBC points at *Ut/M*=98 for different grid densities**.**

If we examine Figures 5.13 closely, we can see that when compared to the experimental CBC results (bold asterisks), both Strelets' results and the simulations using LESTool (32^3 and 64^3 grid : No Model and C_{DES}=0.65) match very well as opposed to Knight *et al*'s results (33^3 and 65^3). The curves corresponding to the 32^3 grid produced using

LESTool are more crooked compared to the 64^3 grid results. This can be attributed to the initial conditions and also because the grid density influences the smoothness of the curve. If the grid density is high the continuity between the points is better connected and the energy variation is better represented. Hence the 64^3 No Model case with 20% dissipation matches well with the CBC results. The Strelets results also match very well with the CBC curve, but the Strelets S-A case with C_{DES}=0.65 tends to flatten out at the end of the curve without actually following the -5/3 slope of CBC curve. Also the Strelets MSST case shows a very high dissipation rate at the end of the curve and drops fairly quickly down without following the CBC curve. But the 64^3 No Model case is comparatively in a better position in behaving well with respect to exhibiting the -5/3 slope and dissipating just the right amount of energy. Regarding the 32^3 grid results produced by LESTool (which can be better seen by zooming in), there are both the polyfit as well as the ordinary 32^3 result but with DES modeling. The polyfit curve, as explained in section 4.1.3, is a better match to the CBC initial condition. Also it can be seen from Figure 5.13 that in general the shape of the polyfit curve matches well with the CBC curve and is less crooked than the other 32^3 curve. Regarding the dissipation rates, in the No Model cases, 20% numerical dissipation seems to be just the right amount of dissipation in obtaining the right match to CBC curve for both the 32^3 and 64^3 grid case. However, when the DES model is incorporated, 10% dissipation seems to be a better choice. This is because DES adds some amount of numerical dissipation which increases the energy dissipation rate at initial time (see discussion of Figure 5.9). So a reduction in the numerical dissipation by adopting a 10% dissipation for the 5^{th} order upwind scheme appear to be a close-to optimal balance to obtain good results.

If we look at the results at non-dimensional time Ut/M=171 (Figure 5.14), we see that as explained before, 20% dissipation both for 32^3 grid and 64^3 grid is a good choice for numerical dissipation while simulating the results using LESTool. Also, if we look at Strelets' results, both of his cases (S-A and MSST) seem to deviate slightly away from the CBC results at the end of the curves in both the cases. But this is not a very large deviation. This happens even in the case of 64^3 No Model case with 20% dissipation but then it quickly adjusts and aligns along the CBC curve by decreasing the dissipation rate slightly. Thus unlike the 32^3 grid case, which is incapable of covering the high wave

number (k- horizontal axis), the 64^3 No Model case with 20% numerical dissipation is the only case which actually matches so well with the experimental CBC spectrum. Again the relative positions of the curves and the matching with CBC curve can be seen clearly when the region is zoomed. As seen after a time evolution of *Ut/M*=98 in Figure 5.13, even at *Ut/M*=171 in Figure 5.14, the results obtained are very encouraging when compared to CBC experimental results, Strelets' simulations and Knight *et al.*'s simulations.

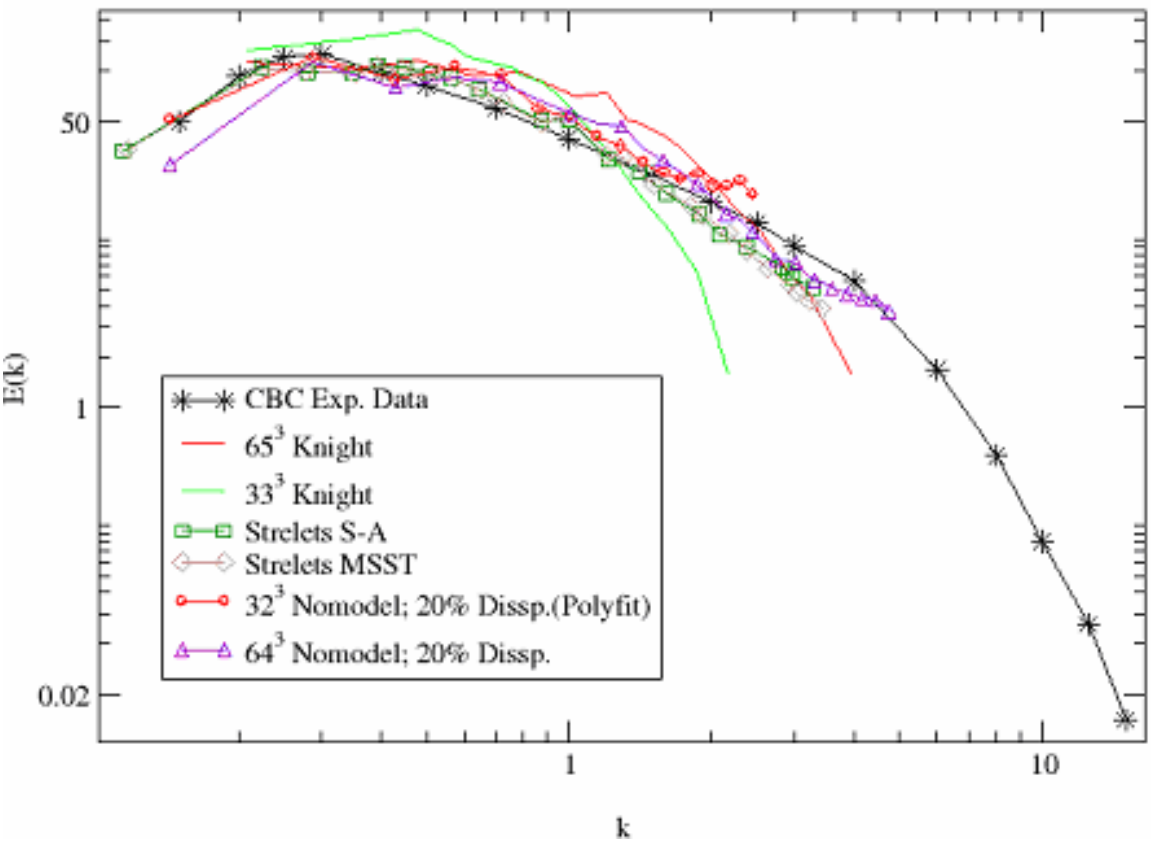

Figure 5.14: Best fit energy spectrum results compared with Knight *et al.*'s results, Spalart's results and Experimental CBC points at *Ut/M*=171 for different grid densities.

5.2.8. Some interesting trends

In the following plots we see the effects of changes in

A). C_{DES}

B). Dissipation

C). Grid Density

In this section, only the trends of the above listed parameters will be shown.

As seen in Figure 5.15, as C_{DES} is increased, the dissipation rate increases. It is actually a more rapid change in the dissipation rate at the peak of the curve. As with other curves in this figure, the dissipation rate further along seems to be almost constant. This trend was also seen when comparing the decay curves (section 5.2.5). There is strong relationship between the behavior of the change in the grid sensitivity parameter, C_{DES} and the numerical dissipation.

As seen in Figure 5.16, as the numerical dissipation is reduced from 100% to 10%, the dissipation rate of the model is reduced. It is very obvious that this general behavior is observed. But unlike the grid sensitivity parameter, C_{DES}, the change in the dissipation rate is not just at the peak. Once the dissipation rate decreases and the curve deviates at the peak, it continues to dissipate energy at that constant rate. That is the reason the energy spectra are not curvilinearly parallel to each other unlike the trend observed in the case of changing of C_{DES}.

Another important trend is the behavior observed when the grid density is changed. From the Figure 5.17, as the grid density increases from 32^3 to 64^4 cube, the turbulence kinetic energy dissipation rate is reduced initially at the peak in the case of the higher density grid. Later, both the grids exhibit almost the same dissipation rate but the low density grid dissipates energy at a slightly higher rate as both the curves are seen to be very slowly diverging. A possible explanation is that as the grid density increases, the inherent numerical dissipation in the model decreases. This happens because the energy is not captured at each and every point and since we have only discrete points, the smaller eddies which are filtered away in this mesh grid take away the energy. Hence this energy is modeled and added to the turbulence model. But the amount of discreteness decreases as the grid density increases, hence the dissipation added to the model keeps decreasing and hence since there is not as much numerical dissipation that is taking place as the simulation evolves.

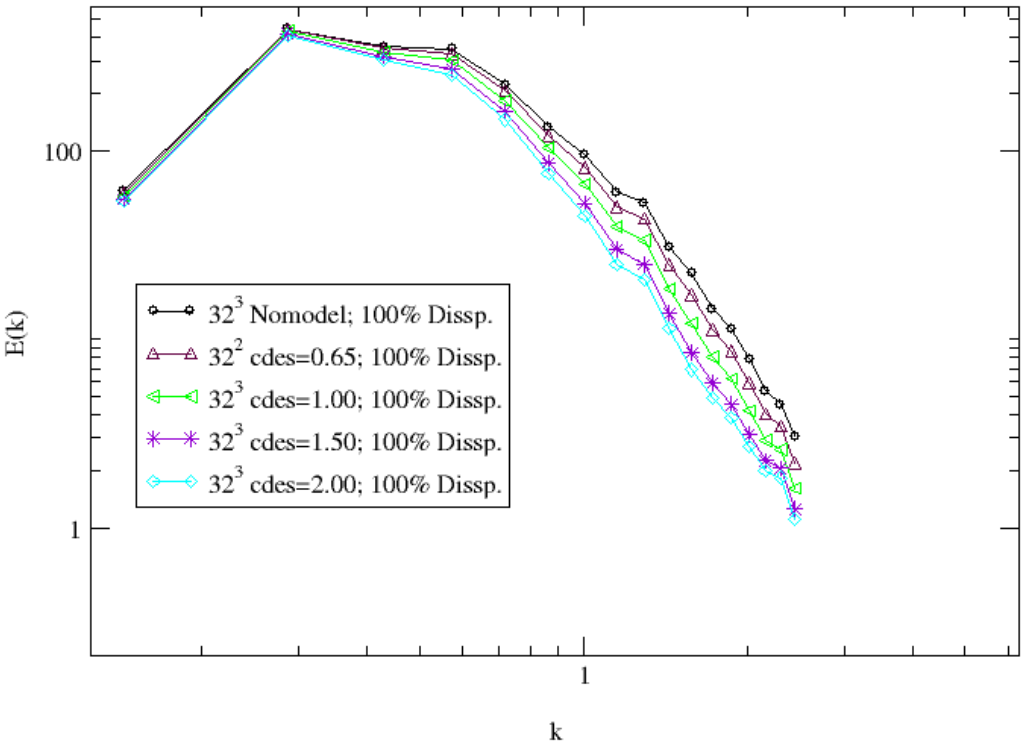

Figure 5.15: The rate of change of dissipation is seen as the C_{DES} is varied from 0.65 to 2.00 along with the No Model case for 32^3 grid at *Ut/M*=98.

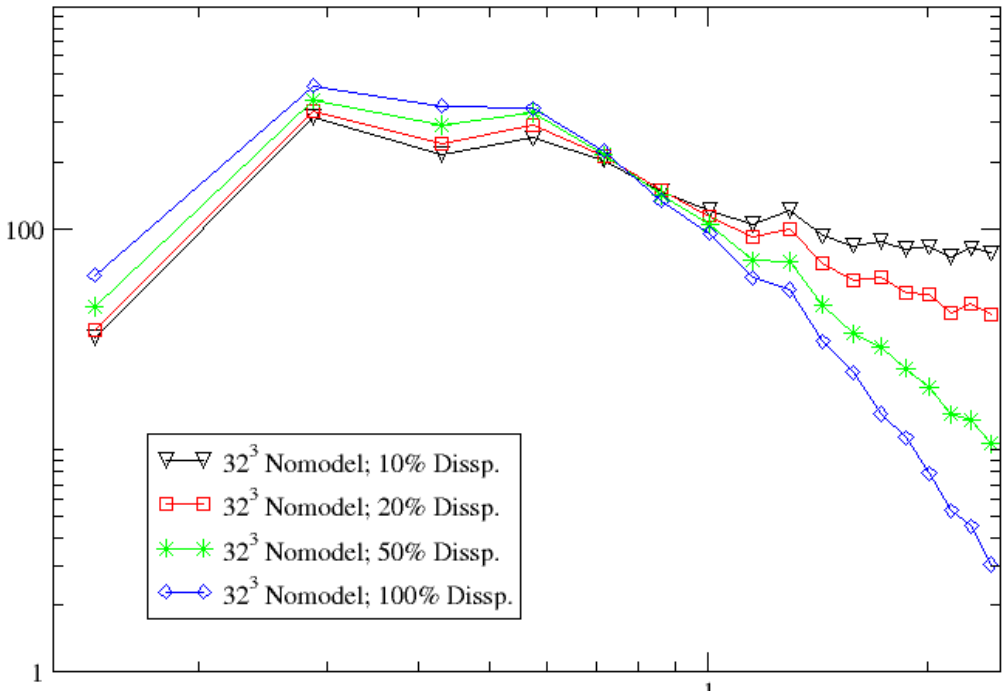

Figure 5.16: The trend energy spectrum follows as the dissipation rate is varied from 10% to 100% for a 32^3 grid at *Ut/M*=98.

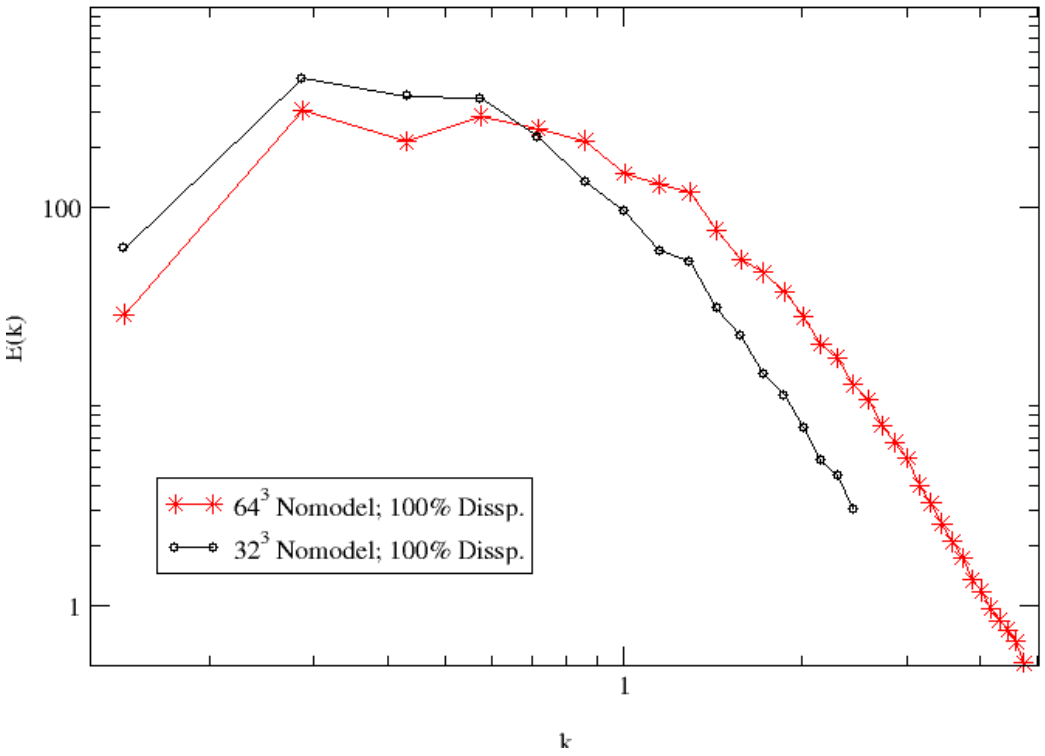

Figure 5.17: The variation in energy spectrum depicted above as the grid density is changed from 32^3 to 64^3 for the No Model case with 100% dissipation at *Ut/M*=98.

5.2.9. Effect of Scaling

In the plots below, the effect of scaling is described using the following

1. The energy spectra at *Ut/M*=98
2. The energy spectra at *Ut/M*=171 and
3. The decay curve

While scaling the graph, the y-coordinates of all the points of the curve are simply multiplied by a scale factor. The scaling factor is a ratio of the area under our initial curve (q.homo) and the area below the CBC curve (cut off at k_{max} of q.homo). Using a scaling factor, q.homo has been scaled and a simulation has been made.

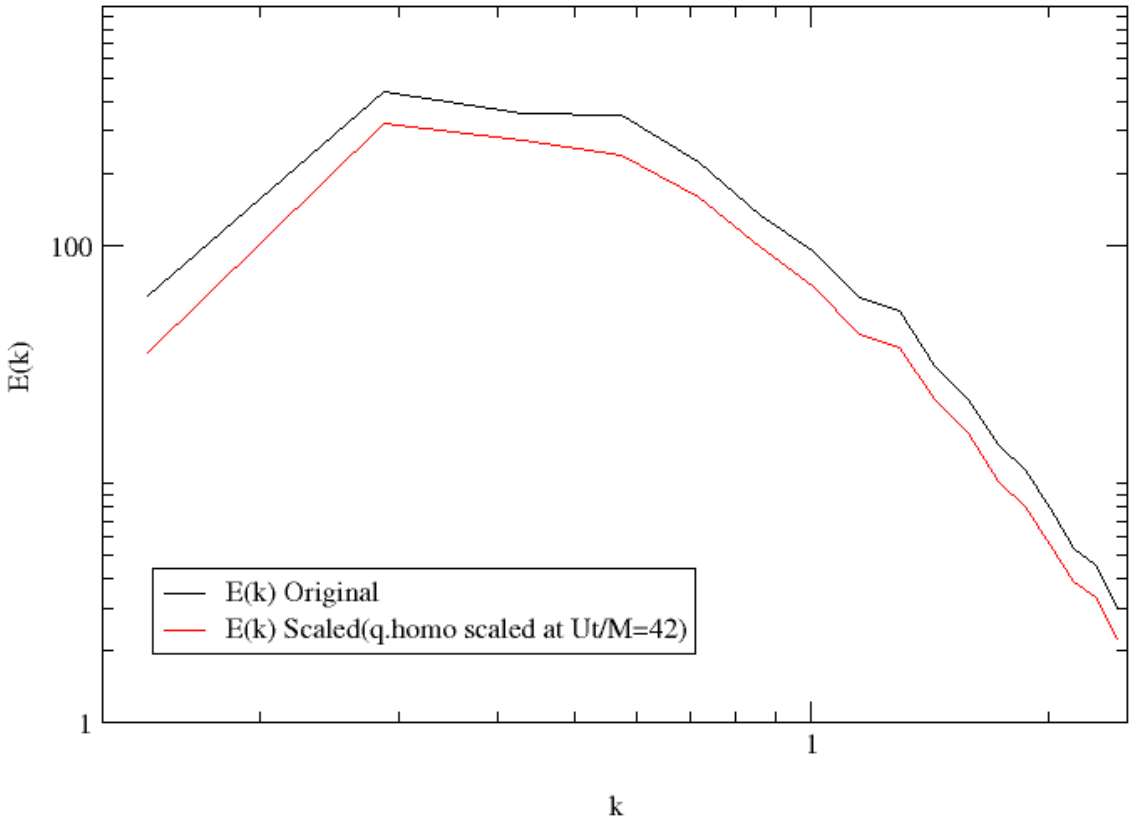

Figure 5.17: The comparison of 'q.homo' and 'scaled q.homo' that evolved thorough time seen at *Ut/M*=98. The scaling has been performed at *Ut/M*=42 to a 32^3 No Model case with 100% dissipation.

As seen in Figure 5.17, at *Ut/M*=98 there is only a magnitude shift (which is expected) but there is no noticeable effect in the change of the slope of the curve. This pattern holds at time *Ut/M*=171 (Figure 5.18) where only a change in the magnitude is seen but there is no change in the actual slope of the curve. So as the curve evolves, the scaling performed on the initial energy spectrum, q.homo does not produce any significant effect on the dissipation rate. So actually, taking the results from a simulation with an unscaled initial condition and scaling the results at later times gives the same results as scaling the initial condition and running the simulation to the desired time.

Also, when the decay curve comparison (Figure 5.19) is observed, there is no significant change produced by the scaling effect. There are two curves, one is the decay curve of a normal 32^3 grid with 100% dissipation No Model case and the other one is the decay plot of same case as the previous one but with a scaling performed on the initial

q.homo energy spectrum at *Ut/M*=42. Since both the decay curves do not shown any significant variance as seen in Figure 5.19 the scaling produces little effect in changing the dissipation rate of the energy spectrum. Thus, by scaling the initial energy spectrum the dissipation rate of the curve is not affected during the simulation as the curve energy spectrum evolves over time. Hence, it can be said that the slope of the initial energy spectrum is the one that has been more significant in affecting the evolution of the spectrum more than the magnitude of initial energy spectrum.

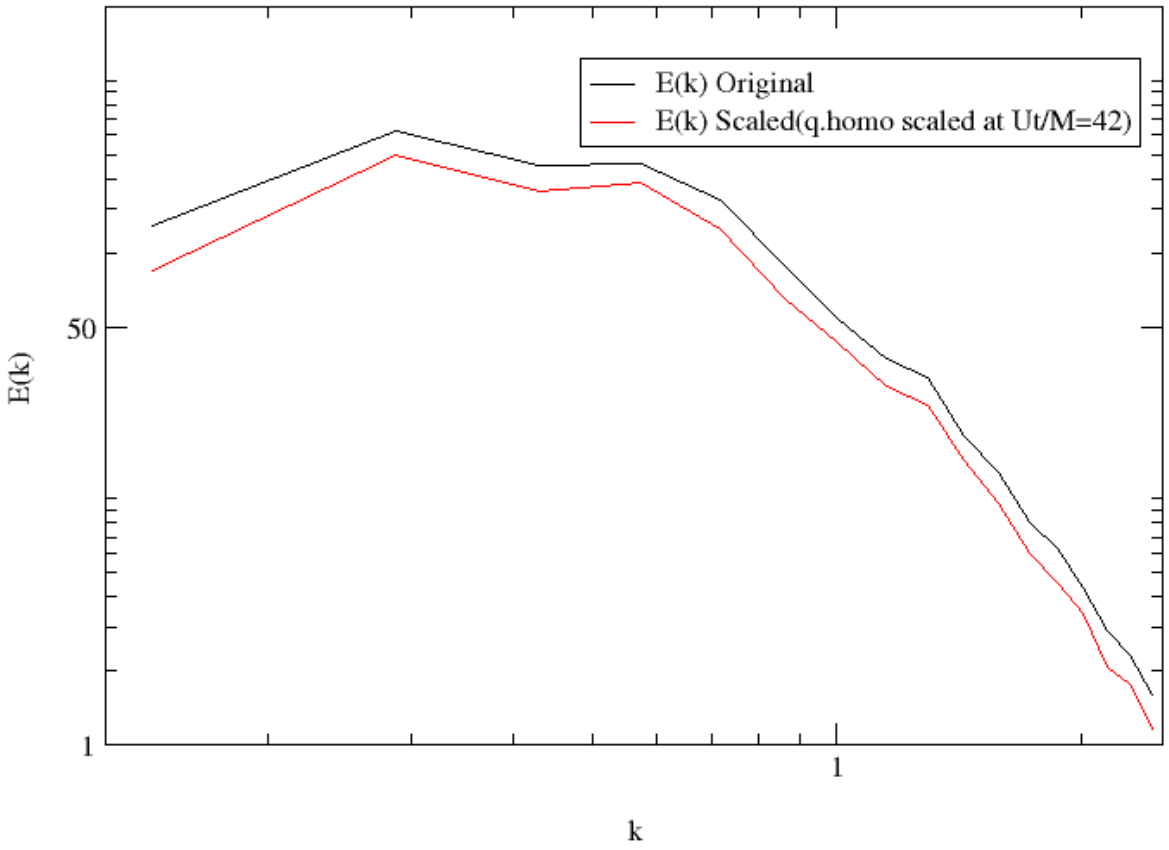

Figure 5.18: The comparison of 'q.homo' and 'scaled q.homo' that evolved thorough time seen at *Ut/M*=171. The scaling has been performed at initial time, *Ut/M*=42 on a 64^3 grid, No Model case with 100% Dissipation.

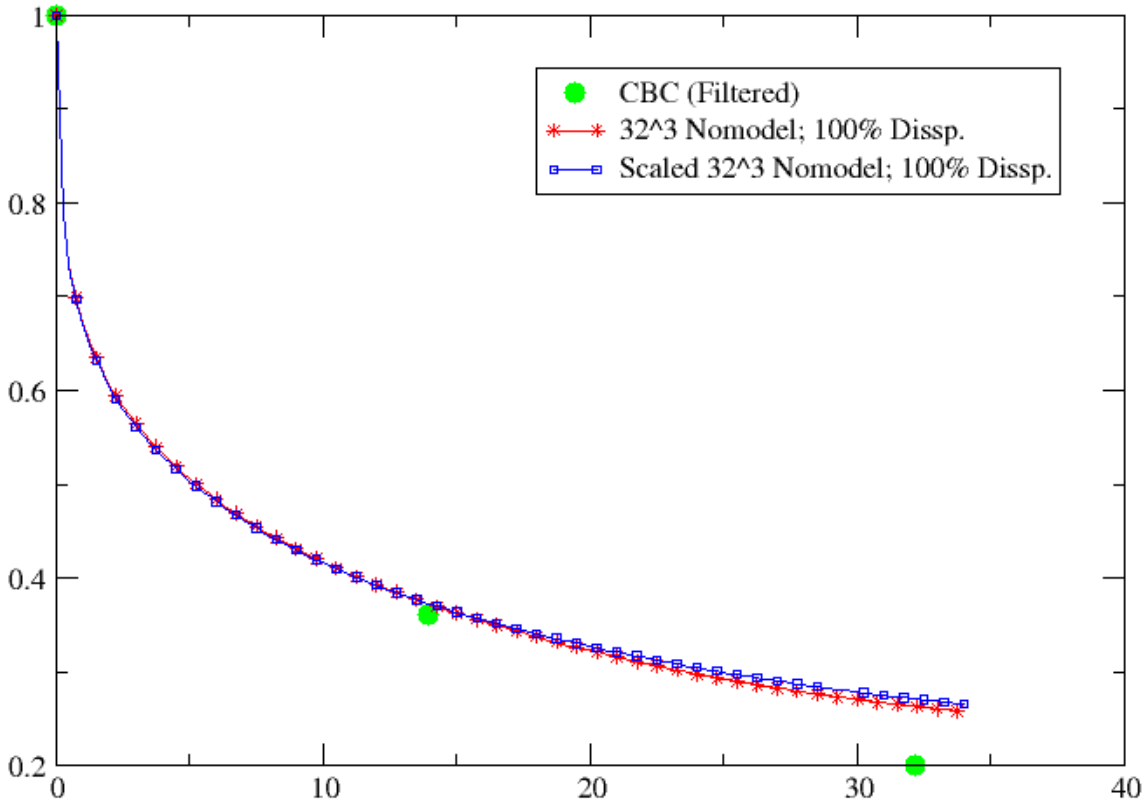

Figure 5.19: The comparison of 'q.homo' and 'scaled q.homo' decay curves for 32^3 No Model, 100% dissipation case. In the case of the scaled decay curve, the scaling has been performed at time Ut/M=42.

The preceding section has provided an overview of the simulation of CBC case using LESTool. It is seen how the initial conditions are produced and compared to Knight *et al.*'s simulations and CBC initial conditions with specific attention to the concept of energy under the energy spectrum. The various results of the energy spectra produced at Ut/M=98 and Ut/M=171 along with the results of energy decay plots were seen. Apart from this, the different trends of effect of the grid sensitivity parameter C_{DES}, grid density and dissipation on the energy spectrum were seen and the effect of scaling the initial energy spectra q.homo were discussed. In fact, these trends will become important when we look at the other case of the simulation of homogeneous turbulence other than the CBC case. This is the Blaisdell's case. These trends will be compared even for the Blaisdell's case and the consistency will be measured which is discussed in Chapter 6.

5.3. Blaisdell's Case

Blaisdell *et al*. performed Direct Numerical Simulation (DNS) studies on homogeneous turbulence. We shall compare our results obtained using LESTool with their results at t=7. The Reynolds number for the case is Re=3640. Cases have been run with 32^3, 64^3, 96^3 and 128^3 grids; for comparison, a 192^3 grid would be a DNS grid comparable to Blaisdell *et al.*

5.3.1. 64^3 grid results

Figure 5.20 shows the initial energy spectrum for the 64^3 grid. It has a top hat energy spectrum as seen from the figure and also seen in the initial conditions seen in section 3.2.2. Using this energy spectrum, simulations varying the C_{DES} value, grid density and the numerical dissipation are completed.

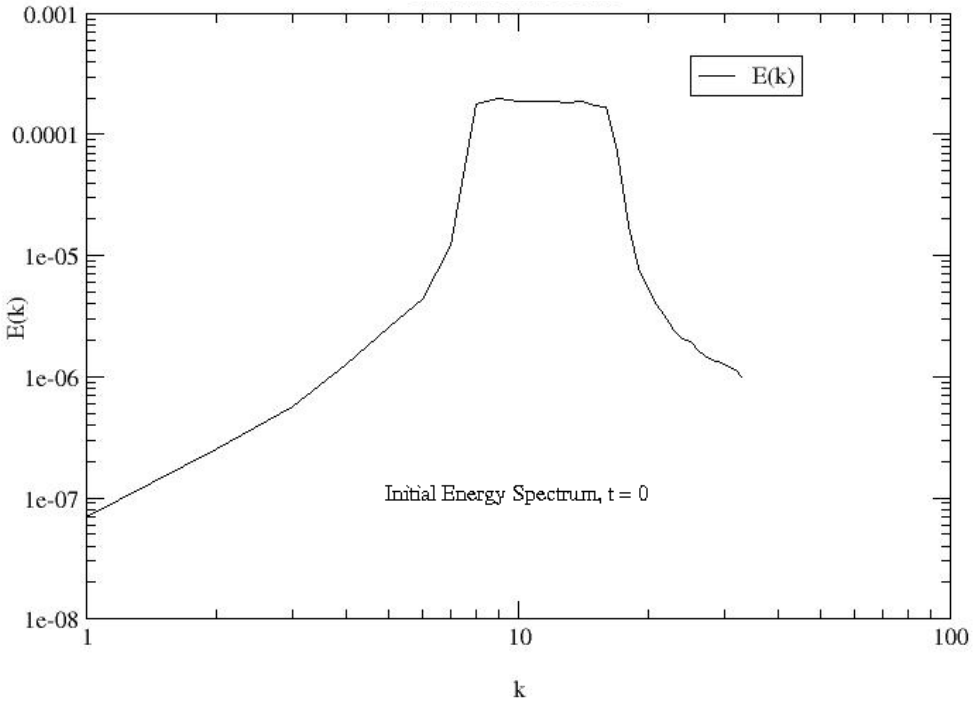

Figure 5.20: Initial energy spectrum produced using LESTool for 64^3 grid.

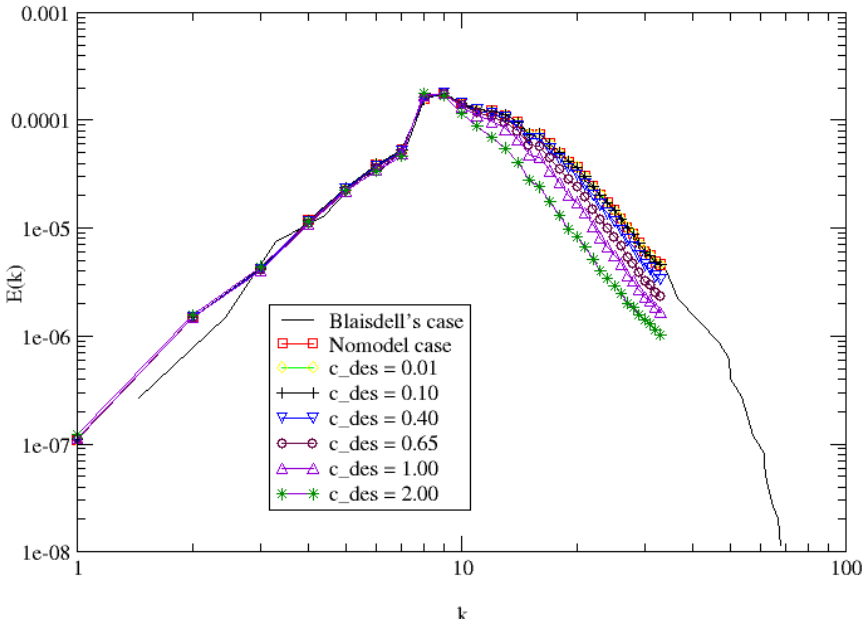

Figure 5.21: (64^3 grid) Comparison of energy spectra for various values of C_{DES} with Blaisdell's spectra at t=7

In the above figure, the Blaisdell's DNS result is indicated by the solid black curve running all the way down. All the other curves with different symbols correspond to simulations run using LESTool for various values of grid sensitivity parameter C_{DES} considered. The significance of Figure 5.21 is seen better close up in Figure 5.22. It can be seen that when a 64^3 grid is used, the No Turbulence Model matches best with the Blaisdell's result. When we look at the DES results, the curve with C_{DES}=0.01 almost merges with the No Model case and Blaisdell's curve.

From Figure 5.22 (a), it can be seen that as the grid sensitivity parameter C_{DES} increases, the energy dissipation rate also increases. The rate of dissipation is highest for C_{DES}=2.00 as seen from the figure. Hence it has the highest slope of all the curves. It is interesting to note that the No Model case (MILES Case) matches well with the Blaisdell's DNS curve. Hence it becomes clear that inherently, for the 64^3 grid, taking a low value for C_{DES} would be the best choice as there is already enough dissipation needed to keep the simulation going in a stable manner. Increasing the value of C_{DES} causes the curve to drift away from the Blaisdell's DNS case. Also, this is a function of the grid

density and numerical dissipation considered. Since all these cases have a 100% numerical dissipation, there is no need of addition of any artificial dissipation by means of the DES model for this grid as seen from the figure. However, if the numerical dissipation were to change or if a different numerical scheme other than the 5^{th} order upwind scheme is to be used, then the results might vary. Presently the 5^{th} order upwind scheme has been used in this case and the C_{DES}=0.01 is the right choice to match the DNS simulation result for the 64^3 grid. The same trend is seen in Figure 5.22 (b) where the Blaisdell's case simulation of the 64^3 grid is shown at t=12.

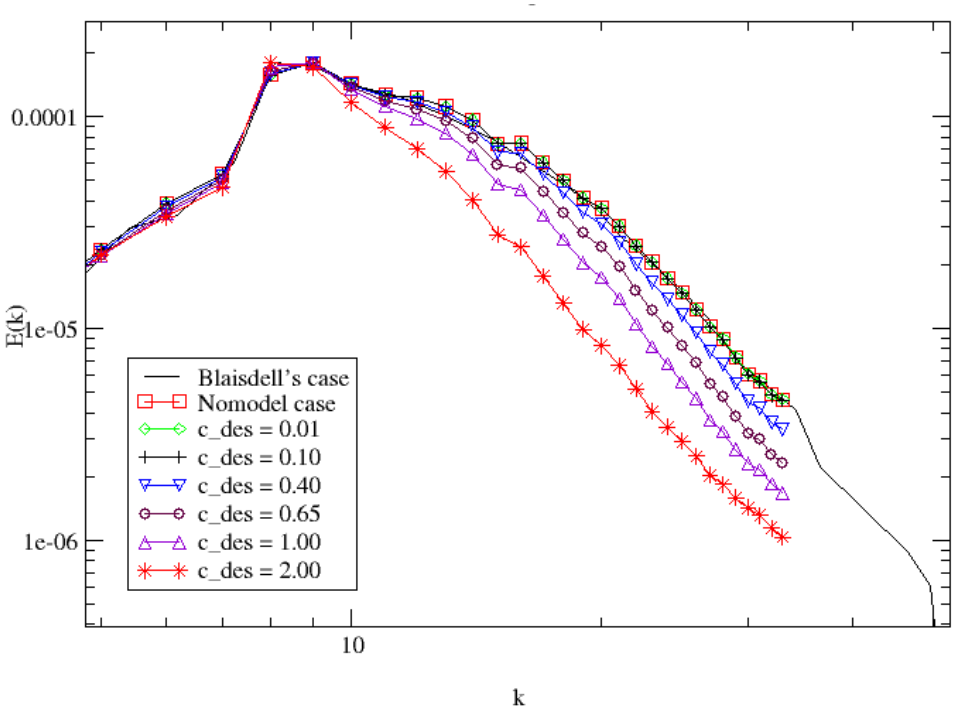

Figure 5.22 (a): (64^3 grid) Comparison of energy spectra for various values of C_{DES} with Blaisdell's spectra at t=7. (Zoomed view)

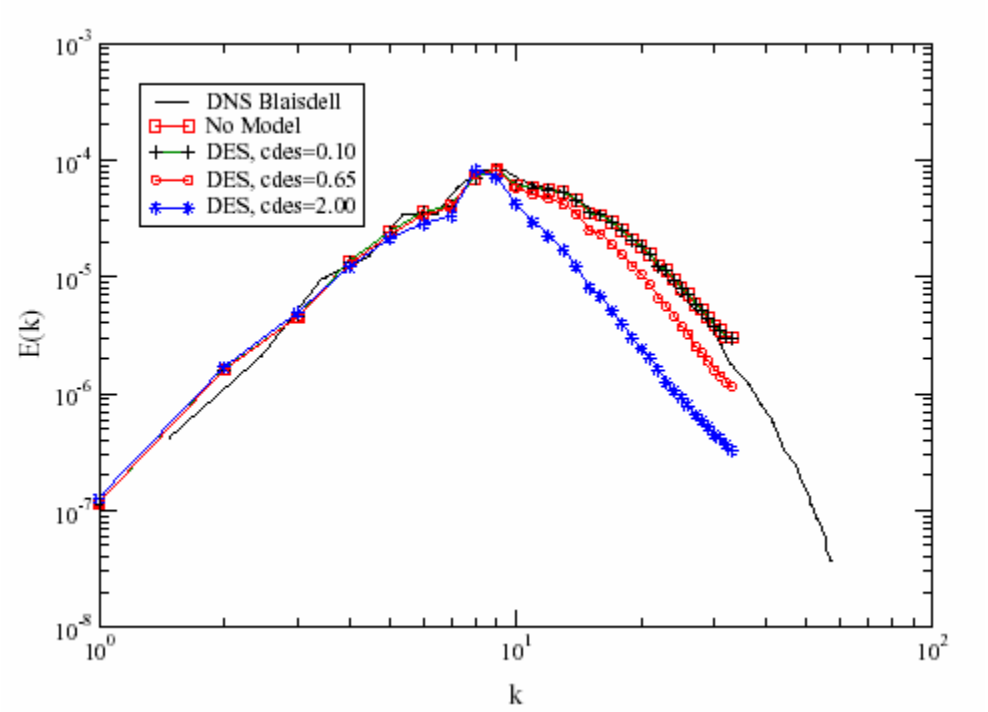

Figure 5.22(b): (64^3 grid) Variation of energy spectrum due to C_{DES} for Blaisdell's case at t=12

From Figure 5.23, we can see how the decay of the turbulent kinetic energy takes place in the Blaisdell's case. The decay rate may depend on many factors including the initial energy, the numerical diffusion of the model, the numerical scheme used and the value of C_{DES} when the Detached Eddy Simulation model is used. Decay curves have been plotted for various values of the grid sensitivity parameter C_{DES} in Figure 5.23. It can be seen that as the value of C_{DES} value increases, the energy decay rate also increases. The decay rate is lowest for the No Model case and C_{DES}=0.01 among the cases considered in the figure. This trend seems to be similar to that seen previously in Figure 5.22. It is interesting to note that the turbulent energy decay rate is almost the same for both the No Model case and C_{DES}=0.01 case. Also both of these cases have displayed similarity in behavior when we looked at the turbulent energy spectrum evolution after t=7.

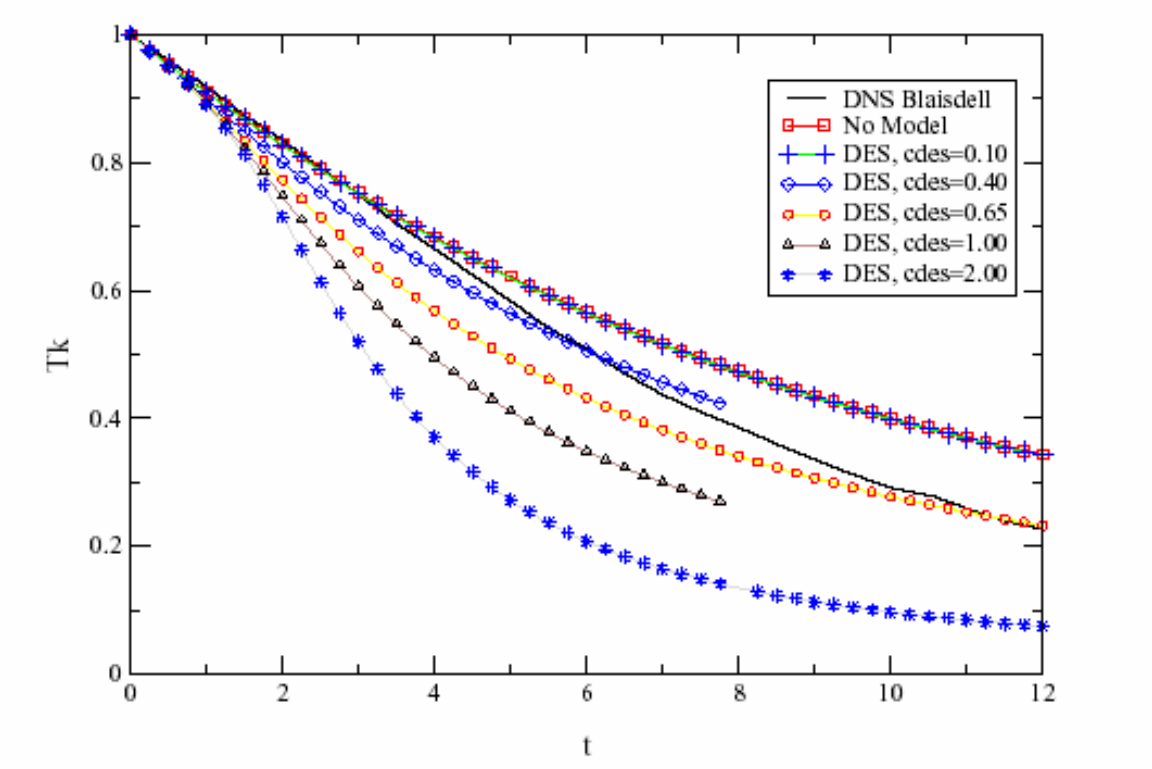

Figure 5.23: (64^3 grid) Comparison of energy decay for various values of C_{DES} with Blaisdell's DNS curve

From the above Figure 5.23, it can also be seen that C_{DES} is a strong factor affecting the turbulent energy decay early in the simulation. After a while the rate of decay is almost the same for all the cases considered above. Thus, over time the turbulent kinetic energy decay changes, starting with a high decay rate and slowly diminishes with time, attaining almost a constant rate at later times irrespective of the grid sensitivity parameter, C_{DES}. But it should be noted that the overall energy of the spectrum at any instant of time is strongly dependent on the value of C_{DES}. As seen above, a higher value of C_{DES} tends to dissipate the energy from the spectrum faster than when a lower value of C_{DES} is chosen. When compared to the Blaisdell's DNS spectra, the DNS curve is close to a value of C_{DES} which is in the range of 0.40 and 0.65. It is more close to C_{DES}=0.65 at later times.

In Figure 5.24, we see the energy spectrum for the 96^3 grid. It can be seen that as the grid sensitivity parameter increases from C_{DES}=0.10 to 2.00, the turbulent energy dissipation

rate increases, the trend that was observed even in the case of the 64^3grid results. But the details in comparison to the Blaisdell's DNS curve are different with the denser grid.

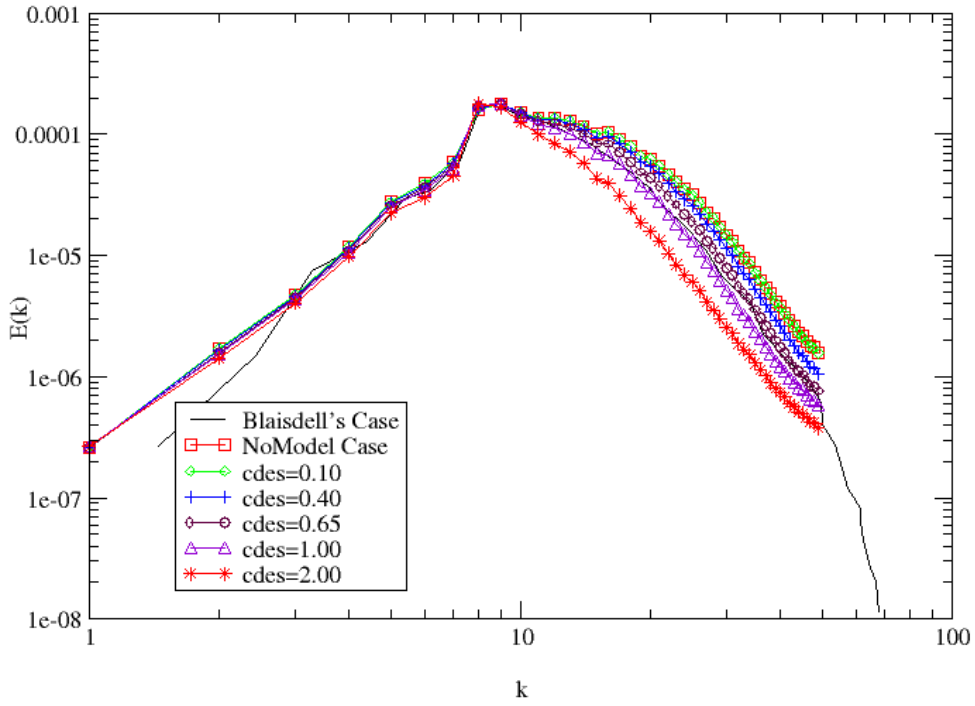

Figure 5.24: (96^3 grid) Comparison of energy spectra for various values of C_{DES} with Blaisdell's DNS spectra as the reference at t=7.

A zoomed version of Figure 5.24 is given in Figure 5.25, depicting the change of the energy spectra results as C_{DES} increases from 0.01 to 2.00 in comparison to the Blaisdell's DNS case. If we look closely, it can be seen that the C_{DES} values of 0.65 and 1.00 are the close matches to Blaisdell's DNS spectra. Initially, for the lower values of *k* the C_{DES}=1.00 is closely aligned with the DNS curve, but for higher values of *k*, the DNS spectra more closely matches the C_{DES}=0.65 curve. Hence for the 96^3grid, a C_{DES} value in the range of 0.65 to 1.00 would be a good value to consider for simulations.

Considering the 96^3 results, it is worth deliberating the mechanisms causing the shifts from the coarser grid results. One way of looking at it is that adding C_{DES} is like adding dissipation to the energy spectrum-the higher the value of C_{DES} the more is the dissipation added. But apart from the C_{DES}, there is an inherent physical dissipation which is added

to the model. But this inherent dissipation gets smaller as we move to higher density grids. This is because the higher density grids are closer to reality (or DNS resolution) than the lower density grids and hence less numerical dissipation needs to be added to the model. Eventually as the grid density gets very large there is no necessity of adding any numerical dissipation to the model or it would be negligible as the modeling effect would no longer be present at very large grid densities.

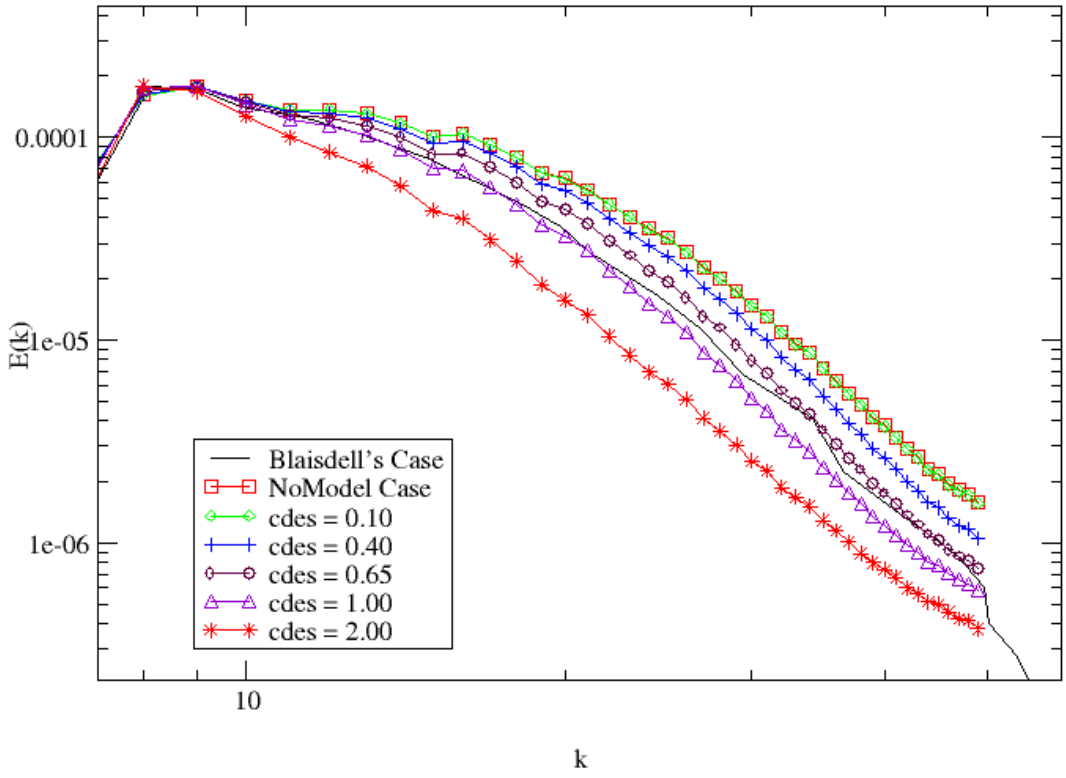

Figure 5.25: (96^3 grid) Comparison of energy spectra for various values of C_{DES} with Blaisdell's DNS spectra as the reference at t=7 (Zoomed View).

So, it can be seen that for the same case, say the No Model Case, the 96^3 grid would have less dissipation compared to the 64^3 grid. This can be seen in Figure 5.25 where the No Model case falls above the Blaisdell's DNS curve since it has relatively higher energy because of the lower inherent dissipation. So as seen from the results, the C_{DES} value close to and greater than 0.65 would be a better choice while using the Detached Eddy Simulation model for the 96^3 grid, while the No Model case is the best choice for the coarser grid.

5.3.2. 96^3 grid results and comparisons

Looking closely at the results of $64^3$and 96^3 in comparison to Blaisdell's DNS case, Figure 5.26 and Figure 5.27 give us a good insight.

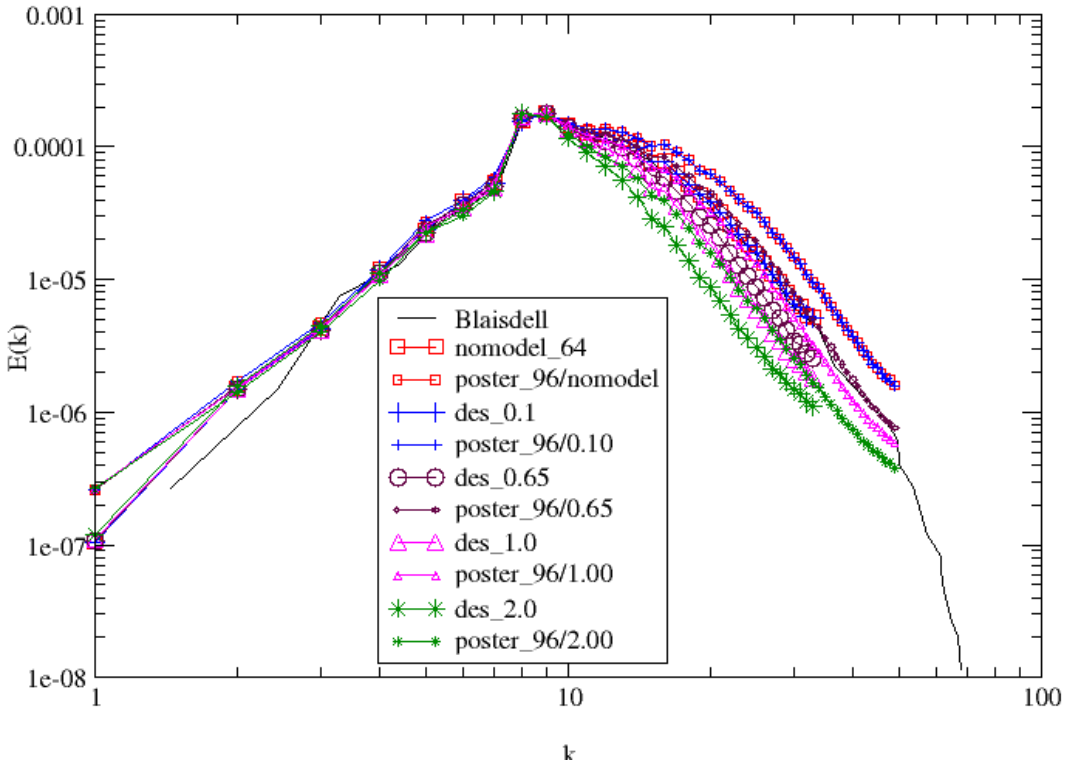

Figure 5.26: Comparison of energy spectra of 64^3 and 96^3 for C_{DES}=0.10, 0.65, 1.00 and 2.00 along with the No Model case and Blaisdell's DNS spectra as the reference.

Considering only the C_{DES} of 0.10, 0.65 and 1.00 which are close to the DNS results we will get to see a good range for both the grid densities considered around the Blaisdell's DNS curve.

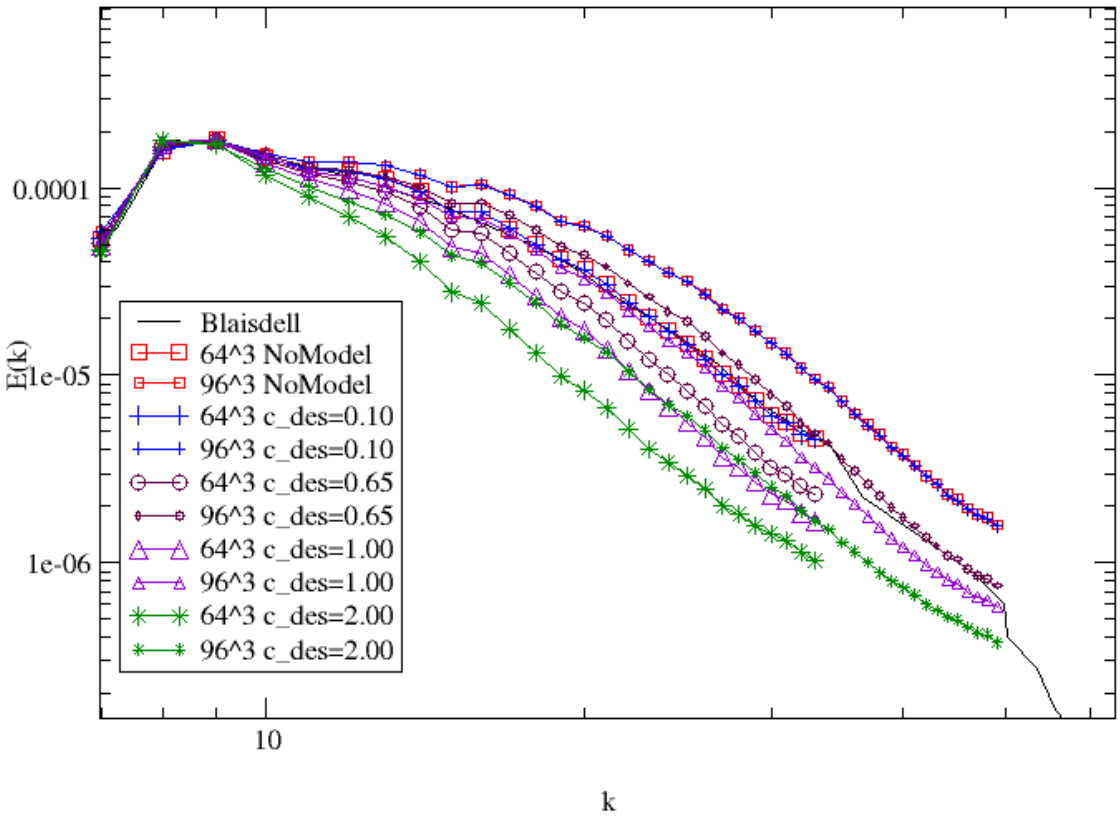

Figure 5.27: Comparison of energy spectra of 64^3 and 96^3 for C_{DES}=0.10, 0.65, 1.00 and 2.00 along with the No Model (MILES) case and Blaisdell's DNS spectra as the reference. (Zoomed version of part of Figure 5.19)

From Figure 5.27, it can be seen that C_{DES}=2.00 and C_{DES}=0.10 for the 96^3 and 64^3 grid results respectively deviate far from the DNS curve and hence can be safely avoided when the 100% numerical dissipation is used. As discussed earlier, the model dissipation and the inherent dissipation of a particular case decide the placement of the energy spectrum. Ultimately, we believe that as the grid density increases, the energy spectrum must coincide with the Blaisdell's DNS spectra without any addition of modeling effect or other artificial dissipation. But when we consider the No Model Case where there is no addition of artificial dissipation or model dissipation, the 96^3 grid deviates from the Blaisdell's DNS curve whereas the 64^3 No Model case matches well. So as the grid density is further increased, the energy spectrum should ultimately approach the DNS spectra. Hence we now look at the 128^3 No model case energy spectra.

5.3.3. 128^3 grid results and comparisons

In the Figure 5.28, we find a summary of results for the No Model case for various grid densities including 128^3, 96^3, 64^3 and 32^3 grids. Coincidentally, the 64^3 grid No Model case is the best match of all with the DNS spectra. However, as argued before the energy spectrum approaches the DNS spectra as the grid density is increased. The placement of the 32^3 grid is lower than the 64^3 grid as the artificial dissipation or the model diffusion is the highest in the 32^3 grid. But it can be clearly seen that as the grid density increases, the model diffusion decreases and also the inherent dissipation also reduces and hence the 128^3 grid is closer to the Blaisdell's DNS curve compared to the 96^3 grid. Though the 96^3 grid and the 128^3 grid seem to coincide for lower values of *k* (horizontal axis), as the grid progresses the 128^3 grid actually approaches the DNS curve more closely than the 96^3 grid as seen from the Figure 5.28.

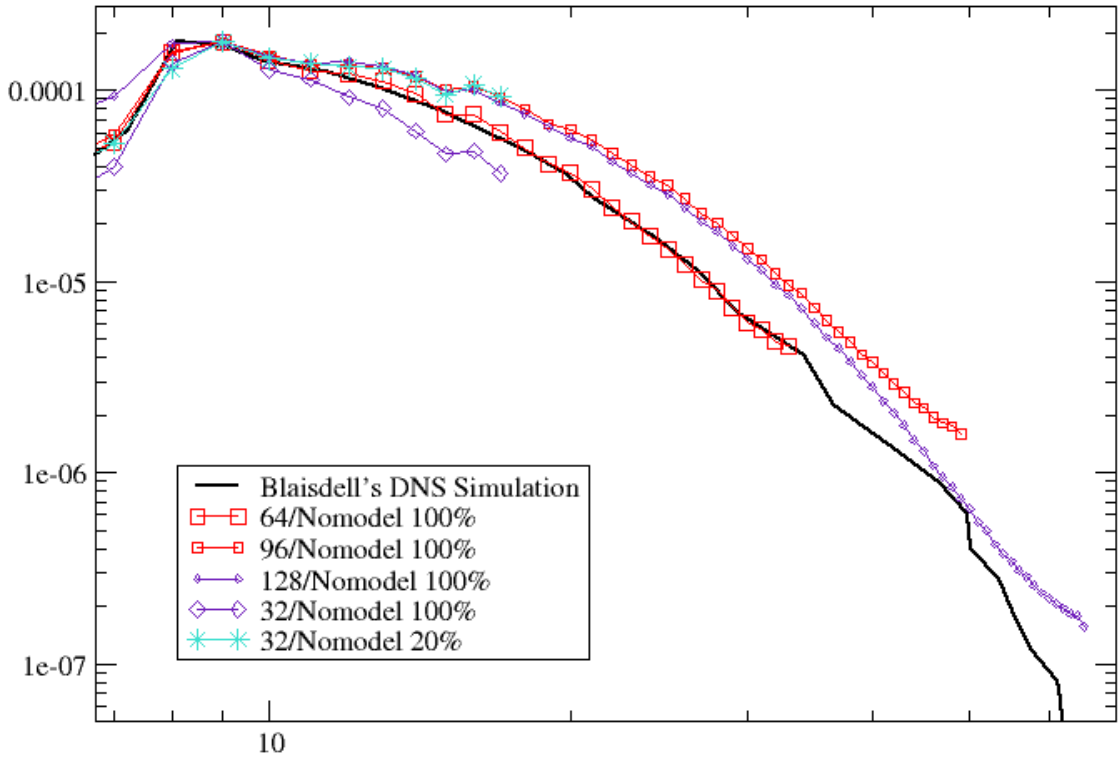

Figure 5.28: Comparison of energy spectra for various grid densities with Blaisdell's DNS spectra as the reference at t=7.

Using a 128^3 grid is obviously costly and time consuming compared to using a lower order grid. In the Figure 5.28, we also see the results for two 32^3 grids in comparison to other results. If dissipation is the major factor differentiating the higher and lower density grids, reducing the numerical dissipation for the 32^3 grid from 100% to 20% should help compensate for the lack of grid points. We see from the Figure 5.28 that by doing this, the resultant curve of 32^3 grid at t=7 actually coincides with the 96^3 and the 128^3 No Model 100% grid results. Therefore, we can actually achieve the right dissipation rate of the higher order grids by reducing the numerical dissipation of the lower density grids.

Alternately, one could use a central-difference scheme with a strong DES effect to create the necessary dissipation. Figure 5.29 presents an example of this approach, using the Detached Eddy Simulation scheme with a 6^{th} order Central difference scheme on a 32^3 grid with C_{DES}=3.00. This produces the right amount of dissipation to match both the 96^3 and 128^3 grid results.

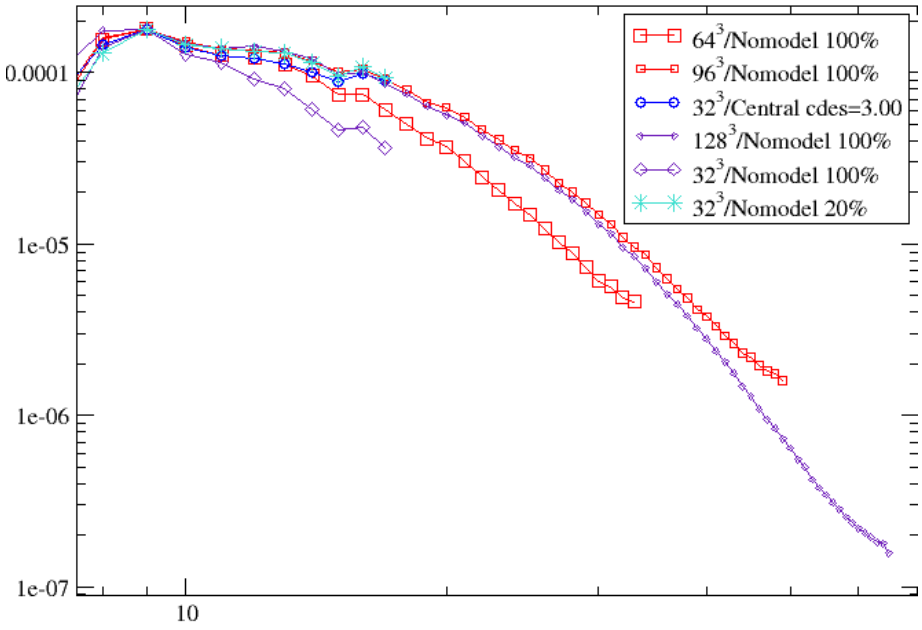

Figure 5.29: Comparison of energy spectra for various grid densities with Blaisdell's DNS spectra as the reference at t=7.

From the results obtained from the comparison with Blaisdell's DNS simulations, it can be concluded that it is important that the grid be first tested before running other cases so that the C_{DES} value is determined properly. As seen from the results obtained from the homogeneous turbulence simulation, the C_{DES} is definitely sensitive to the choice of the grid density and numerical dissipation and the numerical scheme used. More studies can be done with higher order grids to see when (or if) grid independency would be achieved. An open question is whether as the grid density keeps increasing, the model (DES) would finally approach DNS. Based on the 128^3 results, such a possibility remains open, but this will need to be left to future researchers with considerably more computer power.

Chapter 6

Discussions

6.1. Comparison of trends between Blaisdell and CBC Cases

In this report, similarities and differences between the two cases that we have dealt till now will be put across, LESTool simulations of Blaisdell *et al.*[10] and simulations of Comte-Bellot and Corrsin [12]. We shall also investigate if LESTool and DES have behaved consistently across these cases. Hence, we shall look more deeply into some specific aspects of each of the cases.

In the Blaisdell's case, we have run our cases using 32^3, 64^3, 96^3 and 128^3 grid and have compared our results obtained through LESTool with Blaisdell's DNS simulations. In the CBC case, we shall discuss cases run using 32^3, 64^3 and 96^3 grids and have compared our results obtained using LESTool with CBC's experimental results and other standard results from the literature.

6.1.1. Effect of Initial Energy Spectra

Since we are dealing with the simulation of Homogeneous Turbulence, it becomes necessary that we talk about initial conditions. Initial conditions are crucial in any unsteady turbulence model and we shall see how they affect the model.

Figures 6.1 and 6.2 are the initial conditions for the Blaisdell's case and CBC case, respectively. It is worth noticing from the Figure 6.1 and 6.2 (a), (b) and (c) below that as we increase the grid density, the initial condition approaches the standard reference case, i.e., either the Blaisdell's DNS or the CBC curve. This can also be quantitatively seen from the magnitudes of initial energy. In the CBC case, this can be seen very clearly quantitatively and graphically as we move from the 32^3 grid to 64^3 to 96^3 grid.

In the Blaisdell's case, this magnitude is lower for the 64^3 grid (0.0017995) and higher for the 96^3 grid (0.0018034) and should ideally approach the magnitude of energy under Blaisdell's DNS spectrum (0.0035084) at higher grid resolutions. As seen the areas under the curves are measured and we can see how close it gets to the ideal area (Blaisdell's case) as the grid density is increased. This is seen in Figure 6.1 below.

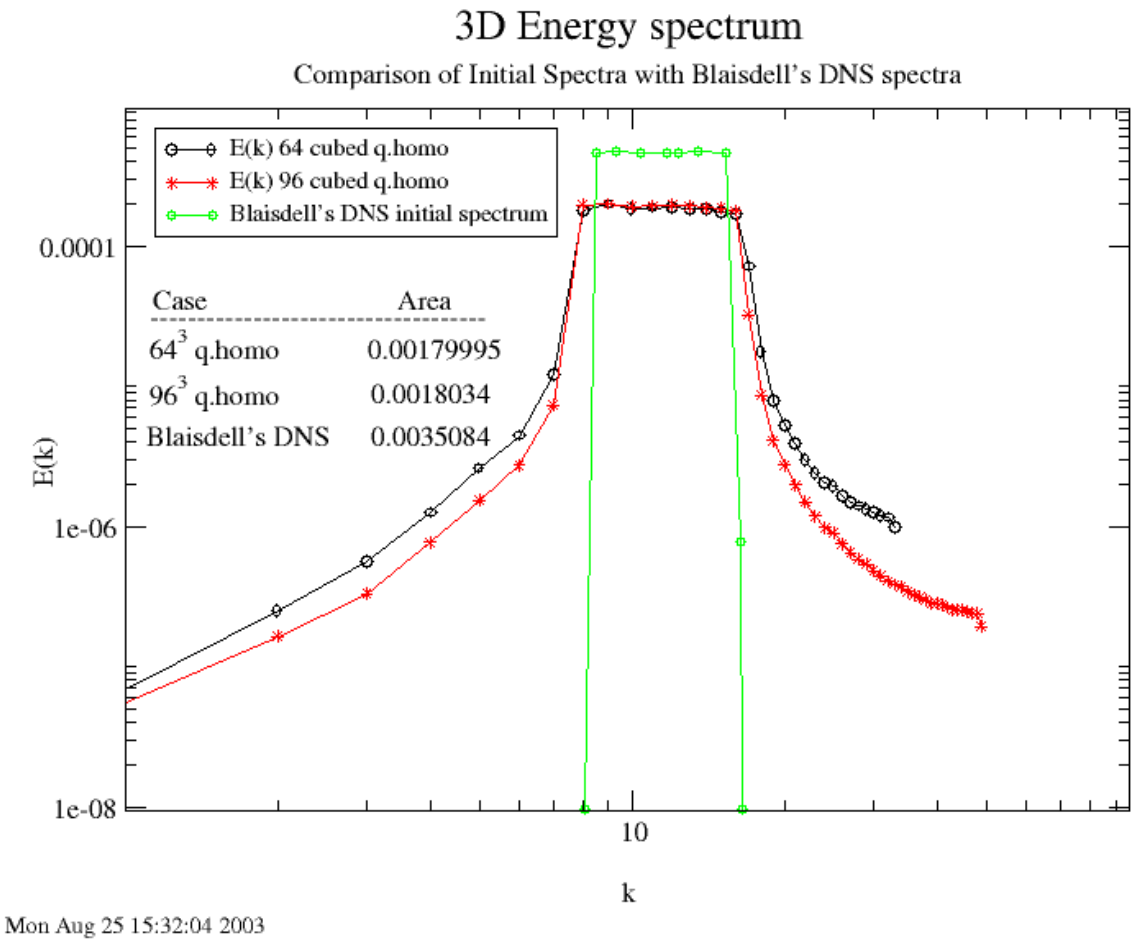

Figure 6.1: Comparison of initial spectra with Blaisdell's DNS spectra noticing the effect of grid density.

Figures 6.2 (a), (b) and (c) show the initial energy spectra for the CBC case. The same trend seen in Blaisdell's case is also seen here, i.e., as the grid density increases, the energy spectrum approaches the Blaisdell's energy spectrum in the Blaisdell's case and in the CBC case, it approaches the Knight's spectrum. Notice that in the case of the 32^3 grid, q.homo curve has an energy of 5.864×10^{-5} and the 64^3 grid curve has an energy of 5.994×10^{-5} and 96^3 grid has an energy of 6.0344×10^{-5} under the curve. Also the energies under the Knight's spectrum (E.dat) are 4.031×10^{-5}, 5.267×10^{-5} and 5.7849×10^{-5} for the 32^3, 64^3 and 96^3 grids respectively. Each of these curves approach the theoretical amount of energy (6.04995×10^{-5}) under the curve (explained in section 5.2.2).

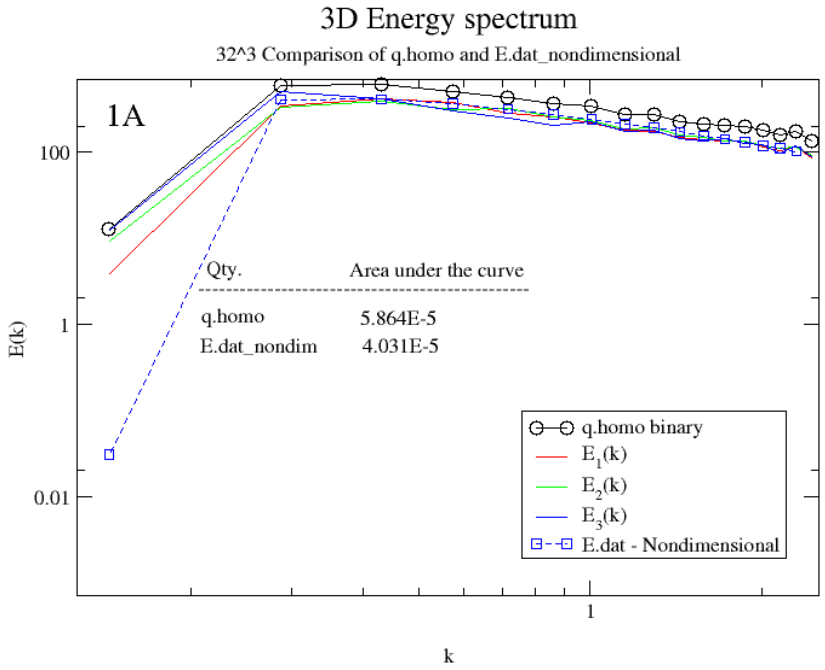

Figure 6.2 (a) 32^3grid initial condition

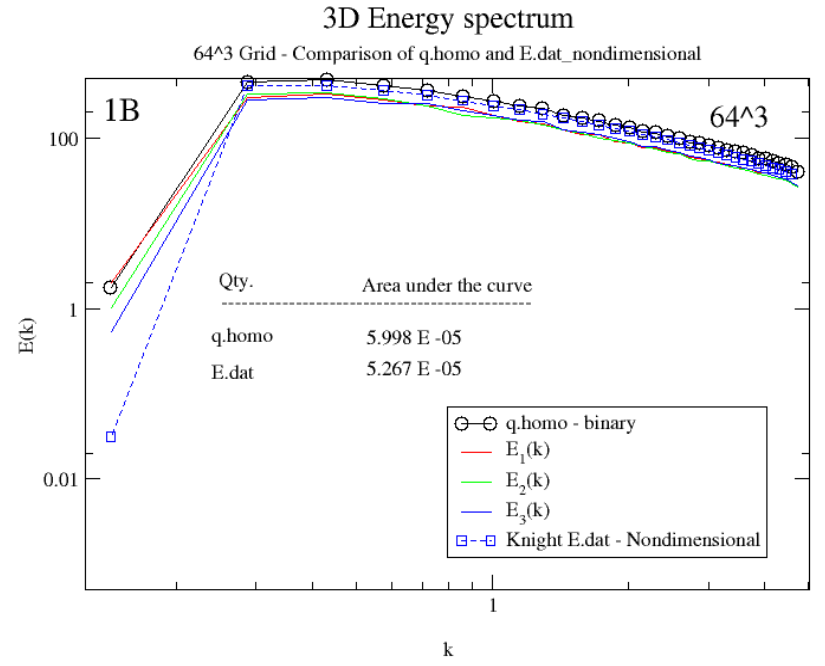

Figure 6.2 (b) 64^3grid initial condition

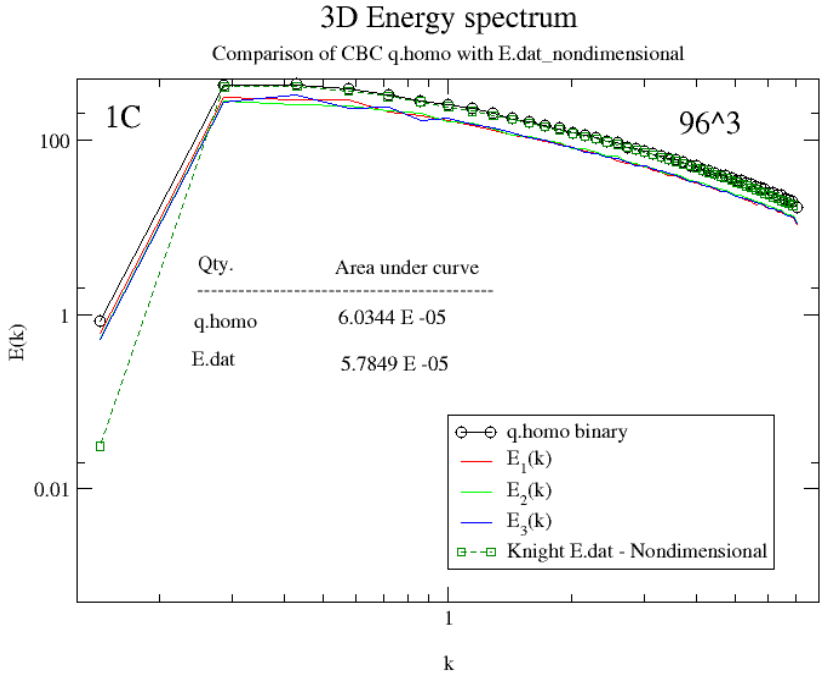

Figure 6.2 (c) 96^3grid initial condition

Figure 6.2: Comparison of initial spectra with Knight et al's spectra noticing the effect of grid density in the CBC case: (a) 32^3grid (b) 64^3grid and (c) 96^3grid.

Therefore in both cases the initial conditions improves noticeably if unsurprisingly as the grid density increases. This consistency establishes a baseline behavioral trend that will be seen again as we examine the effect of other parameters.

6.1.2. Effect of C_{DES}

Here the isolated effect of C_{DES} is examined independent of grid density, dissipation or any other numerical scheme. The Figure 6.3 (a) is produced with 100% numerical diffusion for the 64^3 grid using the 5^{th} order upwind scheme for the Blaisdell's case. Figure 6.3 (b) is shown using the 32^3 grid for the CBC case. As seen from Figure 6.3(a) and Figure 6.3(b), which are the Blaisdell and CBC cases respectively, C_{DES} as expected acts like a dissipation factor. Consistent with the discussion in Chapter 5, as the C_{DES} value is increased in each of these simulation cases, the slope of the curve increases and it becomes much steeper.

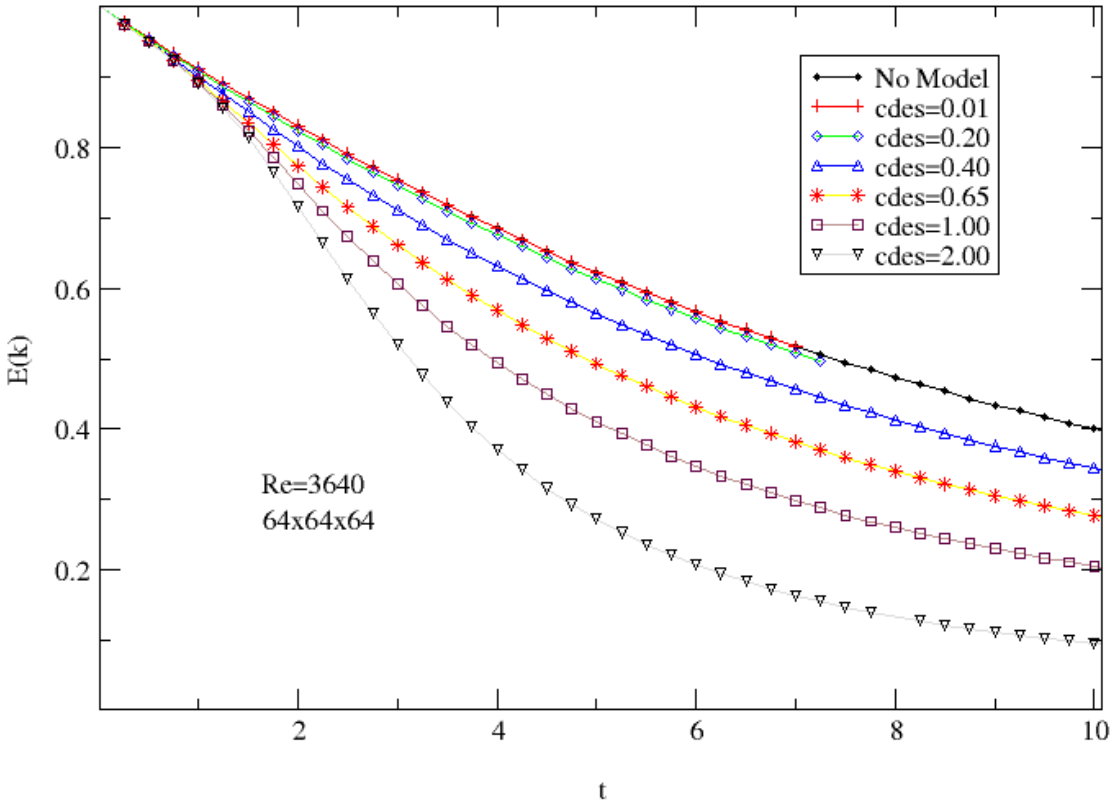

Figure 6.3(a): The effect of C_{DES} is seen clearly in the above Blaisdell's case. C_{DES} varies from 0.01 to 2.00.

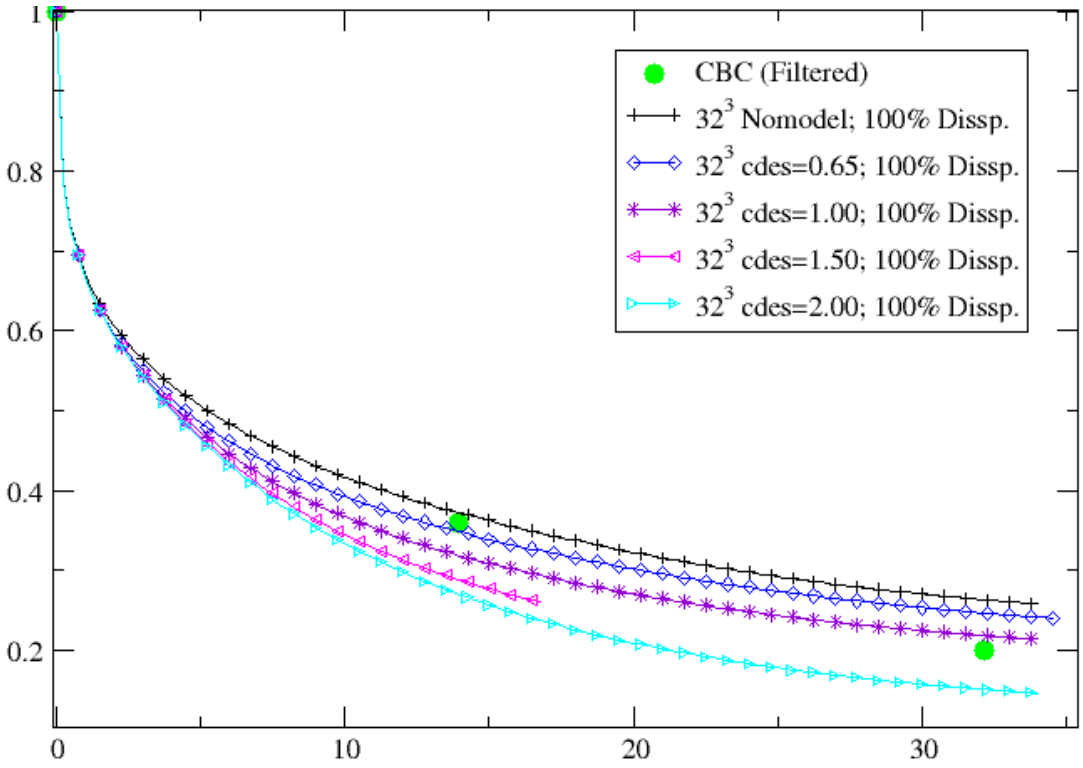

Figure 6.3(b): The effect of C_{DES} is seen clearly in the above CBC's case. C_{DES} varies from 0.65 to 2.00. This is shown for the 32^3 grid only for clarity.

As seen from Figure 6.3 (a) and 6.3 (b), as the value of C_{DES} is increased, the same trend is observed in both the cases – Blaisdell's case and the CBC case.

6.1.3. Effect of Numerical Dissipation

The numerical dissipation strongly affects the shape of the energy spectrum. Two values of numerical dissipation – 20% and 100% have been considered in each of the cases – Blaisdell's case and CBC case. As the dissipation is increased, the curve tends to become steeper. This can be seen in Figures 6.4 (a) and 6.4 (b), as the numerical dissipation decreases the slope of the curve is reduced. Hence the 20% dissipation curve is less steep than the 100% dissipation curve in both the cases. This trend of numerical dissipation is consistent in both cases.

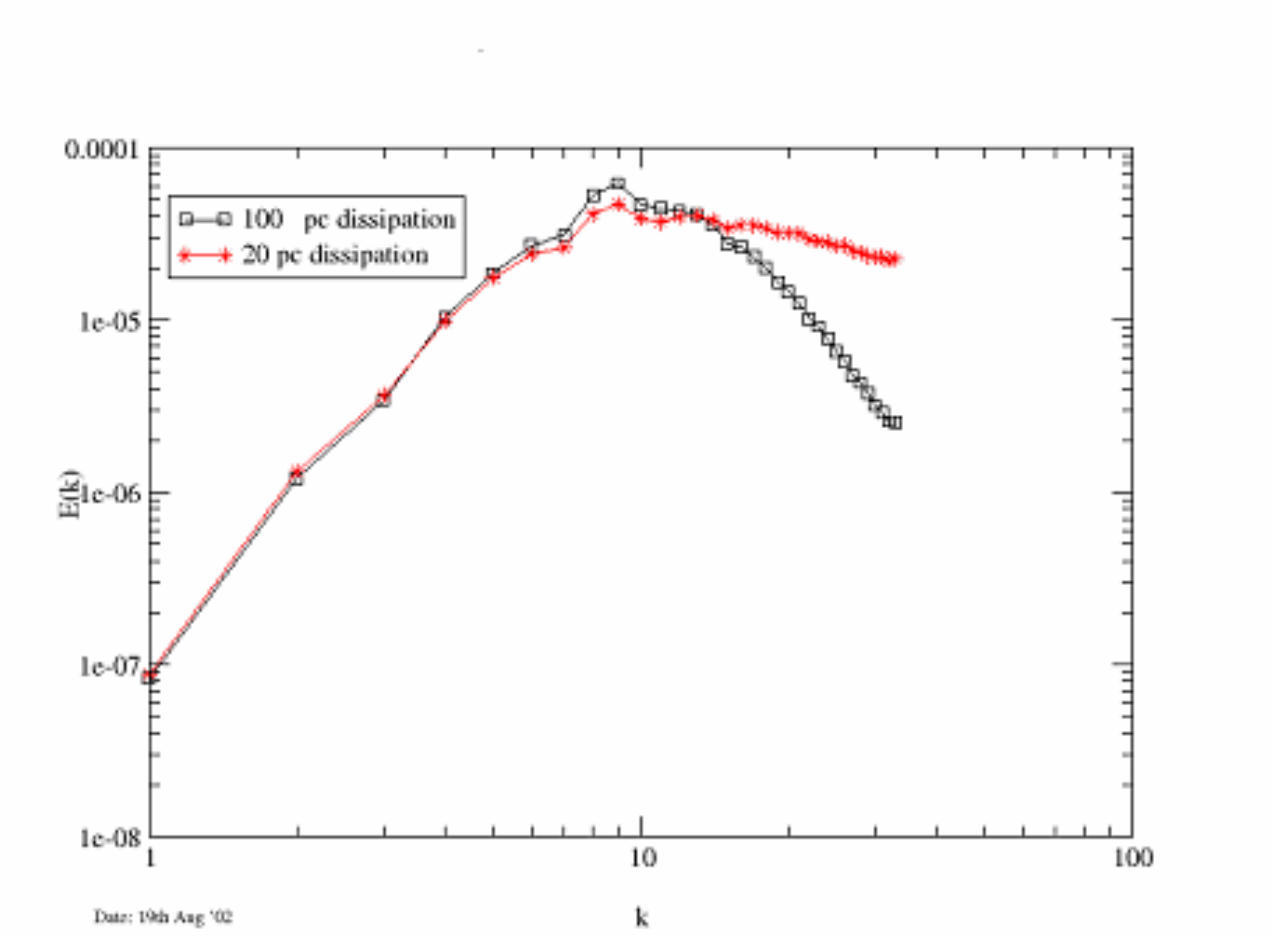

Figure 6.4 (a) Effect of Dissipation at t=7–Blaisdell's Case

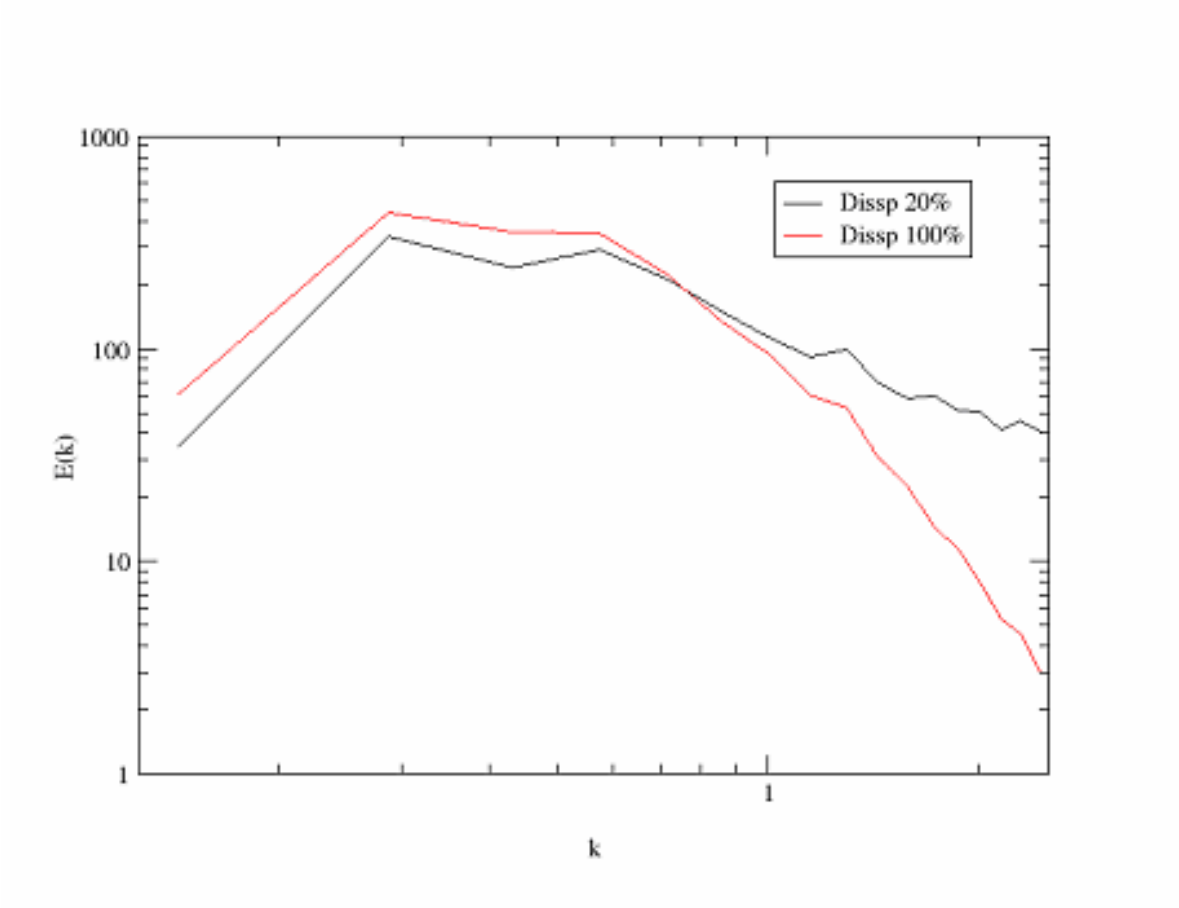

Figure 6.4 (b) Effect of Dissipation at *Ut/M*=98- CBC Case

The above discussed trend of numerical dissipation is seen consistently in both the cases namely Blaisdell's case and CBC case.

6.1.4. Effect of Grid Density

Figure 6.5 (a) and (b) illustrate that as the grid density increases, the slope of the curve decreases. This reduction in the slope is more prominent for lower values of *k* after the peak and later on the slope is almost the same for both the grid density curves. This is because as the grid density increases the artificial dissipation reduces as the modeling effect reduces. This extrapolates to the idea that at nearly DNS resolution, there is no modeling effect at all and the model purely behaves like the DNS scheme. Again, this effect appears to be case dependent.

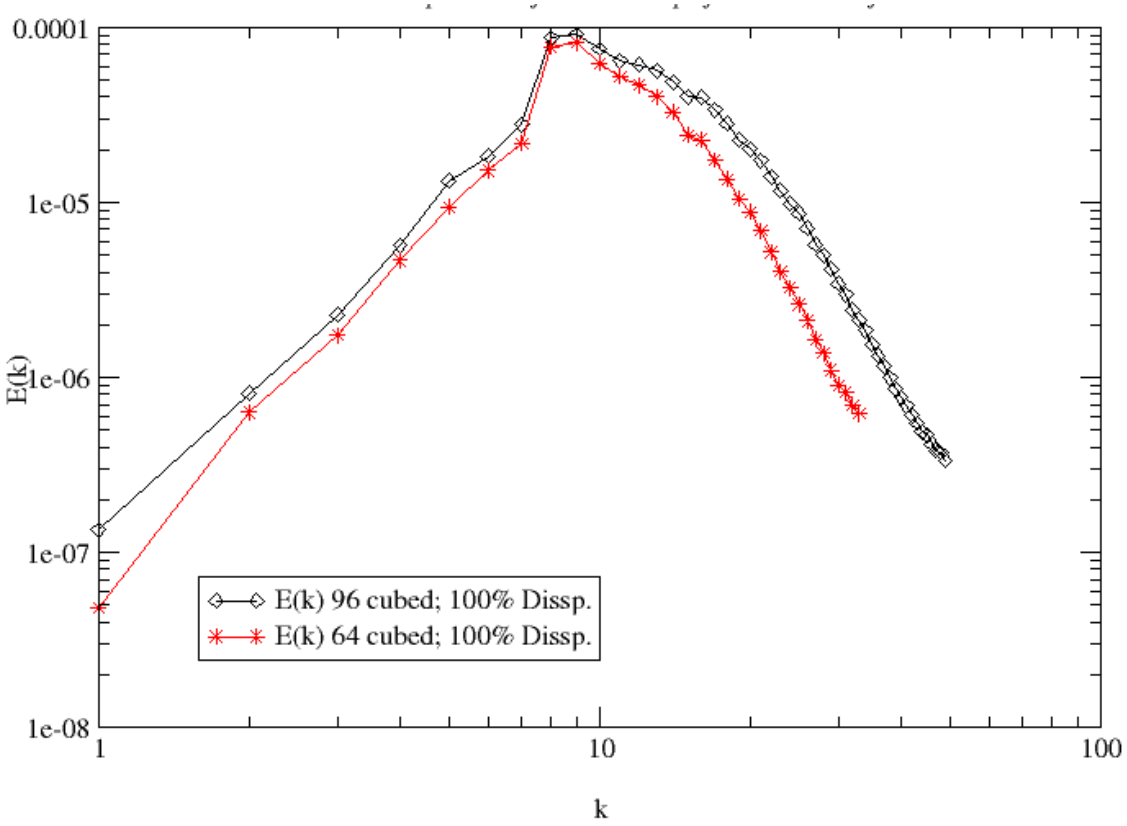

Figure 6.5 (a) Effect of Grid Density at t=7– Blaisdell's Case

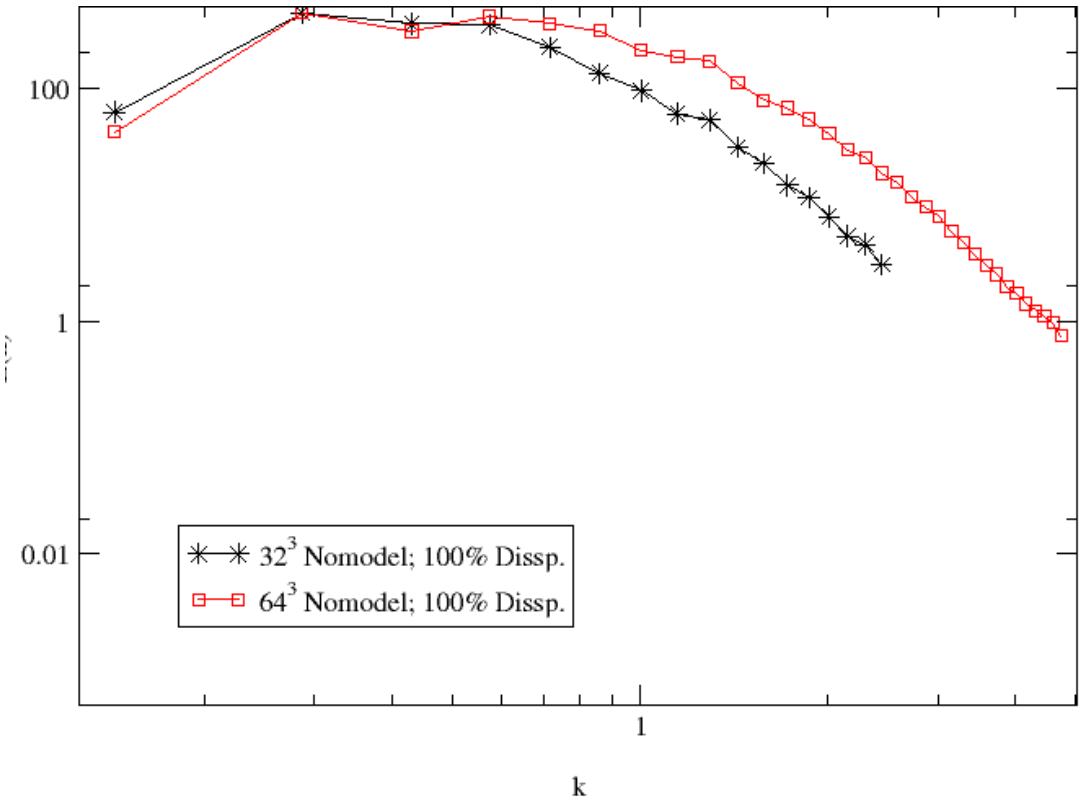

Figure 6.5 (b) Effect of Grid Density for No model Case at *Ut/M*=98– CBC Case

In the above Figure 6.5 (b), the magnitudes are not the actual ones. The curves have been hooked to compare the actual slopes. In other words, the peak points of both the curves have been joined without changing the relative position of the other points of the curve. This is different from the concept of scaling (explained in Chapter 5). Thus we see the isolated effect of grid density on the dissipation rate of the energy spectrum.

As seen from the results below, it can be seen that this behavior of grid density is very consistent in both the cases.

6.2. Review of Present Work

Computational Fluid Dynamics (CFD) has been a very useful tool since many decades. Many observations which were not feasible by carrying out experiments have been made by use of CFD. Over the years, the methods, techniques and approach has been improvised much to solve even complex cases. Yet, turbulence has remained one of the classical problems of physics still unsolved. We shall address some issues in this field

that need attention. This investigation has focused on the most fundamental test case in turbulence, that of homogeneous turbulence. We have run the Homogeneous Turbulence case with two different initial conditions, classified as Blaisdell's case and CBC case. In the Blaisdell's case, we have generated our initial conditions and compared our results with the DNS simulations of Blaisdell et al. In the CBC case, we have generated our initial conditions based on the benchmark experiment performed by Comte Bellot and Corrsin [1971]. Data in this case is specifically available at the initial and two other non-dimensional time evolutions, Ut/M=42, Ut/M=98 and Ut/M=171. Our results have been compared with the experimental data. We have also made comparisons to the numerical results produced by other researchers specifically Knight *et al.* and Spalart *et al.* The results obtained in both the cases are discussed by presenting the comparison of energy spectra and energy decay plots with their respective reference results.

In the present CFD research arena, modeling is the base of simulating any physical flow. But we have not reached a point where we could accurately predict the flow. DNS has been the tool of researchers ever since. It has been very useful in giving us a very good estimate of the flow pattern and properties. It is still a significant method widely used. But the economical burden it puts on the user is not something which could be sidetracked. The cost of DNS computation is proportional to the Reynolds number, $Re^{2.6}$ [18]. So for complicated flows, it becomes extremely difficult to still stick with DNS, even at this moment when computational power costs have slashed and technological advancement have given way to large scale commodity clusters capable of handling heavy jobs. In the case of Reynolds Averaged Navier Stokes (RANS) modeling, it is useful in cases which have only a mild separation of flow across the body and does a good job when there is no separation. But in the case of massively separated flows, it is known that RANS fails. Alternatively, we could use Large Eddy Simulation (LES). LES resolves the larger eddies and models the small scale eddies. But for boundary layer flows, LES resolution is not much different from DNS near the surface of the body.
Hence computationally it's not a widely viable method.

DES provides a unique blend of LES and RANS by tactically applying them at specific locations based on the grid spacing. Very close to the boundary we use the RANS model and far away from the wall we shift to the LES mode and use a subgrid

scale model. By using RANS instead of LES, we will be using 2000 times less number of cells than if we were to use the fully resolved LES mode. [18]

The initial conditions for both these case are generated using the spectral method. A program called 'Crecomp' has been used to generate these initial conditions. In the Blaisdell's case, the initial energy spectrum is a Tophat energy spectrum. This CBC energy spectrum shape was introduced in Chapter 4. In the CBC case, the initial energy spectrum has been generated adhering to the method suggested by Knight *et al* .[2]. Later other methods were presented in Chapter 4 which are modifications of this method which show promise of better initial condition shape.

In the Blaisdell's case with a Reynolds number, Re=3640, cases were run with 64^3, 96^3 and 128^3 grids. For each of the grids, a base case is run which is the No model case or the Monotone Integrated Large Eddy Simulation (MILES) case. This has the full 5^{th} order upwind scheme applied, a state we describe as 100% dissipation. Subsequent cases of less than 100% dissipation as well as Detached Eddy Simulation (DES) were then run in comparison. A 0% dissipation case corresponded to a 6^{th} order central scheme, which is invariably unstable without a DES model (and often is unstable even with one). When we ran with the DES turbulence model, we needed to specify the value for the grid sensitivity parameter, C_{DES}. One of our goals was to test the sensitivity of the DES model to the value of C_{DES}. To investigate this effect, we ran cases with the value of C_{DES} ranging from 0.1 - 2.0. When Spalart *et al.* proposed the DES model, they set the optimum value of C_{DES} as 0.65, which comes from the Homogeneous turbulence simulation [Shur et al]. We have investigated the relevance, importance and sensitivity of this parameter when running the DES model with the value of C_{DES} ranging from 0.1 – 2.0.

Our present discussion is only focused on homogeneous turbulence. It goes without saying that studying homogeneous turbulence alone would not solve the gamut of problems that DES is used in. But, it is important in the sense that Detached Eddy Simulation (DES) in itself is thoroughly investigated. This leads us to say that the sensitive issues that need to be heeded to and the shortcomings in the model would be known. Nevertheless, we would also know how robust and efficient the model is and at the same time the flexibility it provides to the user would also become transparent. This is

critical in advanced research as not only does it save a lot of time for the user but also gives a direction and guidelines in framing the model suiting his requirements. For example, if a user can run a case which requires a very dense grid; by adopting DES, he could probably get the same result by using a coarser grid by choosing the right grid sensitivity parameter C_{DES}, dissipation rate and the appropriate numerical scheme. Thus a smart model with a smart approach gives us the best results.

Numerically, in any computation as the grid density increases the result obtained should converge to the true solution usually. This is because, the physical solution is computationally well represented and the continuity increases as the grid spacing decreases. The limit of the numerical solution as the grid spacing tends to zero should be the actual solution. Of course, the cost keeps rising, but that is a different issue. However, with some numerical models this may not always be true.

The idea in turbulence model is that to keep the simulation stable, usually there is artificial dissipation added to the laminar or physical diffusion which is part of any physical flow. This makes the model stable without diverging. The more the dissipation added the more stable the model is. This artificial diffusion that is added is also called false diffusion. It is also true that as we increase the false diffusion in the model, the solution deviates more from the true solution. So, it is advisable to just add the right amount of artificial diffusion so as keep the code from not diverging. However, it is critical to note that as the grid density increases, the artificial diffusion keeps decreasing. This happens because higher grid densities more fully resolve the eddies that govern the physics of turbulence. Hence it becomes a better representation of reality or the actual physical solution. This means that as we reach the DNS resolution, we should practically lose all modeling effect as there is no need for modeling at that level.

In order to validate the DES model the following tasks were performed

a. Literature survey

b. Grid spacing parameter, C_{DES} studies

c. Grid density dependency

d. Dissipation studies

e. Numerical scheme effects

f. Comparison of results with published results.

There was a lot of work done by many research on Homogeneous Turbulence. Their insight in understanding homogeneous turbulence and modeling it would help us in starting off at a higher stand. DES is not new now and there are a lot of research groups that have used DES to obtain good results. It would also help if we get an insight of their research work.

As already said, C_{DES} studies are an important process of validating DES. Apart from a detailed analysis of the grid spacing parameter C_{DES} , studies on dissipation rates and the numerical schemes are also made. Since LESTool is being used for all our simulations, we need to ascertain if LESTool is the proper tool we have in our hands or not. Other simulations using LESTool have been done, prior to its use on Homogeneous Turbulence. Hence we do not have concerns about using LESTool. Relative comparisons of all our cases and comparisons made with the classical and the present research going on would help us make useful deductions about our research. Hence we are moving in the right direction in tackling the problem at hand and achieving our goal. There are basically three types of Dissipation

1. Dissipation due to the viscosity called 'laminar dissipation'
2. Numerical dissipation
3. Dissipation due to the model also called 'Model Dissipation'

Let us go deeper into these dissipative effects and speculate how they really matter. When we do not use any turbulence model for our simulations, all that matters is the laminar diffusion which exists inherently in any simulation which has to be accounted for in any physical process. Also, when we use the No Turbulence Model which is actually called MILES (Monotone Integrated LES), we do not have any artificial dissipation involved.

The only effect that pure No Turbulence Model would have is the effect of laminar viscosity, which is natural, but we could decrease or increase the numerical dissipation to make the simulation more stable or even just to observe the trend, the way the model behaves.

Truly, dissipation is a stabilizing mechanism. In fluid flows as time progresses, the energy decays in the form of eddies; larger eddies become smaller eddies which in turn break down into even smaller eddies, finally only to be dissipated by the effect of

fluid viscosity and converted into internal energy. Now, this natural phenomenon has to be imitated by a numerical model. How best we can imitate this for the various physical situations that may arise as the case becomes complicated decides how good the model is. There are various models that have been developed over time and there are still models evolving. Some models suit for some flow patterns or situations better than the other, for e.g., RANS is not so good when separation has to be predicted, DES is a better choice, based on some established results. What we use in our research is the Spalart-Allmaras model or more conveniently known as the S-A model. The main parameter which governs this model is C_{DES}. By tuning C_{DES}, we are actually controlling the dissipation rate. Even this is artificial diffusion, which we add to the simulation, but more clearly, this is provided by the model and hence termed as model diffusion. It is important that this parameter be tuned and its significance be understood for this study.

There are many instances where the present researchers have worked on and made use of DES to study cases. Many have got decent results from their studies. But no one has gone to the extent of making a detailed analysis of the model and its parameters. An attempt in that direction as we did is certainly very beneficial and we aim to focus on this aspect.

In our simulations, we have considered the grid densities so as to cover many aspects of our research. One important thing was to see how the model adapts and reacts to the change in grid density. For this we definitely had to have a gradation in grid density. Secondly, we also needed to confirm the concept of grid independence, that is to say that as we keep increasing the grid density the solution should change no more. This happens when we reach the DNS resolution beyond which there wouldn't be any change as all the length scales would have been sufficiently resolved. But the question is, is DES useful if we have to use such highly dense grids. The answer is no, but research in that direction is necessary to confirm that. The idea of the model is that we use a grid which suits our budget and problem and then use an appropriate value of C_{DES} and dissipation rate, choosing a proper numerical scheme to get satisfactory results without having to use huge resources in terms of computation and economy.

The work that we have done is very beneficial to the research community. However, it doesn't give an exhaustive analysis of the model. To do that more time and

testing is needed. But at this point, we have covered many aspects providing a good insight into the working of the model.

Apart from working on homogeneous turbulence, this work can be extended to flow over a cylinder. We could use the same analysis used in homogeneous turbulence. It would be a good case to support and ascertain the present trend of results.

The limiting factors for this present research work are the time, computational resources and compatibility. Though, we have good computer resources, to run cases with grid density of 96^3 and higher, it is a heavy task on the IRIX(SGI) machines used and even on the NCSA machines it takes up a lot of time. We have excellent Linux clusters which could be put to use, but the MPI version of LESTool suitable for the Linux platform is in the process of development. So since this problem will be solved soon, we should have good resources to build our cases in any future study.

Chapter 7
Conclusions and Future Work

7.1.Conclusions and Recommendations

A comprehensive examination along with different trials in each of the test cases has much to reveal. Initially, starting off on the test cases, the effect of initial conditions was considered. In this case, two different aspects of initial conditions are important which are (1) The magnitude of the spectrum, which is the value of the area under the curve. (2) The shape of the spectrum which is a representation of the slope of the curve. The slope of the curve is of great importance. It helps us in determining the decay rate and how the decay rate changes and also allows us to compare with other cases and study the trend of the simulation.

Based on the above observation, it has been seen that the magnitude of the initial condition has a strong effect, although the shape especially in the CBC case where the wave number is low (nearer to the peak) plays a vital role. Also, by scaling the curve, the effect of magnitude in the initial conditions can be nullified. But the shape of the curve is crucial in terms of obtaining accurate results. So an effort has to be put in obtaining a proper shape and magnitude in terms of the initial conditions.

It has been seen in both our test cases that numerical dissipation has had a very great impact on the quality of results. It is clear that increase in dissipation gives us stable results, but also introduces artificiality in the model. As seen, we have the best results when we have the least percentage of numerical dissipation. We have run all our cases including the No Model case with the 5^{th} order upwind scheme. As we reduce the percentage of numerical dissipation, we approach the 6^{th} order central difference scheme. Hence, as seen if we were allowed to use this scheme we would get good results. But in our case, some of the No Model cases get unstable when using the central difference scheme. Hence, the best solution is using a 5^{th} order upwind scheme with 20% dissipation. This has produced very good results.

Though the study of high Re flow would be more interesting and useful for testing the DES (Detached Eddy Simulation) model, choosing a low Re (as in the Blaisdell's case) also would be very beneficial in drawing many important conclusions about the

behavior of the model and the interdependencies of various parameters within the model and its implications on the results.

The effect of grid density has been studied appropriately within the limitations that were placed. It has been seen that high density grids have consistently given us good results and in fact better results than the corresponding low density grid results. It is evident and also has been explained before why this is so. The high density grid better represents the physical flow compared to the low density grid. In the low density grid, the intermediate filtered out physical quantities have to be estimated properly and it depends on the model how well they are represented. However, low density grids also have given us decent results. The contention is that, when we use a turbulence model which models the flow accurately taking into account the information lost with the small-scale eddies, we gain in many ways. First of all, if we did not have the necessity of modeling, we would as well use the DNS (Direct Numerical Simulation) scheme to run our cases. But this is not feasible and not a practical solution because of the amount of time, cost and resources that would be needed especially for flow with high Re numbers and complicated geometries. Thus modeling shows us an easy way out by optimizing all that are available within limits and simultaneously obtaining decent results.

In the present case, using the DES model, we can use the lower density grid to obtain very good results if we were to use the right value of C_{DES} and the proper numerical scheme with the numerical dissipation that is appropriate. From the results that have been obtained, for most situations, it would be better to use a central difference scheme. But if the central difference scheme if unstable, the 5^{th} order upwind scheme with a numerical dissipation of 10-20% would be ideal. The value of C_{DES} that DES model could work well is in the range of about 0.2 - 0.65. Since No Model scheme has been giving decent results in the Blaisdell's case for 64^3 grid, and since lower the C_{DES} closer is the model to No Model, it is better to use a low value of C_{DES} for coarser grids and a higher value of C_{DES} for denser grids but not higher than 0.65. Also, from a series of observations in the CBC case, a numerical dissipation of 40-50% with a C_{DES} of 0.65 has given us the best decay curve results. The shape or slope of the curve was mainly influenced by the numerical dissipation, whereas the C_{DES} influenced in shifting the curve or changing the overall magnitude of the curve. So ideally, it is a proper combination of

the C_{DES} and the numerical dissipation that works out best, but as a general guideline, what was proposed earlier would be good enough.

7.2.Future Work

A lot of findings have been made in the present research work. But still, as always, there is scope for improvement by way of development of better models and better propositions. The present research has been limited to the case of homogeneous turbulence investigating the DES model. But LESTool can actually be used to handle many more test cases. A consistency in all of these research results would mean a more stable code, reliable results and would help in getting affordable solutions. LESTool is known to have given good results for channel flow based on an earlier work at University of Kentucky, Lexington. DES could be implemented into it and the results could be assessed quickly to gain a better perspective. Also, as an extension to the present work, the flow over a cylinder can be considered and studied for different Reynolds numbers.

Appendix A
Crecomp

The program *Crecomp* is mainly intended to create the initial conditions for homogeneous turbulence. It creates the velocity, density and temperature fields with a prescribed energy spectrum in Fourier space. For creating a divergence free energy spectrum, first the fields are initialized with random numbers. Then the Fourier transformation of the velocity components is performed and a projection onto a wave number vector computation of the compressible and incompressible velocity components is done. Next, the prescribed energy spectrum is computed and a back transformation is done. Finally, the spectrum is normalized and the data is written for LESTool.

The energy spectrum is defined in defined in the fashion the user desires using the input file. In the CBC case, the initial energy spectrum was defined using the curve fit of the data points taken from the CBC paper (Genevieve Comte-Bellot *et al*., 1971). Knight *et al.* (1991) proposed this technique of polynomial curve fitting and the method has been utilized along with exploring other possible ways. Here is the part of the code which explains the polynomial curve fitting for the generation of initial conditions.

```
!+ the experimental spectrum by Comte-Bellot and Corrsin
   SUBROUTINE spec_cbc(kmax, akf, spksol)
     integer, intent(in) :: kmax
     real(prec), intent(out) :: akf(kmax)
     real(prec), intent(out) :: spksol(kmax)

     real(prec), parameter :: L = 43.787
     real(prec), dimension(0:4), parameter :: alpha = &
       (/ 4.7935398, -1.3284141, -0.2146974, -0.0314604, -0.0169870 /)

     real(prec) :: ak, akl, E11
     real(prec) :: E11log(kmax), lak(kmax)
     integer :: k
```

```
  do k=1,kmax
    ak = 2.0_prec*pi*real(k,prec) / L
    akf(k) = ak
    lak(k) = log(ak)
    akl = log(ak)
    E11 = alpha(0) + alpha(1)*akl + alpha(2)*akl**2 + &
        alpha(3)*akl**3 + alpha(4)*akl**4
    E11 = exp(E11)
    e11log(k) = log10(E11)
    spksol(k) = E11*( 0.5_prec*(alpha(1) + 2.0_prec*alpha(2)*akl + &
        3.0_prec*alpha(3)*akl**2 + 4.0*alpha(4)*akl**3)**2 + &
        alpha(2) - alpha(1) + (3.0_prec*alpha(3)-2.0_prec*alpha(2))*akl &
        + (6.0_prec*alpha(4) - 3.0_prec*alpha(3))*akl**2 - &
        4.0_prec*alpha(4)*akl**3)
  end do
  open(nspc, file='e11.dat')
  write(nspc, *)'# k, e11'
  do k = 1, kmax
    write(nspc, '(2e16.5)') lak(k), e11log(k)
  end do
  close(nspc)
END SUBROUTINE spec_cbc
```

References

[1] A. Hamed, D. Basu, K. Das, AIAA 2003-0549, *"Detached Eddy Simulations of Supersonic Flow Over Cavity"*.

[2] Andrei Travin, Michael Shur, Michael Strelets, Philippe Spalart, Federal Scientific Center, Seattle, WA, *"Detached Eddy Simulation Past a Circular Cylinder",* Flow, Turbulence and Combustion 63: 293-313, 1999.

[3] Arne Johansson, Department of Mechanics, KTH, Sweden, *"Engineering Turbulence Models and Their Development, With Emphasis on Explicit Algebraic Reynolds Stress Models",* Manuscript.

[4] Aroon K. Viswanathan, Kory R. Klismith, James R. Forsythe, Kyle D. Squires, Aerospace Sciences Meeting 2003, Jan 2003, Reno, Nevada, "*Detached Eddy Simulation around a Forebody at High Angle of Attack"*.

[5] Daniele Carati, Sandip Ghosal, and Parviz Moin, Center for Turbulence Research, Stanford University, California, *"On the representation of backscatter in dynamic localization models",* Phys. Fluids 7 (3), March 1995.

[6] Doyle Knight, Gang Zhou, Nora Okong and Vijay Shukla, " Compressible Large Eddy Simulation Using Unstructured Grids", AIAA Paper, 1998.

[7] Evangelos T. Spyropoulos and Gregory A. Blaisdell, Purdue University, West Lafayette, Indiana, "Evaluation of the Dynamic Model for Simulations of Compressible Decaying Isotropic Turbulence", AIAA Journal, Vol. 34, No. 5, May 1996.

[8] Fotini V. Katopodes, Robert L. Street, Joel H. Ferziger, Environmental Fluid Mechanics Laboratory, Stanford University, CA, *"Subfilter-Scale Scalar Transport For Large-Eddy Simulation",* Technical Report 2000-K1, March, 2000.

[9] F. R. Menter, M. Kuntz and R. Bender, CFX Germany, Otterfing, *"A Scale-Adaptive Simulation Model for Turbulent Flow Predictions",* 41st Aerospace Science Meeting and Exhibit, Reno, Nevada, 6-9 January 2003.

[10] G. A. Blaisdell, N. N. Mansour, W. C. Reynolds, Department of Mechanical Engineering, Stanford University, *"Numerical Simulations of Compressible Homogeneous Turbulence",* Report No. TF-50, January 1991.

[11] G. Erlebacher, M. Y. Hussaini, C. G. Speziale, T. A. Zang, NASA Langley Research Center, Hampton, VA, *"Toward the Large-Eddy Simulation of Compressible Turbulent Flows",* J. Fluid Mech. 238, 155-185, 1992.

[12] Genevieve Comte-Bellot, Stanley Corrsin, "Simple Eulerian time correlation of full and narrow-band velocity signals in grid-generated, 'isotropic' turbulence", J.Fluid Mech., 1971.

[13] G. R. Ruetsch and M.R. Maxey, Center for Fluid Mechanics, and Computation, Brown University, Providence, Rhode Island, " Small-scale features of vorticity and passive scalar fields in homogeneous isotropic turbulence", Phys. Fluids A 3 (6), June 1991.

[14] James R. Forsythe, Klaus A. Hoffman, Fluids 2000, June 2000, ' *Detached Eddy Simulation of a Supersonic Axisymmetric Base Flow with an Unstructured Solver".*

[15] James R. Forsythe, Klaus A. Hoffman, Russel M. Cummings, Kyle D. Squires, Journal of Fluids Engineering, Dec 2002, "*Detached-eddy simulation with compressibility corrections applied to a supersonic axisymmetric base flow".*

[16] J. R. Chasnov, Center for Turbulence Research, NASA Ames Research Center, Moffet Field, California, *"Similarity states of passive scalar transport in isotropic turbulence",* Phys. Fluids 6 (2), February 1994.

[17] L. Biferale, G. Boffetta, A. Celani, A. Lanotte, *"The decay of homogeneous anisotropic turbulence",* Phys. Fluids, Vol. 15, No. 8, August 2003.

[18] L. Temmerman, "Near-Wall Modelling in Hybrid LES/RANS Schemes for High Reynolds Number Flows", Short Report.

[19] Massimo Germano, Ugo Piomelli, Parviz Moin, and William H. Cabot, Center for Turbulence Research, Stanford, California, " A dynamic subgrid-scale eddy viscosity model", Phys. Fluids A 3 (7), July 1991.

[20] Meng Wang, Pietro Catalano, Gianluca Iaccarino, Center for Turbulence Research, Annual Research Briefs, *"Prediction of high Reynolds number flow over a circular cylinder using LES with wall modeling"*, 2001.

[21] M. Shur, P. R. Spalart, M. Strelets, and A. Travin, Engineering turbulence modeling and experiments, "*Detached-eddy simulation of an airfoil at high angle of attack",* Proceedings of 4th International Symposium on Engineering Turbulence Modeling and Measurements, 1999.

[22] M. Strelets, "*Detached Eddy Simulation of Massively Separated Flows*", 39th AIAA Aerospace Sciences Meeting & Exhibit, 8-11 January 2001, Reno, NV.

[23] N. V. Nikitin, F. Nicoud, B. Wasistho, K. D. Squires, P. R. Spalart, *"An Approach to Wall Modeling in Large-Eddy Simulations",* Phys. Fluids, Vol. 12 (7), pp. 1627 – 1632, July 2000.

[24] O. J. McMillan, J. H. Ferziger, *"Direct Testing of Subgrid-Scale Models"*, AIAA 17th Aerospace Sciences Meeting, New Orleans, LA, Jan. 15-17, 1979.

[25] P. D. Ditlevsen, M. H. Jensen and P. Olesen, Niels Bohr Institute, Copenhagen, Denmark, *"Scaling and the prediction of energy spectra in decaying hydrodynamic turbulence",* arXiv:nlin.CD/0205055 v4, Sep 2002.

[26] P. R. Spalart, S. R. Allmaras, Boeing Commercial Airplane Group, Seattle, WA, *"A One-Equation Turbulence Model for Aerodynamic Flows",* 30th Aerospace Sciences Meeting and Exhibit, Reno, NV, January 6-9, 1992.

[27] Spalart P.R., Jou W.H., Strelets M., Allmaras S.R.: *Comments on the feasibility of LES for wings, and on a hybrid RANS/LES approach*, 1st AFOSR Int. Conf. on DNS/LES, Aug. 4-8, 1997, Ruston, LA. In: Advances in DNS/LES, C. Liu and Z. Liu Eds., Greyden Press, Columbus, OH, USA (1997).

[28] Richard Anderson, Charles Meneveau, Department of Mechanical Engineering, The Johns Hopkins University, MD, *"Effects of the Similarity Model in Finite-Difference LES of Isotropic Turbulence Using a Lagrangian Dynamic Mixed Model",* Flow, Turbulence and Combustion 62: 201-225, 1999.

[29] Robert A. Clark, Joel H. Ferziger, W. C. Reynolds, *"Evaluation of subgrid-scale models using an accurately simulated turbulent flow"*, J. Fluid Mech., Vol. 91, part 1, pp. 1-16, 1979.

[30] Robert D. Moser, John Kim, Nagi N. Mansour, *"Direct numerical simulation of turbulent channel flow up to* Re_τ*=590",* Phys. Fluids, Vol. 11, No. 4, April 1999.

[31] S. M. de Bruyn Kops and J. J. Riley, "Direct numerical simulation of laboratory experiments in isotropic turbulence", Department of Mechanical Engineering, University of Washington, Seattle, Phys. Fluids, Vol. 10, No. 9, September 1998.

[32] S.Scott Collis, " Numerical Simulation of Homogeneous Turbulence", Report, 1998

[33] Subrata Roy, Sagar Kapadia, James D. Heidmann, Proceedings of ASME Turbo Expo 2003, "*Film Cooling Analysis Using DES Turbulence Model"*.

[34] T.S. Lund, Center for Turbulence Research, Annual Research Briefs, *"On the use of discrete filters for large eddy simulation",* 1997.

[35] Ugo Piomelli, Department of Mechanical Engineering, University of Maryland, MD, "*Large eddy and direct simulation of turbulent flows",* Short course delivered at *CFD2001 - 9* ^{e} *conférence annuelle de la Société canadienne de CFD*. Kitchener, Ontario, May 2001.

[36] W. E. Mell, V. Nilsen, G. Kosaly, and J. J. Riley, Department of Mechanical Engineering, University of Washington, Seattle, *"Investigation of closure models for nonpremixed turbulent reacting flows",* Phys. Fluids 6 (3), March 1994.

Vita

Sai Kumar Doddi was born in December 1978 in Hyderabad, India. He did his schooling at Jyothi Vidyalaya High School. He then attended A.P.R. Junior College, Bhadrachalam and Nalanda Junior College, Hyderabad and then passed the Intermediate Public Examination. He obtained his Bachelors degree in Mechanical Engineering from Indian Institute of Technology, Madras in May 2001. During his M.S program at University of Kentucky, Lexington he was briefly involved with the student chapter of A.I.A.A and the voluntary activities of A.S.C.E.